UNIVERSITÀ DI PISA

Dipartimento di Fisica
Scuola di Specializzazione in Fisica Medica

Tesi di Specializzazione

IN VIVO DOSIMETRY AND PRE-TREATMENT QA WITH GAFCHROMIC EBT3 IN RADIOTHERAPY

Relatrice:
Dott.ssa Valentina Ravaglia

Candidata:
Dott.ssa Alessia Giuliano

Anno Accademico 2014/2015

Contents

List of Figures

List of Tables

List of Acronyms

CBCT Cone Beam Computed Tomography

CCD Charge Couple Device

CRT Conformal Radiation Therapy

CT Computed Tomography

DPI Dots Per Inch

FFF Flattened Filter Free

HDR High Dose Rate

HN Head and Neck

IMRT Intensity Modulated Radiation Therapy

KV Kilo Voltage

LiPCDA Lithium salt of pentacosa-10,12-diyonic acid

MLC MultiLeaf Collimator

MU Monitor Units

MV Mega Voltage

OD Optical Density

PTV Planned Target Volume

PV Pixel Value

QA Quality Assurance

RGB Red Green Blue

ROI Region Of Interest

SAD Source Axis Distance

SBRT Stereotactic Body Radiation Therapy

SD Standard Deviation

SRS Stereotactic RadioSurgery

SRS Stereotactic RadioTherapy

SNR Signal to Noise Ratio

SSD Source Surface Distance

TIFF Tagged Image File Format

TBI Total Body Irradiation

TPS Treatment Planning System

TSET Total Skin Electron Therapy

VMAT Volumetric Modulated Arc Therapy

Introduction

The development and the spreading of complex treatment modalities in radiotherapy, such as Intensity Modulated Radiation Therapy (IMRT), Stereotactic Radiosurgery (SRS), and Volumetric Modulated Arc Therapy (VMAT), have provided great achieving in reducing dose to healthy tissues and delivering radiation targeted for very specific lesions. On the other hand, these techniques are characterized by high dose gradients and considerable time and space variations of dose rate and beam fluence, leading to an increase of the complexity of treatment planning and delivery. For these reasons, more specific dosimetric solutions are necessary to the radiotherapy treatment verification and quality assurance (QA).

Among the various types of dosimeters, at present GafChromic EBT3 films represent one of the most powerful tools to perform QA with high accuracy and measure absolute dose in radiotherapy. They have very high spatial resolution, weak energy dependence in a wide photon energy range, and no angular dependence. Furthermore, radiochromic films present the advantages of easy handling, being insensitive to room light, self-developing, and they can be digitalized using a common flatbed charge couple device (CCD) scanner. The characteristics of near-tissue equivalence, effective point of measurement very close to the clinically relevant and recommended depth for skin of 70 μm [1,2] and the possiblility of being cut and positioned at various locations on the patient, allow to use EBT3 film as in vivo dosimeter and evaluate skin dose during radiotherapy treatments.

This thesis aims to describe the use of GafChromic EBT3 films for pre-treatment QA applying both single channel and multichannel methods, and to report and analyse skin dose measurements using radiochromic film as in vivo dosimeter.

In first place, an overview of the main principles, characteristics and applications of radiochromic films and of flatbed scanner dosimetry is provided (see Chapter 1). Secondly, the setting out of the scanning protocol and the characterization of the scanner are described in Chapter 2. Then, an account of the calibration measurements is given, focusing on fit analyses performed for single channel dosimetry with red color channel. Moreover, data calibration has been also performed with a method that combines green and blue channels data together [3,4] and using multichannel dosimetry [5] (see Chapter 3).

With the purpose of validating GafChromic film dosimetry method, film readings have been compared with data measured through PTW 2D-Array 729 irradiated with different standard fields. Afterwards, pre-treatment QA measurements have been performed with EBT3, and absolute dose maps have been compared with TPS calculations using γ-analysis [6] (see Chapter 4).

Finally, in vivo measurements performed during radiotherapy treatments are described. Skin dose was evaluated on patients undergoing helical tomotherapy treatments for different pathologies, including head and neck, brain cancer and sarcoma. Moreover, measurements on patients with breast cancers treated at Linac both with 3D conformal radiotherapy (3D-CRT) and VMAT, and skin lesions treated with Plesio-Röntgen therapy have been considered. Then, in vivo measurements, analysed with GafChromic dosimetry, have been compared with TPS planned doses, investigating on factors possibly related to discrepancies between expected and measured doses (see Chapters 5 and 6).

Chapter 1

GafChromic film dosimetry

The advancement and the diffusion of complex treatment modalities in radiotherapy, such as IMRT, SRS, and VMAT, have provided great achievement in reducing dose to healthy tissues and shorted treatment time, and have allowed dose delivery targeted for very specific lesions. These techniques are characterized by high dose gradients, small fields, and high time and space variations of dose rate and beam fluence, leading to an increase of the complexity of treatment planning and delivery. For these reasons, more specific dosimetric solutions are necessary to the radiotherapy treatment verification and quality assurance (QA) [7]. In radiotherapy, dosimetry aims to quantifying the energy deposited in a medium in terms of absorbed dose to water. An ideal dosimeter should be stable, insensitive or predictable in response to environmental factors such as temperature, pressure and humidity. Moreover, it should be small in size enough to provide high spatial information as well as producing minimal perturbations of the beam. It should be water equivalent to allow interpretation of dose relative to tissue and also to avoid perturbations and other artifacts. The response to radiation is desired to be independent on energy and dose rate for Mega-Voltage (MV) photons and electron beams, and ideally be linear in its response, with sensitivity to both small and large doses. Other more practical considerations include that it be non-toxic for in vivo dosimetry purposes, cheap, reliable and reproducible [8].

Among the various types of dosimeters, at present radiochromic films represent one of the most powerful tools for QA in radiotherapy. They have high spatial resolution, weak energy dependence in a wide photon energy range, near-tissue equivalence and no angular dependence. These dosimeters also present the advantages of easy handling, being insensitive to room light and self-developing, and they can be digitalized using a common flatbed charge couple device (CCD) scanner equipped with a transparency unit for transmission measurements. Nevertheless, radiochromic film dosimetry presents some disadvantages, such as a complex and quite time-consuming processing, intrinsic film inhomogeneity and non-uniform scanner response in the direction of the CCD array. In this chapter a description of the physical principles and applications of radiochromic films will be provided, focusing on the GafChromic EBT3 commercial films, that at present are the most used commercial films in radiotherapy.

1.1 Overview of GafChromic film models

Much of the early work on radiochromic materials can be attributed to the National Institute of Standards and Technology (NIST, US). In 1965 McLaughlin et al. firstly reported on the development of colorless solid solutions of particular materials, called derivatives of triphenyl methane molecule, that underwent radio-syntesis to produce dyes. The initial forms of radiochromic media had a useful dose range of 10^3 to 10^6 Gy, hence their use was limited to high dose applications such as food irradiation, medical instrument sterilization

and other industrial applications. The possibility for new non-industrial applications appeared when a new radiochromic film medium was developed in 1986. This film was named GAFchromic^{TM} and was produced by ISP Technology, a division of GAF Chemical corporation (GAF Corporation, Wayne, NJ). The acronym GAF was derived from the company's pre-1968 name of General Aniline and Film Corporation. In 1991 the GAF Chemical Corporation was publicly listed and it is now known as International Speciality Products Inc. (ISP). The particular dye in GafChromic medium was found to be an order of magnitude more sensitive than previous types and could be used to map distributions with lower doses occurring in medical applications [8].

The materials in radiochromic films which are responsible for the coloration are known as crystalline polyacetylenes, in particular diacetylenes, and upon thermal annealing or radiation exposure they undergo polymerization. The particular diacetylene monomer which composes GafChromic EBT films is the lithium salt of pentacosa-10,12-diyonic acid (LiPCDA) [9]. In the raw manufactured form diacetylene crystals are too large to provide useful sensitivity, hence they are dissolved in a solvent, which has the added advantage of improving the light resistance of the polyacetylenic crystals. These dissolved crystals are then dispersed in a binder such as an aqueous gelation solution. After further processing to remove the alcohol solvent the binder is coated onto a substrate, upon drying crystals become fixed in orientation. Possible substrate materials include polyester, ceramic, glass, and there can be additional coatings in the active layer to reduce UV sensitivity and to act as anti-oxidizing layer [8]. McLaughlin et al. demonstrated that the emulsion mechanism of color production in GafChromic films was a first order solid state polymerization and reported that post-irradiation polymerization continued to occur, most notably within the first 24 hours following exposure [10]. The diacetylene monomers upon heating, UV or ionizing radiation exposure undergo progressive 1,4-polymerisation leading to the production of colored polymer chains that grow in length with level of exposure (see Fig. 1.1). The radiation sensitivity of the crystal is also dependent on the particular end groups, with the lithium salt of PCDA used in GafChromic EBT being sensitive to doses as low as 1cGy, several orders of magnitude more sensitive than the earlier radiochromic films.

ISP manufacturers a range of radiochromic films under the product name GAFchromic^{TM}. The difference between each type of film relates to whether it is constructed with a single or double active layer film, if it is reflective or transmissive film, its physical dimension, and the specific chemical composition of the active layer. In the mid 2000's a film was released called GAFchromic^{TM} EBT. The active layer was a variation of the monomer used in the previous films, and was a hair like version of the LiPCDA crystal [9]. The atomic composition of EBT is (42.3% C, 39.7% H, 16.2% O, 1.1% N, 0.3% Li and 0.3% Cl). The inclusion of the moderate atomic number element chlorine (Z = 17), provided a Z_{eff} of 6.98 making it near tissue equivalent. The new active layer was also found to have a good sensibility in a dose range of 0.01-8 Gy. In 2009 the production of EBT film was discontinued and replaced by EBT2. The EBT2 film had the same active component as EBT but with a yellow dye added to the active layer and it was also constructed as a single layer instead of double (see Fig. 1.2). The film has a slightly narrower active layer than EBT and lightly different overall atomic composition. The Z_{eff} of EBT2 is 6.84 compared to 6.98 for EBT, and close to Z_{eff} of water (7.3). Several works have been published studying some EBT and EBT2 properties, such as film homogeneity [11, 12], scanning orientation dependence [13–17], energy dependence [14, 18–20], absorption spectra [21], postcoloration behavior [12, 14, 15, 17, 18, 22, 23], high-dose dependence [17], temperature dependence [9, 17, 24] and ambient light sensitivity [17].

In 2011, ISP released a new film generation, the GAFchromic^{TM} EBT3 film (see Fig. 1.3). This film is made by laminating an active layer between two identical polyester layers, which makes the product more robust and allows water immersion. While the active layer
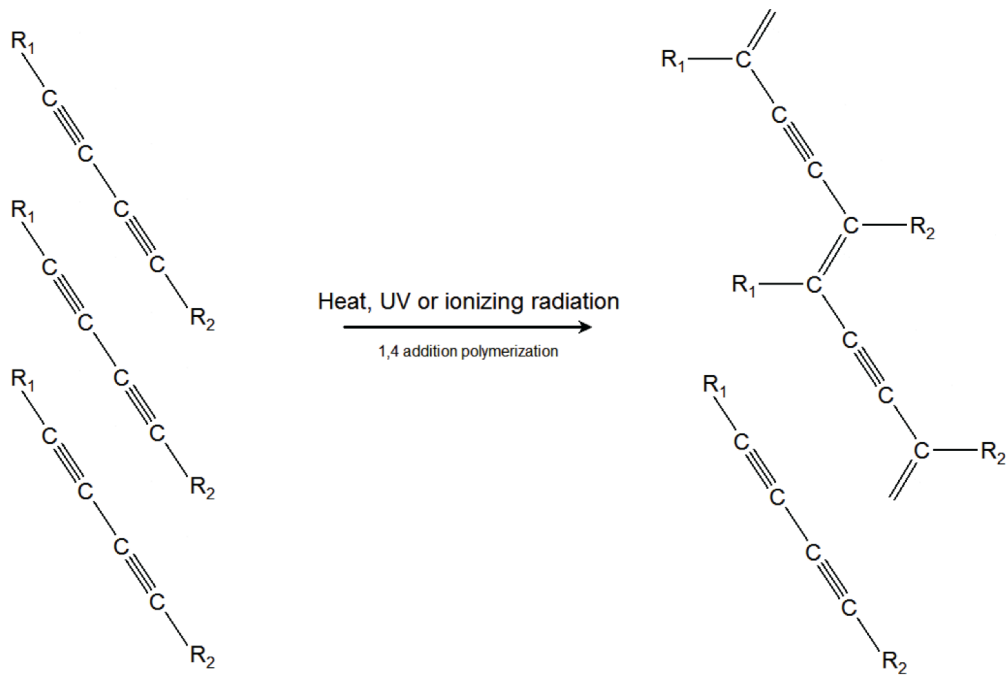
Figure 1.1: The diacetylene monomers undergo a 1,4 polymerization upon exposure to heat, UV or ionizing radiation [8].
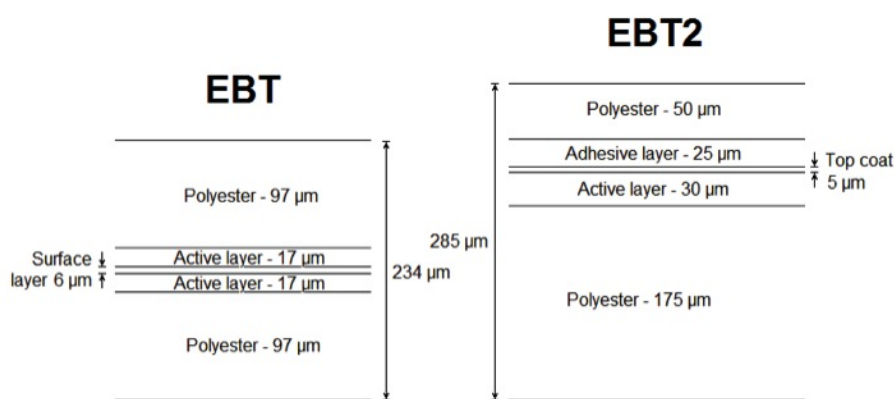
Figure 1.2: An illustration of the physical configuration of GAFchromic^{TM} EBT compared to EBT2. EBT2 has a slightly thinner active layer and an asymmetric design [8].

composition and response are unchanged, the real EBT3 improvements are: the symmetric structure that will avoid the potential errors in optical density measurements due to scanning side in EBT2, the matte polyester substrate that prevents Newtons Rings formation, and the presence of fiducial marks that allows for the film automatic alignment if required [25]. The dynamic range of this film is designed for best performance in the dose range from 0.2 to 10 Gy, making it suitable for many applications in IMRT, VMAT and brachytherapy. For measurement of doses substantially greater than 10 Gy other GafChromic film models are preferred, such as EBT-XD or MDV3, while the use of HD-V2 is indicated for still higher dose measurement.

The structure of EBT3 film is shown in Fig. 1.4. The film is comprised of an active layer, nominally 28 μm thick, sandwiched between two 120 μm matte-polyester substrates. The active layer contains the active component, a marker dye, stabilizers and other components giving the film its near energy independent response. The thickness of the active layer will vary slightly between different production lots. The yellow marker dye incorporated in EBT3, in conjunction with a Red Green Blue (RGB) film scanner and a commercial or homemade software, enables the dosimetry process to benefit from the application of triple-channel dosimetry [28]. The polyester substrate of EBT3 has a special surface treatment containing microscopic silica particles that maintain a gap between the film surface and the glass window in a flatbed scanner. Since the gap is nearly ten times the wavelength of visible light, formation of Newton's Rings interference patterns in images acquired using flatbed scanners is prevented.

Dosimetric study on EBT3 performed by Casanova Borca et al. [25] confirms that the red channel has a greater response up to 10 Gy. The green channel exceedes the red one for doses above 10 Gy, indicating it could be preferable to use the green channel at higher doses. Instead, the blue channel has a lower response gradient at any dose because the signal has a weak dose dependence while having a strong dependence on the thickness of the active layer. This makes the blue channel less useful than the other channels for dose measurements. In addition, measurements of postirradiation development with time have been reported in literature. Regarding this aspect, EBT3 films showed the same behavior as EBT2 [17,23]. Casanova Borca et al. reported that between 24 h and 72 h after irradiation the variations in net optical density (net OD, see Eq. 1.2) were less than 0.005 for all doses between 0.3 and 4 Gy. Then they studied the variation of net OD measured at 30 min, 1 h, 2 h, 6 h after irradiation with respect to net OD measured 24 h after irradiation. They showed that between 1 h and 24 h after irradiation, the variations in net OD were less than 0.010 for all doses under study. Moreover, between 2 and 24 h after exposure, changes in the net OD were less than 0.008 (see Fig. 1.5) [25].

Finally, Casanova Borca et al. [25] demonstrated that EBT3 film response is nearly independent on radiation energy used in IMRT treatments, within the uncertainty of the measurement, thus confirming previously published data on EBT2 [20]. Differences between films were negligible with values less than 1% for doses up to 4 Gy, comparing 6 MV and 15 MV energies and three different dose rates (100 MU/min, 300 MU/min, 600 MU/min). Other studies have been set up on EBT3 energy dependence considering both the MV and the Kilo-Voltage (KV) regions. Rubinstein et al. showed that in KV region, EBT3 has significant energy dependence showing decrease in film-sensitivity with decreasing beam energy. However, the film resulted practically energy independent for MV Photon & Electron beams including Cs-137 [26]. Furthermore, Villarreal-Barajas et al. reported that for a given dose of 1 Gy of kVp Xray, the response relative to Co-60 using the three color channels decreases with decrease in kVp, reaching a maximum under response of about 20% for the 70 kVp. A significant under response of about 5% was observed at 300 kVp. Instead, responses of MV Xray beams with respect to Co-60 at the 1 Gy dose level showed no statistically significant difference [27].

5

Figure 1.3: GafChromic EBT3 available in format: 8"x10", 25 sheets/box (Ashland, Medical dosimetry, www.gafchromic.com).
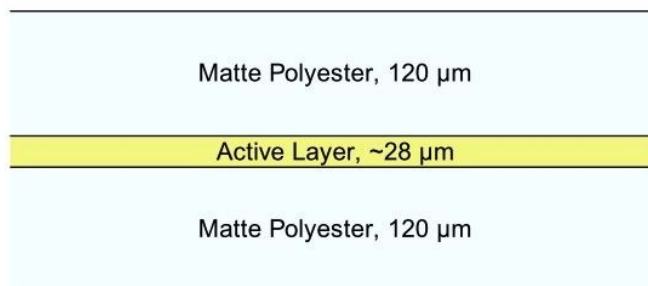
Figure 1.4: Configuration of GafChromic EBT3 dosimetry film (www.gafchromic.com).
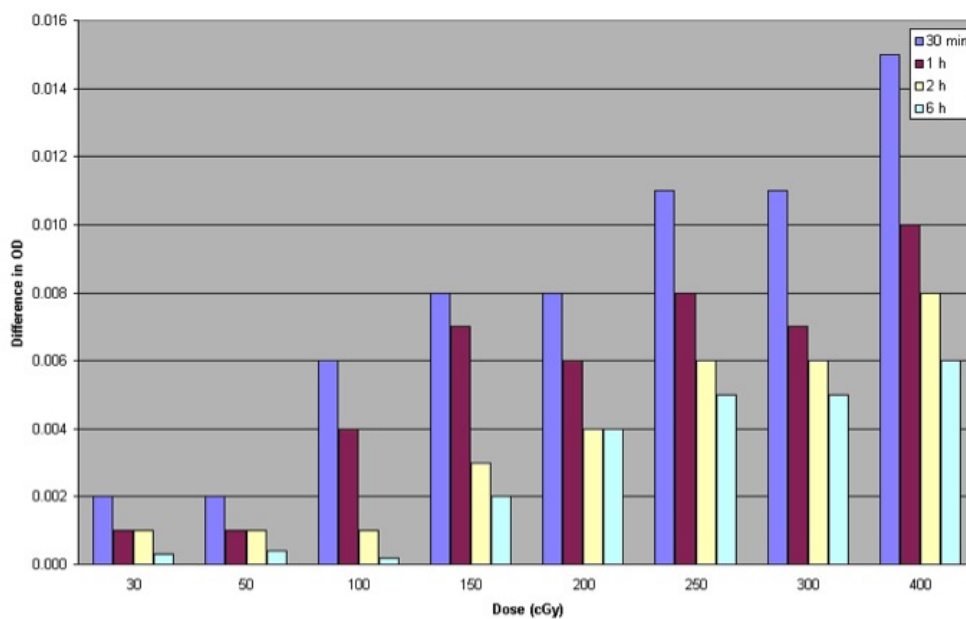
Figure 1.5: Variation of net optical density after 30 min, 1h, 2 h, and 6 h compared to 24 h after irradiation at eight different dose levels [25].

1.2 GafChromic film dosimetry system

As for other types of dosimeters, by using a certain protocol a radiochromic film dosimetry system can provide a measurement of absolute dose. However, to convert the response of the film into absolute dose, the calibration curve is needed. It has to be determined for a given radiochromic film dosimetry system, which consists of a film model, particular densitometer used, and protocol together, under reference conditions and using a reference radiation beam quality. The very same motive is applied to other dosimetric systems in the clinic. On the other hand, absolute dosimeters report an absolute dose as a result of dose measurement without an a priori knowledge of the dosimeter's response to a certain reference beam quality. Up to now, absolute dosimeters have been designed, developed and maintained in Radiation Standard Laboratories only. Currently used absolute dosimeters are: Free Air Ion Chamber, Calorimeters and Fricke-gel dosimeters [29].

Response of radiochromic films to radiation is commonly expressed in terms of the change in its optical density (netOD), that represents the difference in optical densities of the same film piece sampled after and before irradiation. The optical density (OD) is the function of the wavelength at which the absorbance was sampled. In other words, the measured OD could be considered a sole property of the film only if sampled by spectrophotometer where the measured OD refers to the particular wavelength of the absorption spectrum. On the other hand, many optical densitometers are employed (particularly flatbed document scanners) that use broad band fluoroscopic visible light sources. For the optical densitometers that do not employ monochromatic light sources, OD change is a rather complex convolution between the film absorption spectrum ($A(\lambda)$), the linear CCD array sensitivity spectrum ($S(\lambda)$) and the emission spectrum of the fluorescent light source of the scanner ($E(\lambda)$), which can be expressed as [29]:

$$OD = \log_{10} \frac{I_0}{I} = \log \left(\frac{\int_{-\infty}^{+\infty} E(\lambda) \cdot S(\lambda) \cdot d\lambda}{\int_{-\infty}^{+\infty} E(\lambda) \cdot A(\lambda) \cdot S(\lambda) \cdot d\lambda} \right), \tag{1.1}$$

where I_0 and I are the incident and transmitted light intensities respectively. It is important to remark that for every particular radiochromic film dosimetry system the sensitivity curves will be different [30]. One should also remember that manufacturer may change the chemical composition of the film layers. So even for the same film model, the sensitivity and hence the calibration curve may change from one film batch to the other. In fact, a good practice is to measure a new calibration curve if the film batch has changed, indicated by manufacturer on the box.

OD depends on the thickness of the film, but also on the wavelength of the incident light. Radiochromic films have an inherent color that develops during radiation exposure, and the optical absorption varies by wavelength [23]. OD is determined using a color flatbed scanner which digitalizes the image and measures the film response over different wavelength bands divided into red, green and blue in the visible spectrum. The absorbance spectrum of the active layer for GafChromic EBT3 has a peak of 636 nm after exposure to ionizing radiation, which means that the maximum sensitivity for optical density measurements is obtained with the red color (see Fig. 1.6).

The process of radiochromic film dosimetry can be divided two distinct steps. Firstly, the generation of the calibration curve, during which film samples are irradiated to known dose values. In second place, an irradiated film with unknown dose can be read applying the calibration curve. During the calibration phase, a reference radiation source must be used, which has been previously calibrated following an a priori established reference dosimetry protocol (TRS 398 [31] or TG-51 [32], for example). Once the radiation source is characterized, reference irradiation takes place by exposing several pieces of film to different dose values. Pixel values (PV) of the transmission scan on a flatbed document scanner are
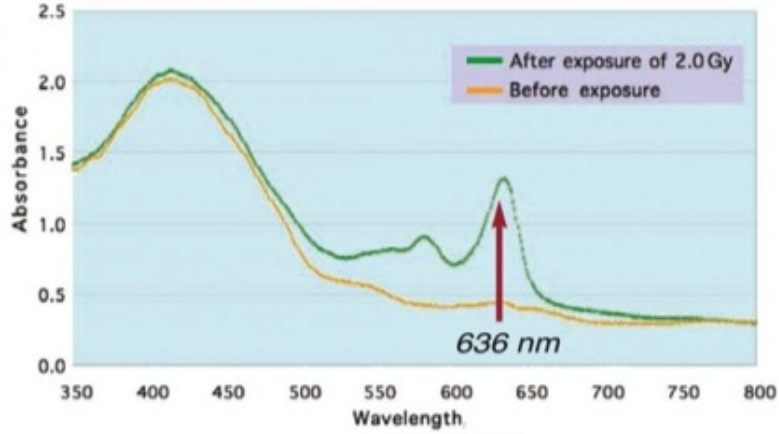
Figure 1.6: Absorption spectra of EBT3 film as a function of wavelength, before exposure (the yellow line) and after irradiation corresponding to 2.0 Gy (the green line) http://www.rpdinc.com/.

sampled over predefined region of interest (ROI) and change in OD is calculated for every film piece:

$$netOD = OD_{after} - OD_{before} = \log_{10} \frac{PV_0}{PV_{after}} - \log_{10} \frac{PV_0}{PV_{before}} = \log_{10} \frac{PV_{before}}{PV_{after}}, \quad (1.2)$$

where PV_0 represents the pixel value of non attenuated beam and for a 16-bit image amounts to 2^{16}. To use the calibration results for future dose measurements, the common practice with GafChromic films is to plot dose as a function of the measured netOD, and then fit the data with an appropriate function using the method of least squares. Fig. 1.7 illustrates schematically the reference dosimetry protocol established to measure absolute dose of a plan dose distribution in an IMRT plan using only the red channel of the scanned RGB image. The use of the red color channel is commonly adopted in the current practice, but it does not exclude the possibility of using the other color channels, especially if higher doses are to be measured with a given radiochromic film dosimetry system.

1.2.1 Flatbed scanner dosimetry

To determine the amount of dose delivered to a film, its change in the absorbance is measured. In order to quantify this change the optical density of the film needs to be measured using a scanning densitometer system. The ready availability and low cost of flatbed scanners make them attractive for use as densitometers. One particular make and model, the EPSON 10000XL, has been specifically recommended by ISP for use with their GafChromic EBT films.

A flatbed scanner is usually composed of a glass pane (or platen), under which there is a white light fluorescent source which illuminates the pane, and CCD detection system that move together to scan the film. The movement direction of the light source will be called the y-axis and the direction parallel to the light source the x-axis (see Fig. 1.8). The unit contains a combined mirror-lens optics forming a reduced image of the illuminated line of the scanned object on a CCD detector array. These devices can operate in transmission or reflection mode. The most basic difference between transmission and reflection mode is that in reflection mode most of the detected light has passed through the film twice, this increases the sensitivity to low doses but leads to quicker saturation at higher doses. The image produced by a CCD scanner is usually of 16-bit resolution in the channel of interest, for a color channel this will mean 48-bit images are required as 16-bits will be allocated to each of the red, green and blue color channels.
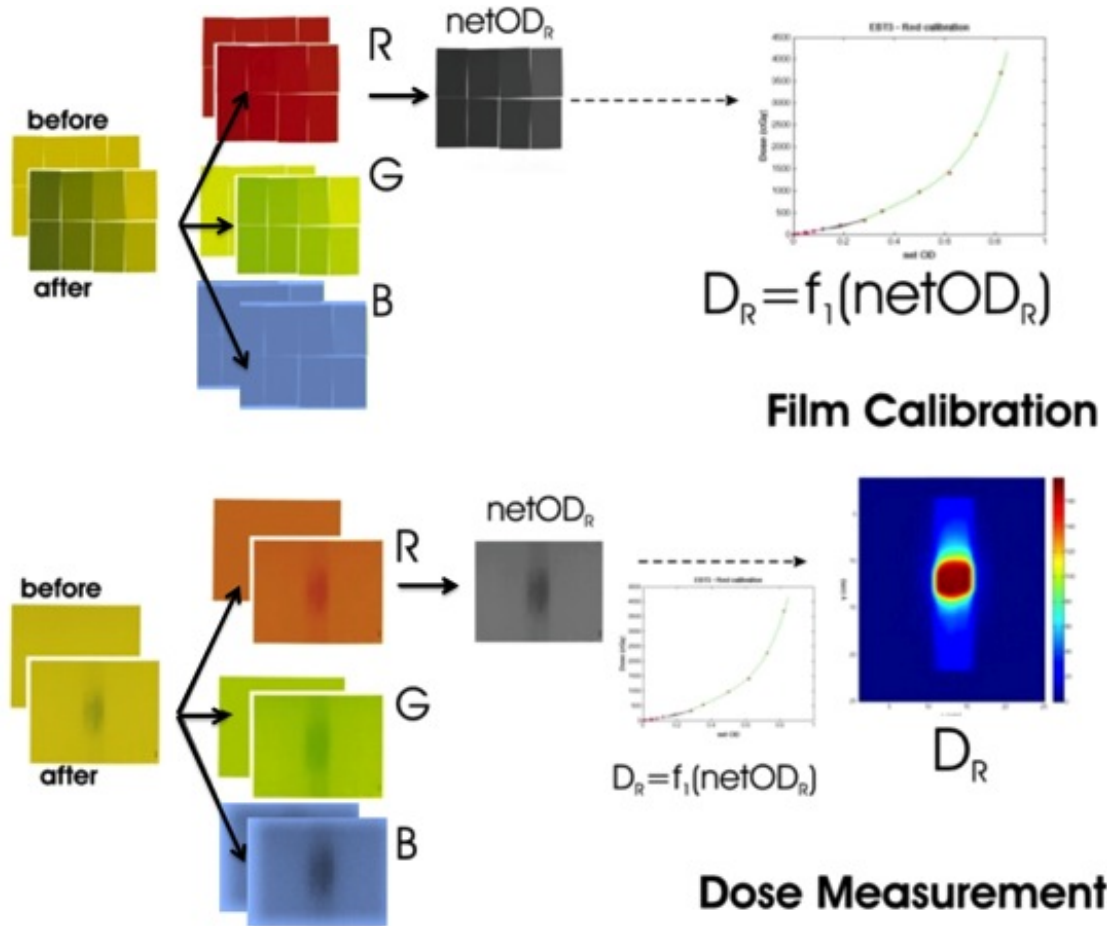
Figure 1.7: Summary of radiochromic film reference dosimetry protocol. Top: calibration of radiochromic film dosimetry system. Bottom: measurement of an unknown map of dose [29].

Fluorescent light sources can have an emission spectrum that covers the entire visible spectrum and may include ultraviolet and infrared. Fig. 1.9 shows the emission spectrum for the Xenon cold cathode ray tube that is found in the Epson 10000XL scanner type, also shown are the spectral sensitivities in the red, green and blue channel for the CCD typically used in flatbed scanner. As can be noticed, the red channel is well suited for GafChromic dosimetry with a peak sensitivity between 600-650 nm [8].

OD range and Warm-up

As described by Gonzalez et al. [36], the OD range of a scanner used for film dosimetry is limited to saturation and noise. As the OD increases, saturation causes the rate of change of the output to become smaller as the input signal increases, whilst at the same time the amount of noise remains fairly constant or increases. The combined effect leads to a degradation of the signal-to-noise ratio at high optical densities. The nominal maximum of OD for the EPSON 10000XL scanner is of 3.8.

A warming up period has been observed for scanner fluorescent lamps. If possible the scanner and lamp should be turned on 30 minutes prior to use to allow the temperature to stabilize. For some scanners, such as the EPSON 10000XL, it is not possible to independently switch the light source on without scanning, hence to warm up the lamp scanning must be performed. Typically the scanner response stabilizes after the first 3-4 scans. Several authors report various scanning methodologies, but each contains either a warm-up period or the rejection of the first 2-3 images, followed by averaging of the next 3 images [8].

Noise

In addition to the microscopic non-uniformity of the film, the flatbed scanner will introduce additional noise due to electronics. By averaging multiple successive scans the amount of noise can be reduced [37, 38]. Ferreira et al. reported that a large decrease in noise was achieved by repeating scans twice, and a maximum improvement occurred after 4 scans. As the number of repeated scans increased beyond four there was degradation in image quality and the noise became to increase again [8].

To reduce noise caused by imperfections in the film the images can be processed using a filter, such as Wiener filter [37]. The 2D Wiener filter uses a local estimate of the noise power spectrum and is therefore suitable for dosimetry as it preserves systematic variations in the film's OD. To minimize film to film variations, averaging across multiple films can be done. In a study by van Battum et al. on EBT and the uncertainties associated with using a flatbed scanner they concluded that using at least two films reduced the impact of inherent film non-uniformity and reduced the overall uncertainty of EBT dosimetry down from 1.8% to 1.3% [39]. Decreasing scanner resolution can also improve dose accuracy by averaging out the noise. Using a resolution of 72-75 dpi provides a good compromise between image resolution and noise [38, 40].

Stability

The stability of scanners have been studied by performing numerous repeat scans. When using radiochromic film a gradual increase in OD was observed following the initial warm-up period. Several factors contribute to this growth. The response of the film is temperature dependent, as multiple scans are made the temperature of the glass plate increases and then the film also heats up leading to a change in response [24]. Another contributing factor to the increase in OD with multiple successive scans is the presence of UV wavelengths in the fluorescent light. Most radiochromic films demonstrate some sensitivity to UV light, and when they are scanned using the standard white light fluorescent tube the UV component
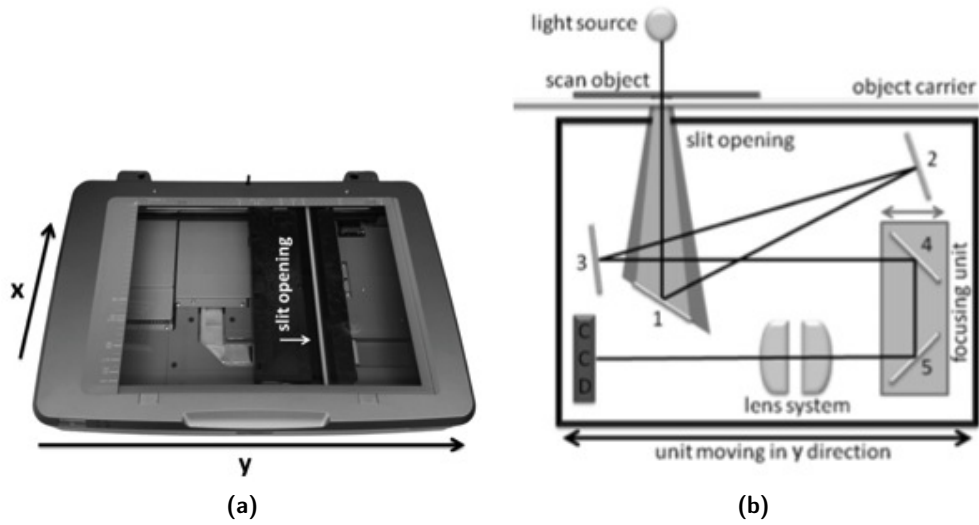
Figure 1.8: The Epson Expression 10000XL flatbed scanner. (1.8a) The scanner bed, the coordinates y (movement direction of the lengthy light source) and x (parallel to the lengthy light source) and the movable imaging unit below the lengthy light source. (1.8b) Cross section (not to scale) of the light recording unit. Its box has a width of 15.8 cm, length of 39 cm and height of 8 cm. It moves in the y direction, and the x direction is perpendicular to the drawing plane [35].
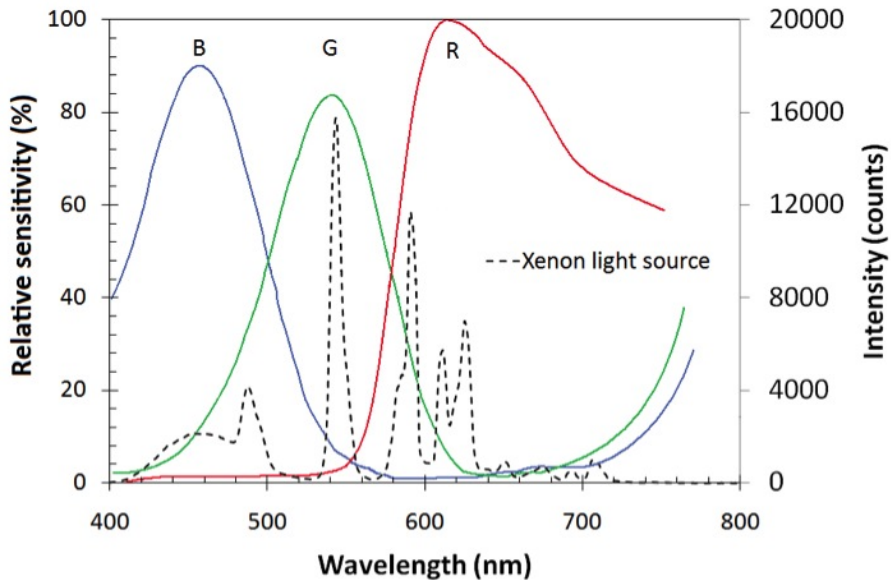
Figure 1.9: Typical spectral sensitivities of the red, green and blue channels of a CCD of the type used in flatbed scanners, also shown is the emission spectrum of the Xenon cold cathode ray tube used in the EPSON 10000XL flatbed scanner [8].

11

results in additional polymerisation. Limiting the number of scans to fewer than 10 will minimize this effect [8].

Uniformity

The non-uniformity of the scanned light field on flatbed scanners has been well documented and it is one of the largest sources of error if left uncorrected [24]. The non-uniformity is essentially limited to the direction perpendicular to the scan direction (x-axis in Fig. 1.8), this being parallel to the light source. The non-uniformity has been shown to be dependent on OD and can be greater than 10% across the entire scan area. The non-uniformity study across the EPSON 10000XL scanner will be extensively described in the second chapter. However, the effect of this non-uniformity is that the pixel value behaviour along the x-axis has a parabolic trend, with the maximum located in the central axis of the scanbed.

Devic et al. suggest several possible contributing factors to the non-uniformity: geometrical inefficiency with CCD elements at the edge capturing fewer photons, light leackage, diference between reflections in the central region and in region close to the edges of the scanning bed and the optics used to focus the light at the CCD array [8,47]. To minimize the uncertainty associated with light non-uniformity, several methods have been suggested. The simplest method is to scan the films in the centre of the scanner which has minimal non-uniformity. An alternative approach is to is to use a transparent film or filter of constant OD, and scan it over the entire flatbed producing a correction matrix.

Orientation

Landscape orientation of the film means that the long side of the film points in the x direction, while in portrait orientation the long side is pointing in the y direction. The scan response of radiochromic films is sensitive to orientation of the film on the scanner. This behaviour is caused by the anisotropic scattering of the photons emitted by the scanner when passing through the polymer network, and the polarization of the transmitted light by the needle-like shape particles of film active component that are preferentially aligned parallel to the direction in which the film was coated that is parallel to the short edge of the film. Casanova Borca et al. reported that EBT3 film shows a difference up to 4.5% in net OD between portrait and landscape orientation [25]. Measurements showed lower dependence to those published for EBT2 by Andreas et al. ($\approx$7-9%) [17], although greater than that published by Desroches et al. ($\approx$2%) [16]. Moreover, Schoenfeld et al. scanned EBT3 films exposed to doses between 0 Gy and 20.9 Gy and placed on the scanner in landscape and portrait orientation, also with and without the application of a neutral density filter to correct non-uniformity (see Fig. 1.10 for results). By comparing between landscape and portrait orientation the optical densities measured at the same dose, the orientation effect can be recognized: the measured optical density is always higher when the film is scanned in portrait orientation. The parabola effect, on the other hand, is represented by the lateral increase of the measured optical density, shaped as an upward-bent parabola with its deepest point near the centre of the light source and with a dose-dependent weight of the quadratic term. An increase in optical density towards the ends of the x-axis of up to 8.4% for landscape orientation and up to 12% for portrait orientation was observed [35].

Conversely, due to the symmetric structure of EBT3, differences from film face-up versus face-down scan orientation were negligible, with values less than 0.7% for doses up to 4 Gy [25]. The side independent scanning can be considered the most important improvement of EBT3 film with respect to EBT2, which showed a net OD difference between the two sides approximately equal to 2% which may significantly affect relative and absolute dose measurement [16]. In practice, the EBT3 film can be scanned with either side facing the
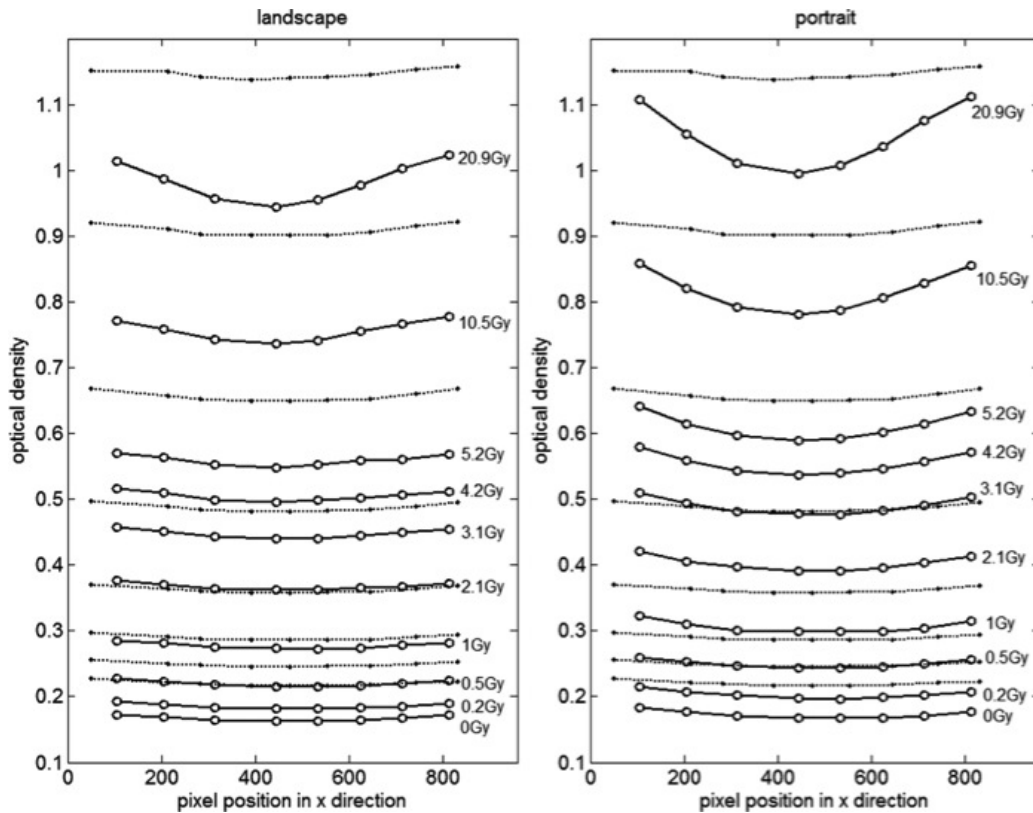
Figure 1.10: The orientation and parabola effects in landscape (a) and portrait (b) orientation of EBT3 films exposed to doses from 0 to 20.9 Gy (full lines), in comparison with scans of neutral density filters with different optical densities (dotted lines) [35].

light source, but in the measurement and analysis of calibration, care must be taken not to mix films acquired in portrait orientation with those acquired in landscape.

Spatial resolution

It has been reported that the active component of GafChromic film is capable of resolving greater than 1200 lines/mm, due to the physical size of the crystal [10]. When dispersed in emulsions of different thickness the true resolution is likely to deviate from this value. In either case Gafchromic film is capable of very high spatial resolution, and for accurate dosimetry the film response should be uniform over very small and large distances. Hence the spatial resolution is only limited by the scanning resolution, which is 2400 dots per inch (dpi) for the EPSON 10000XL. Nevertheless, Ferreira et al. reported that as the resolution of the scanning system decreased the amount of noise also decreased, as determined by the standard deviation within a ROI (2x2 mm^2) for EBT2 film (see Fig. 1.11) [38]. This is the reason why the most common values for scan resolution are 72-75 dpi, which correspond roughly to 0.3 mm.

1.3 Radiochromic films applications

Radiochromic film has been used for a variety of medical applications, but with the advent of the GafChromic media and the even more sensitive EBT3 product, there has been a rapid uptake of radiochromic film for use in radiotherapy dosimetry.

For accurate quantitative dosimetry to be performed with radiochromic film there must be adequate measures in place to account for the variety of film and densitometer dependent
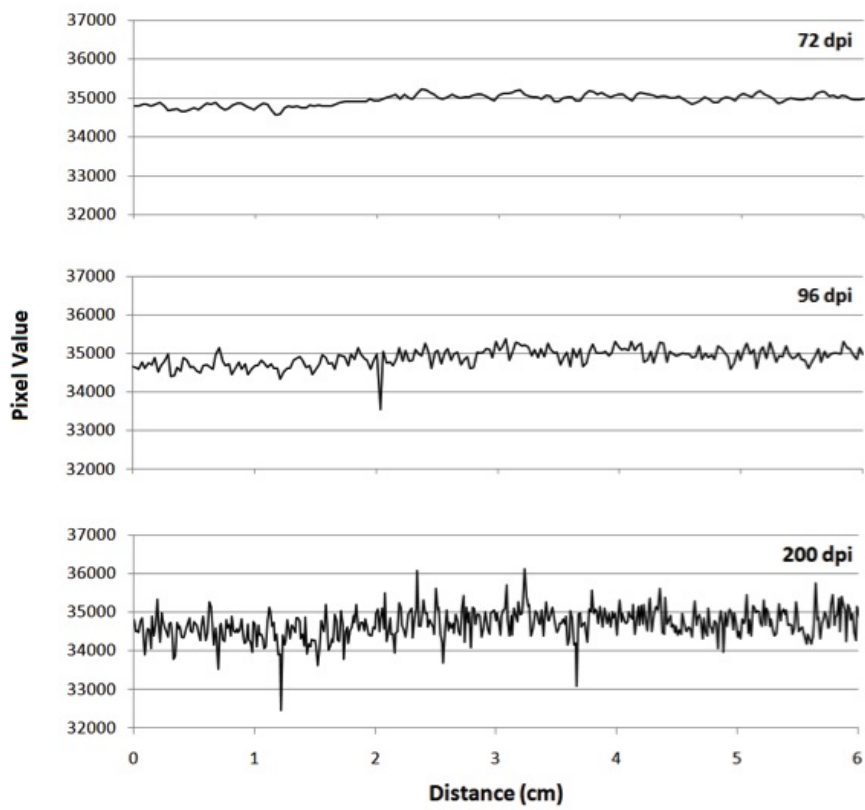
Figure 1.11: Profiles measured across the same region of GafChromic EBT2 film using different scan resolutions. As the scan resolution decreases the amount of noise also decreases [8, 38].

properties. With such measures in place radiochromic film can be adopted to collect high resolution data that characterizes various properties of the linear accelerator, such as micromultileaf leackage and trasmission, to perform small stereotactic field dosimetry [8, 42], and proton beam dosimetry. The water resistance and near tissue equivalence of EBT3 films allow them to be used in water phantoms to perform accurate dosimetry.

The high resolution of GafChromic film makes it favourable for performing high resolution qualitative measurments. GafChromic film has been used to verify isocentre alignment for proton beams, on linear accelerators also, and for periodic QA in Tomotherapy.

There have been a number of published papers describing the use of GafChromic films in brachytherapy. In this field they have been used to determine the TG-43 parameters for the Cs-131 and Cs-132 seed sources [45], and to access dose heterogeneity in intra-operative HDR brachytherapy and for high dose rate (HDR) brachytherapy QA.

One of the most common uses of GafChromic films is to perform quality assurance of IMRT treatments, for which EBT films were specifically designed. With the complexity of IMRT planning and delivery requiring increased verification of treatment delivery, radiochromic films provide a fast and reliable mean of accurately recording the dose distribution. The insensitivity to room light and lack of chemical processing also allow it to be incorporated into a variety of phantoms. Moreover they are used for pre-treatment QA in SRS and VMAT, and thanks to their high spatial resolution they are suitable for small lesions typical of Stereotactic RadioTherapy (SBRT).

In addition to its use for verifying patients treatments, radiochromic film shows a great potential for two dimensional clinical dosimetry of electron beams [43, 44], and it has been found useful in total skin electron therapy (TSET) in vivo [45]. Radiochromic films can be also used to measure not only the small electron cutout output, which represents very labor intensive and time consuming process, but, it provides complete dose distribution within measuring plane that may help radiation oncologist in dose prescription from a given treatment.

The ability to cut and bend the film allows it to be positioned at various locations on the patient and have challenging dosimetry, such as skin folds. In fact, GafChromic films have many attractive characteristics that make them candidates for in vivo skin dosimetry such as, high spatial resolution, near-tissue equivalence, weak energy response, angular independence. Moreover, the equivalent depth in water of the effective point of measurement for EBT radiochromic films has been determined as 153 μm [47], which is very close to the clinically relevant depth for skin of 70 μ recommended by ICRP [1] and ICRU [2]. For example, Su et al. have applied GafChromic EBT as an in vivo dosimeter in total body irradiation (TBI) dosimetry to evaluate entrance and exit doses in various locations of patient surface. Moreover, Avanzo et al. performed in vivo measurements to evaluate dose to the skin in helical tomotherapy [46]. In this study the sites of treatments included scalp, brain, head and neck, cranio-spinal axis and lower limbs. To give another example, Roland et al. measured and compared skin dose for prostate and head-and-neck patients treated on various IMRT delivery systems (serial and helical tomotherapy, IMRT step and shoot), observing that the TPSs always overestimate the average skin dose in all three systems [48].

Chapter 2

Flatbed scanner characterization

In this chapter the preliminary measurements performed to characterize the flatbed scanner are described. The scanner response has been studied in terms of reproducibility, stability and uniformity. Moreover, the variation of the mean pixel readout between consecutive readings and between different protocols was evaluated for the three colour channels with the aim of setting up a general scanning protocol for the dosimetric readings.

2.1 Reading protocol

A flatbed scanner, Epson Expression 10000XL (Seiko Epson Corporation, Nagano, Japan), and its software, EPSON Scan v3.49I, were used to digitalize the films (see Fig. 2.1 and 2.2). The EBT3 were scanned in professional mode, which gives the greatest control of image colour and quality, and the scanning parameters were set as follows:

- film type: positive film;

- spatial resolution: 75 dpi;

- type of image: colour 48-bit;

- document dimensions: width 419.1 mm, height 309.9 mm.

All filters and image enhancement options were turned off and the scans were saved as tagged image file format (TIFF). The films were scanned in portrait orientation (i.e., long edge of the film parallel with the long edge of the scan bed), which have been shown to be more sensitive to changes in the optical density of the film [33]. A polycarbonate frame with markers in correspondence to the centre of the scanner were developed to guarantee a good reproducibility in film positioning on the scan bed. Since the films were scanned in colour 48-bit mode, each Red Green Blue (RGB) image was composed by three 16-bit matrixes, in which red, green and blue signals are added together in various ways to reproduce a deep array of colours. Hence, each pixel of a single colour matrix assumes a value in the range [0 , $2^{16} - 1$].

2.2 Preliminary measurements in the centre of the scan bed

In first place an evaluation of the necessity of a scanner warm-up in order to obtain a stable pixel value response was performed. The same irradiated EBT3 film was scanned in three different conditions:

1. the scanner is turned on, then, after 30 minutes of warm-up and 5 blank scans, 15 consecutive measurements of the film are taken;

Figure 2.1: Scanner Epson Expression 10000XL (Seiko Epson Corporation, Nagano, Japan), https://www.epson.it.
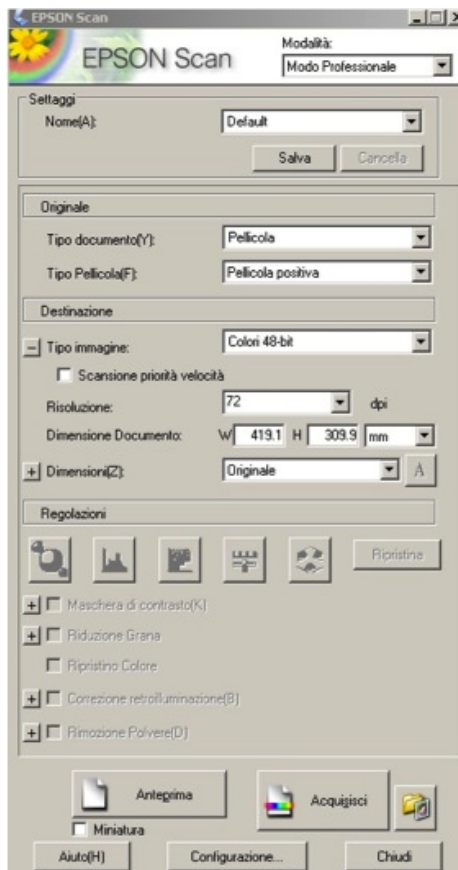
Figure 2.2: The EPSON Scan dialog box.
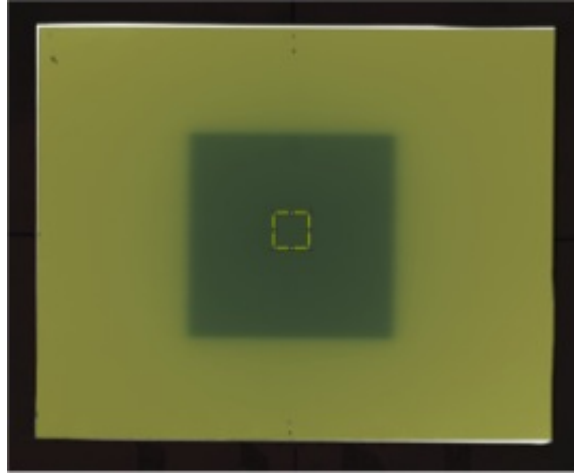
Figure 2.3: Scan of an irradiated Gafchromic EBT3 film. The measurements of mean and standard deviation of pixel values is computed in a fixed central ROI with area of 50x50 pixels.

2. the scanner is turned on, then the film is scanned 15 consecutive times;

3. the scanner is turned on, then, after 30 minutes of warm-up, 15 consecutive scans of the film are made.

Each group of measurements has been acquired in about 15 minutes and distant in time from the others. The mean and the standard deviation of the pixel values in a Region Of Interest (ROI) of 50x50 pixels taken in the centre of the film have been computed with ImageJ software (https://imagej.nih.gov/ij/) for each set of measurements and for each channel (see Fig. 2.3). The results of the measurements, shown in Fig. 2.4, demonstrate that the responses in the red and green channels are quite stable if compared with the results in the blue channel, where a slow growing trend can be appreciated in the three sets of measurements. Considering the blue channel only, the average pixel values appear a little more stable in the first condition, leading to prefer the first measurement approach. Nevertheless, the differences between the results obtained in the three approaches are so little highlighted that it can be concluded that the scanner warm-up will not substantially change the results in terms of pixel values of the scanned film, especially if they will be averaged in a ROI and between a small group of consecutive scans. To be thorough, the results in terms of mean and standard deviation in the three measurements conditions between the various scans are summarized in Table 2.1. Moreover, the results have been presented in terms of maximum deviation from the mean pixel value and expressed in percentage (see Table 2.2). From these it is confirmed that the more stable result in the blue channel is obtained from the approach 1, but here the maximum deviations in the red and green channels are a bit larger than those obtained with protocols 2 and 3. Then, to reach a compromise between these situations, we decided to follow the first protocol. Hence, after a period of about 30 minutes of warm-up of the scanner and after a couple of blank scans, we acquired the desired film.

2.3 Studying the reading response along the scan bed

With the aim of characterizing the response of the scanner along x and y directions (see Fig. 2.5) for the three colour channels, the same piece of film has been scanned in various positions along both the axes. Moreover, in order to understand the dependence of the readout both on the position of the film and on its mean pixel value, that is inversely
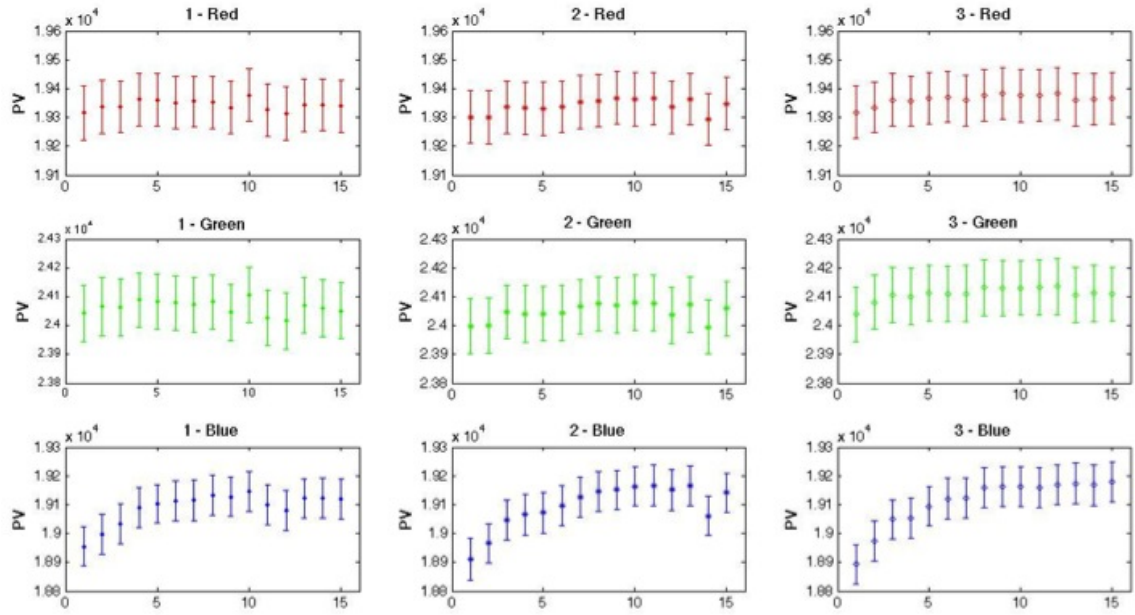
Figure 2.4: Comparison of the mean pixel values in the central ROI of 50x50 pixels between the three measurement conditions (1, 2 and 3) and the three channels with respect to the number of scans.

Table 2.1: Comparison of the global mean pixel values (PV) and standard deviations in the central ROI of 50x50 pixels between the three measurement conditions (1, 2 and 3) and the three channels.

Color channel	Measurement 1	Measurement 2	Measurement 3
Red	19343 ± 18	19339 ± 25	19364 ± 18
Green	24063 ± 24	24047 ± 29	24110 ± 25
Blue	19090 ± 54	19096 ± 76	19109 ± 84

Table 2.2: Comparison of the maximum deviation from the mean of the average pixel values in the ROI between the various measurement conditions (1, 2 and 3) and for the three channels.

Color channel	Measurement 1	Measurement 2	Measurement 3
Red	0.18%	0.15%	0.11%
Green	0.17%	0.14%	0.11%
Blue	0.29%	0.38%	0.36%
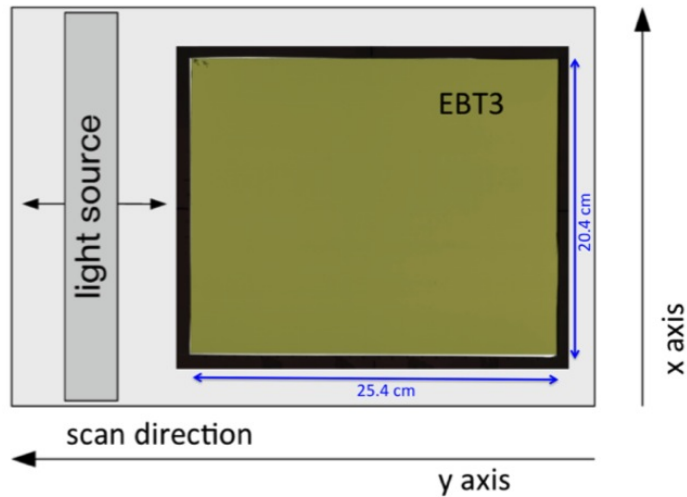
Figure 2.5: Definition of x and y directions of the scanner. The y axis coincides with the scan direction, instead the x axis is transversal to it.

proportional to the exposed dose, a set of square pieces of EBT3 films were irradiated at different uniform doses. For this purpose, seven film samples of 5x5 cm^2 were cut from the same film and irradiated perpendicularly with a 10x10 cm^2 open field from a 6 MV radiation beam (Linac Synergy Agility, Elekta) to seven levels of uniform doses. Hence, the film pieces presented different OD levels, within a range of [0.2,1.4] for red, [0.2,1.1] for green and [0.4,0.9] for blue channel. For the sake of simplicity, they were called level 1 to 7 with increasing dose and OD.

2.3.1 Response along the scan direction

With the aim of studying the scanner reading in the motion direction of its light source, each film sample was scanned in five consecutive positions to cover the length of 25.4 cm every 5 cm along the y axis. The film in each position was scanned five times, then the mean and the standard deviation of the pixel values were evaluated in a ROI of 50x50 pixels (about 1.7x1.7 cm^2 with 75 dpi) placed at the centre of the piece of film. These evaluations have been repeated for the three colours to assess eventual differences in the channels behaviours. The design of the measurements is clarified in Fig. 2.6, and the plots of the results at different doses are reported in Figures 2.7, 2.8 and 2.9 for red, green and blue channels respectively. To allow a comparison between the figures, the size of the range of the y axis has been set equal for all of them and the mean PV have been normalized to the central value. As can be appreciated from these figures the trend of the measurements is rather constant. Moreover, the average PV for each dose level and for each channel have been computed (see Table 2.3). As can be seen, the percentage errors on the mean PV are below the 0.5% for all the dose levels and for all the channels, leading to consider the conclusion of a constant scanner reading signal along the y axis to be reliable. Moreover, it can be noticed that the signal is a bit noisier when the exposure level of the film is lower.

2.3.2 Response along the x direction of the scan bed

With the intention of assessing the scanner behaviour on the x axis, each film sample was scanned in four consecutive positions to cover the length of 20.4 cm every 5 cm along the x axis. In each location the film was scanned five times and the mean and the standard deviation of the PV were evaluated in a ROI of 50x50 pixels located at the centre of the piece of film.
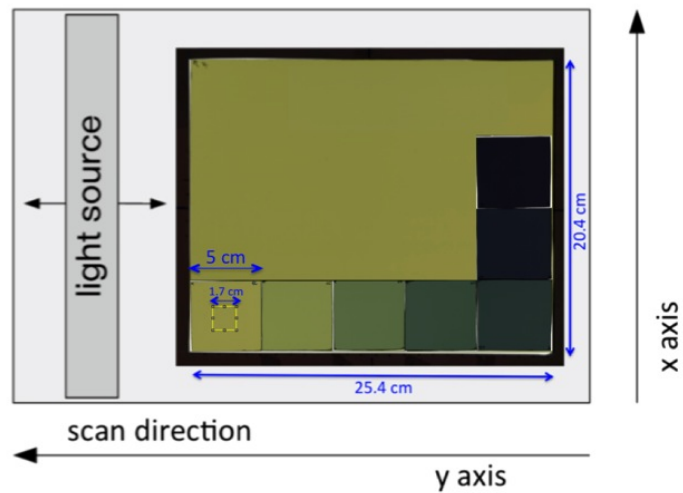
Figure 2.6: Experimental set up for the study of the scanner readout along its axes and with film portions (5x5 cm^2) exposed at different doses, hence having different OD levels. The mean PV was evaluated in a ROI centred in each piece and sized 50x50 pixels (about 1.7x1.7 cm^2 with 75 dpi).
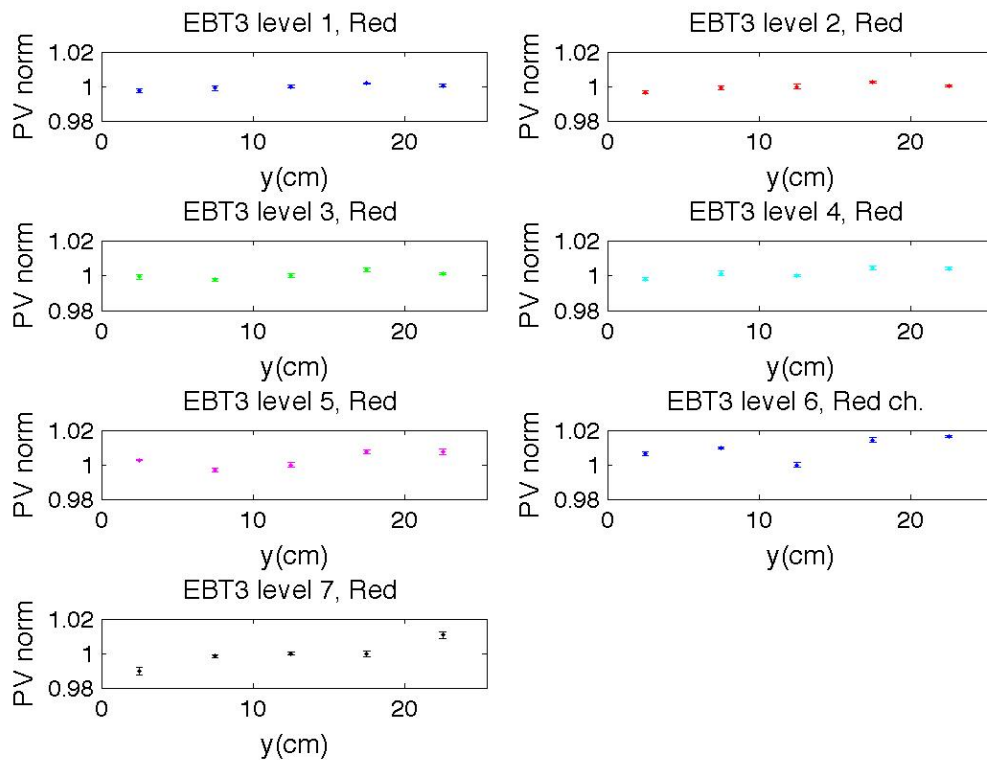
Figure 2.7: Evaluation of mean PV normalized to the central value along the y axis for seven OD levels for the red channel.
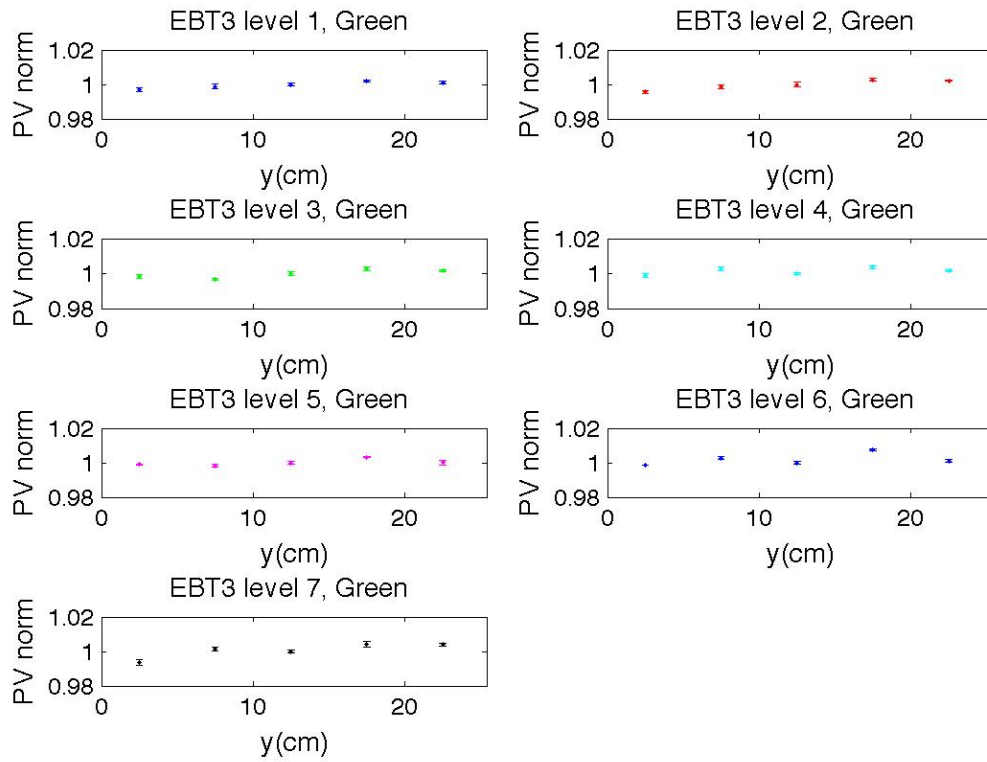
Figure 2.8: Evaluation of mean PV normalized to the central value along the y axis for seven OD levels for the green channel.

Table 2.3: Comparison of the percentage variations of the mean PV along the y axis between the channels and for different OD levels.

OD level	Red	Green	Blue
Level 1	0.2%	0.2%	0.2%
Level 2	0.2%	0.1%	0.5%
Level 3	0.2%	0.3%	0.5%
Level 4	0.3%	0.2%	0.4%
Level 5	0.5%	0.2%	0.5%
Level 6	0.01%	0.04%	0.3%
Level 7	0.01%	0.04%	0.02%
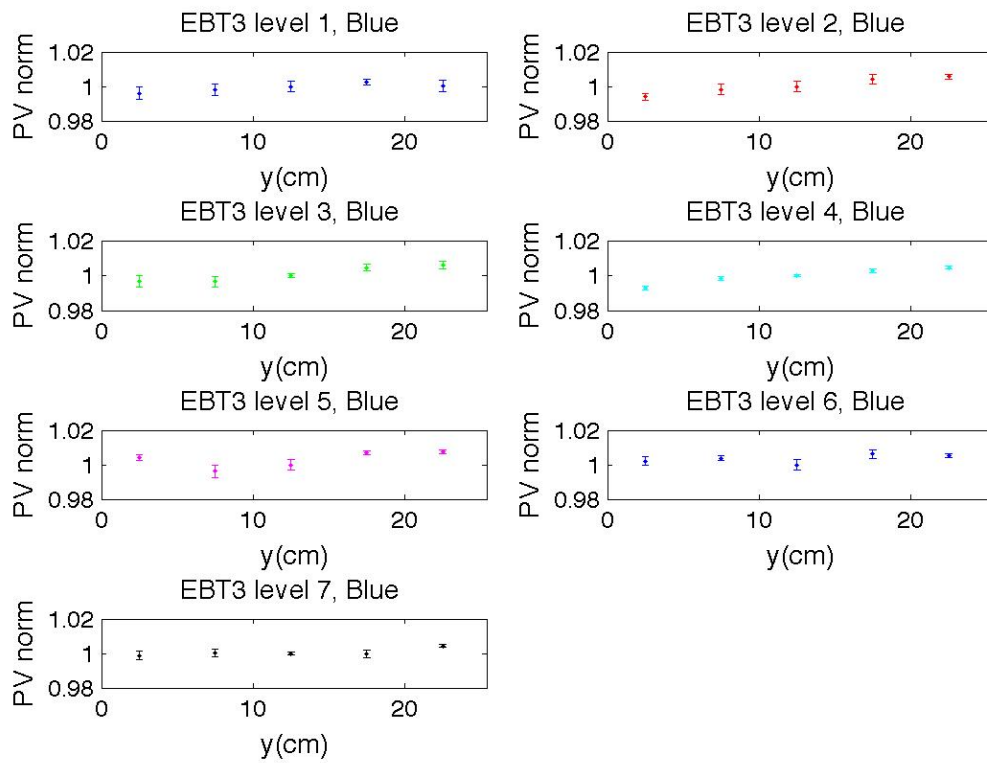
Figure 2.9: Evaluation of mean PV normalized to the central value along the y axis for seven OD levels for the blue channel.

Red channel

Firstly, the measurements in the red channel have been analyzed. The mean PV showed a parabolic trend with a decrease of the readout proportional to the distance from the centre of the scanner. Moreover, the difference in PV from the periphery to the centre was more accentuated when the mean OD increased, reaching for example the 14% less than the signal at the centre when considering OD level 7 at distance of 8 cm from the central axis, which corresponds to an increase in dose of about the 20% . This result is not surprising, in fact several authors have applied parabolic corrections in the direction of the CCD camera for the red channel [13, 24, 47, 49–53, 65], because such deviations would considerably alter the resulting dose map. Therefore, data were firstly fitted with a parabolic curve with three parameters ($y = p_1x^2 + p_2x + p_3$) to verify that the maxima were at the centre of the scanner (see Fig. 2.10 and Table 2.4 for the results), then a two parameters fit with a fixed point of maximum was applied. The x coordinates of the maxima (x_{max}) were computed from the fitted curves and the mean value was obtained from the three highest OD level curves, where the best fits were obtained. The mean x_{max} was 10.2 cm, then the fits were repeated with the curve $y = ax^2 - 2x_{max}a + c$, with the aim of achieving a consistent correction map for those points on the scan bed that are not in the central axis. The results of these fits are showed in Fig. 2.11 and Table 2.5. The fitted parables normalized at the maximum are shown in Fig. 2.12, where it is evident the need of a parabolic correction when the mean OD and the dose increase. From the fitted parameters, a parabolic correction method can be set up. With this purpose, the parameters a and c should be fitted with respect to a quantity that is proportional to the dose, such as the maximum pixel value of the correspondent parabola (see Fig. 2.13 and Table 2.6 for the results of these fits). The idea of the correction is that each PV of a new map will be corrected proportionally both to its value and to its distance from the central axis. This will be done calculating the parameters a and c of the parabola from the PV and then a correction factor k such that $k \cdot PV$ will be equal to the pixel value at the centre of its parabola. More in detail, if x_i is the position of the pixel, PV its scanned pixel value and f its parabola, the correction factor k will be:

$$k = \frac{f(x_{max})}{f(x_i)} = \frac{c - ax_{max}^2}{ax_i^2 - 2x_{max}ax_i + c}. \tag{2.1}$$

k will always be major than 1, in fact the pixel values must be augmented proportionally to their distance from the central position and to the correspondent dose. Therefore, the dose associated with the corrected PV will be lower than the value that it would have had without a parabolic correction. This method makes the approximation of estimating the parabola for each pixel from its PV, but this value is always lower than the real one that would be necessary for a more correct calculation of the parameters, that have been fitted with respect to the pixel value on the central axis. This correction method will be applied to pre-treatment QA dose maps, that will be discussed in one of the next chapters.

Green and blue channels

The mean and the standard deviation of the pixel values extracted from the ROIs located along the x axis have also been analyzed in the green and blue channels for the various OD levels. Here, differently from the red channel, the deviations from the mean PV in the central axis are less pronounced. The plots of the mean PV normalized at the maximum value with respect to the x coordinate are reported in Fig. 2.14 and 2.15 for both channels. As it can be noticed, the average deviations from the maximum value are of 1-2% for the green channel, and of 1-3% for the blue one. Moreover, it is not evident a trend in the measurements but the it is clear that the blue channel is noisier than the others. It cannot be easily and reliably identified a correction method for the deviations from the maximum
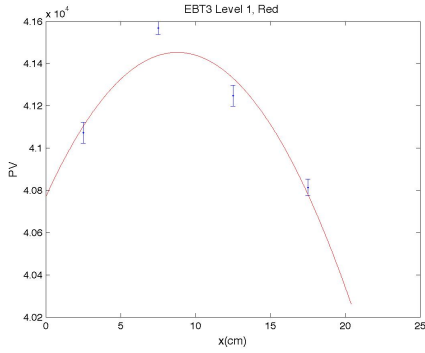
(a) Red PV versus x position, OD level 1.
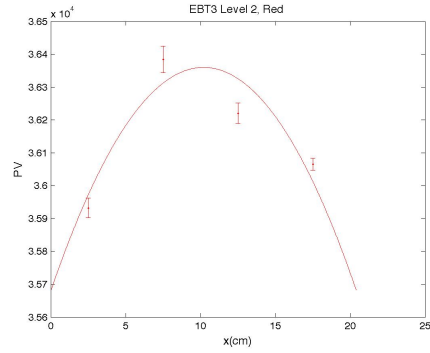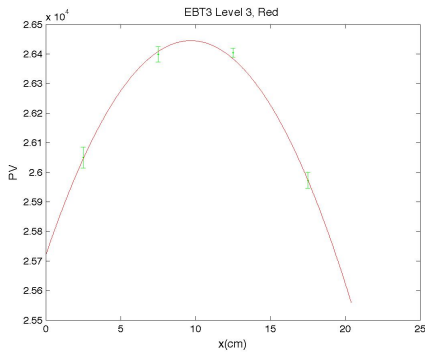
(b) Red PV versus x position, OD level 2.

(c) Red PV versus x position, OD level 3.
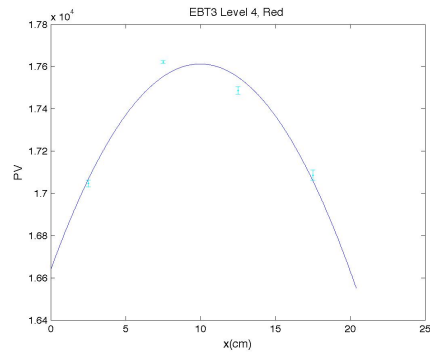
(d) Red PV versus x position, OD level 4.

(e) Red PV versus x position, OD level 5.

(f) Red PV versus x position, OD level 6.

(g) Red PV versus x position, OD level 7.

Figure 2.10: Parabolic fit $(y = p_1 x^2 + p_2 x + p_3)$ of the PV versus the position along the x axis at various OD (level 1 to 7).

Table 2.4: Results of the parabolic fit ($y = p_1x^2 + p_2x + p_3$) of the PV versus the position along the x axis at various OD levels. The estimated values of the coefficients (with 95% confidence bounds), the R-square and the position of the maximum are reported.

OD level	p_1	p_2	p_3	R-square	x_{max} (cm)
Level 1	-8.838	155.4	4.077×10^4	0.9092	8.8
	(-47.34, 29.66)	(-610.5, 921.3)	(3.772×10^4, 4.381×10^4)		
Level 2	-6.523	133.2	3.568×10^4	0.8277	10.2
	(-45.3, 32.25)	(-638.9, 905.2)	(3.241×10^4, 3.894×10^4)		
Level 3	-7.718	149.6	2.572×10^4	0.9977	9.7
	(-12.41, -3.024)	(54.53, 244.7)	(2.536×10^4, 2.608×10^4)		
Level 4	-9.764	194.9	1.664×10^4	0.9596	10.0
	(-35.21, 15.68)	(-327, 716.7)	(1.445×10^4, 1.884×10^4)		
Level 5	-10.49	214.5	1.171×10^4	0.9998	10.2
	(-12.62, -8.358)	(166.7, 262.3)	(1.147×10^4, 1.195×10^4)		
Level 6	-12.42	254.1	6502	0.9994	10.2
	(-16.45, -8.384)	(171.3, 336.8)	(6139, 6864)		
Level 7	-13.68	282.3	4755	0.9999	10.3
	(-15.44, -11.93)	(246.3, 318.3)	(4597, 4913)		

Table 2.5: Results of the parabolic fit ($y = ax^2 - 2x_{max}a + c$) of the PV versus the position along the x axis at various OD levels. The estimated values of the coefficients (with 95% confidence bounds) and the R-square are reported.

OD level	a	c	R-square
Level 1	-7.602	4.06×10^4	0.6009
	(-26.45, 11.25)	(3.918×10^4, 4.204×10^4	
Level 2	-6.527	3.568×10^4	0.8277
	(-15.59, 2.533)	(3.494×10^4, 3.641×10^4	
Level 3	-7.462	2.567×10^4	0.9384
	(-13.28, -1.645)	(2.525×10^4, 2.608×10^4)	
Level 4	-8.981	1.664×10^4	0.9654
	(-14.15, -3.81)	(1.627×10^4, 1.701×10^4)	
Level 5	-10.45	1.172×10^4	0.9997
	(-11.03, -9.87)	(1.167×10^4, 1.176×10^4)	
Level 6	-12.43	6508	0.9992
	(-13.51, -11.35)	(6421, 6596)	
Level 7	-13.77	4780	0.9971
	(-16.03, -11.5)	(4607, 4952)	

Table 2.6: Results of the fits of the parameters a and c of the parabola versus the maximum PV. The theoretical curves, the values of the parameters (with 95% confidence bounds) and of the R-square are reported.

| parameter	fit function	fitted parameters			R-square
a	$f(z) = p_1z^4 + p_2z^3 + p_3z^2 + p_4z + p_5$	p_1	-2.686×10^{-17}	(-4.204×10^{-17}, -1.169×10^{-17})	0.9995
		p_2	2.586×10^{-12}	(1.064×10^{-12}, 4.107×10^{-12})	
		p_3	-9.397×10^{-8}	(-1.464×10^{-7}, -4.149×10^{-8})	
		p_4	0.001693	(0.000983, 0.002403)	
		p_5	-21.2	(-24.18, -18.22)	
c	$f(z) = p_1z^2 + p_2z + p_3$	p_1	-1.349×10^{-6}	(-1.607×10^{-6}, -1.091×10^{-6})	1
		p_2	1.084	(1.067, 1.101)	
		p_3	-1942	(-2229, -1654)	
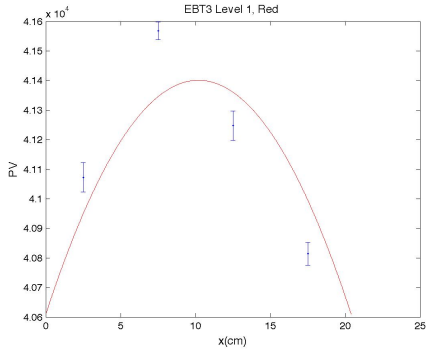
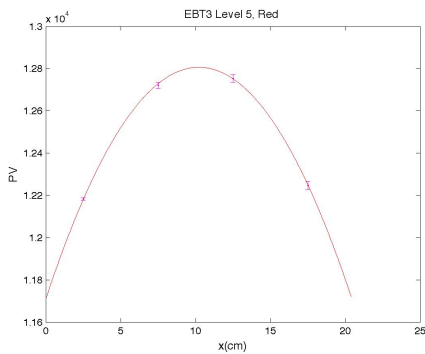**(a)** Red PV versus x position, OD level 1.
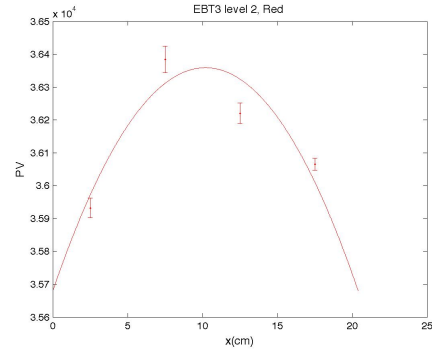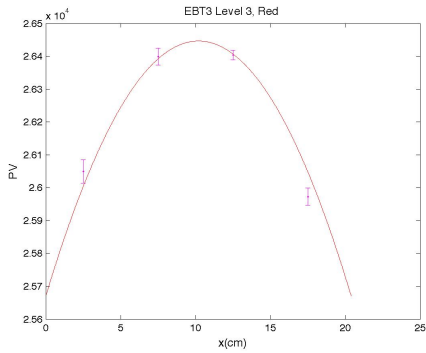
(b) Red PV versus x position, OD level 2.
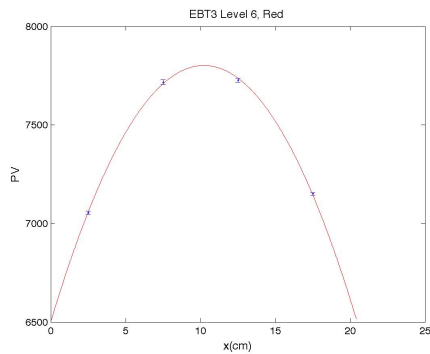

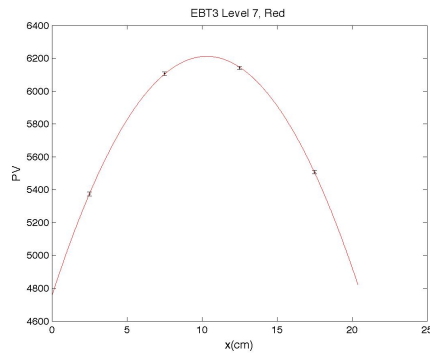**(c)** Red PV versus x position, OD level 3.
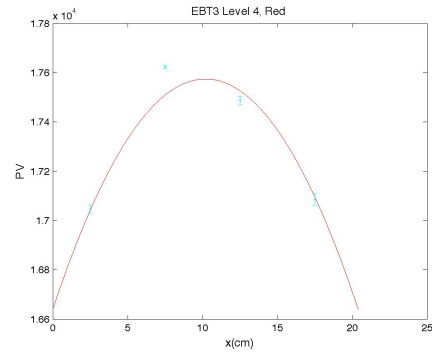
(d) Red PV versus x position, OD level 4.
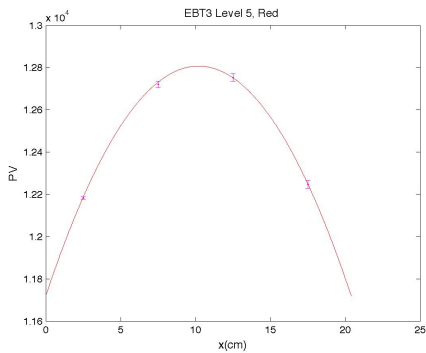
(e) Red PV versus x position, OD level 5.
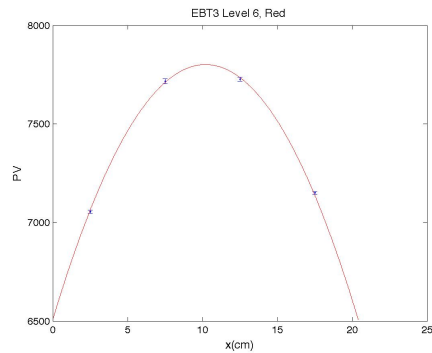
(f) Red PV versus x position, OD level 6.
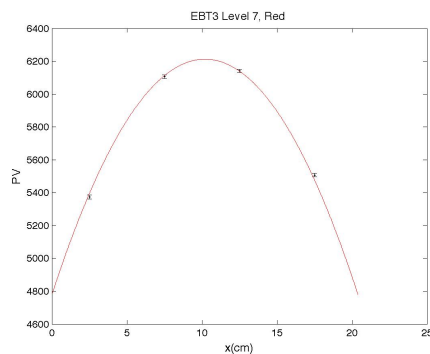
(g) Red PV versus x position, OD level 7.

Figure 2.11: Parabolic fit $(y = ax^2 - 2x_{max}a + c)$ of the PV versus the position along the x axis at various OD levels, having fixed the maximum of the curves equal to the central position of the scanner.

27
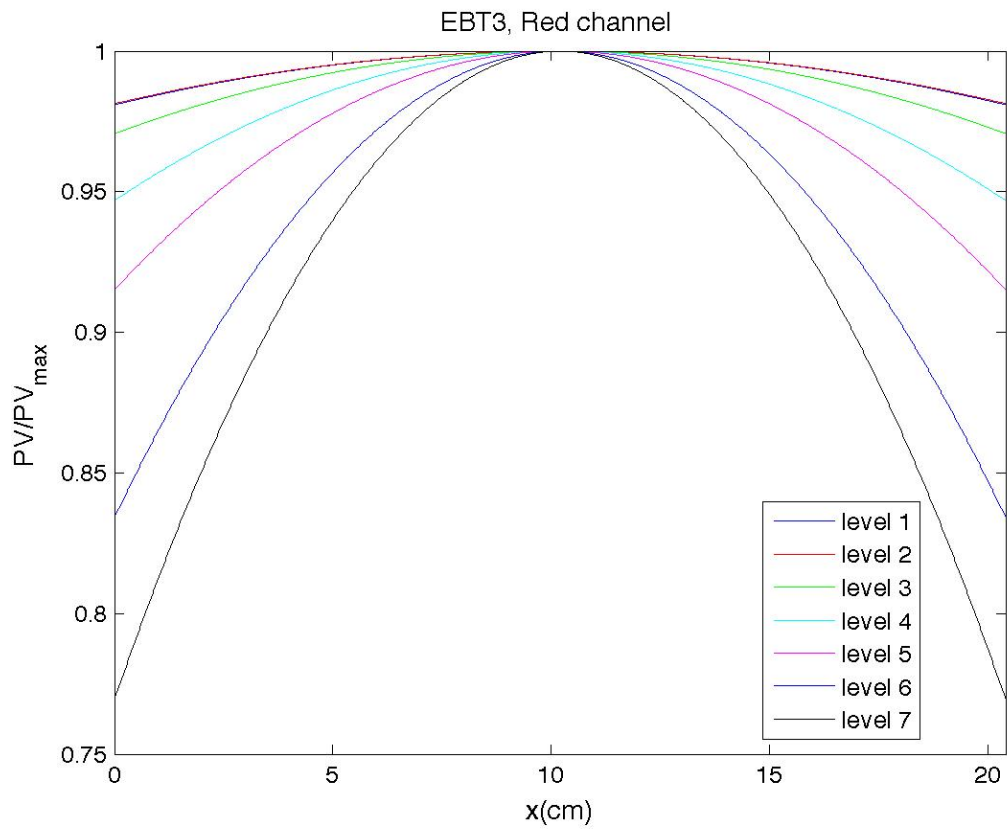
Figure 2.12: Comparison between the parabolic curves fitted with 2 parameters and the point of maximum fixed at the centre of the scanner (x_{max}=10.2 cm). The plotted curves are relative to different OD levels and they are normalized to the maximum PV of each curve.
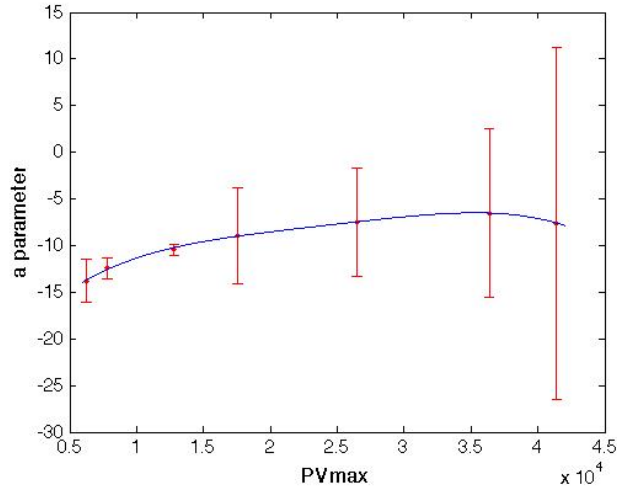
(a) Fit of the parameter a with the function $f(z) = p_1 z^4 + p_2 z^3 + p_3 z^2 + p_4 z + p_5$.
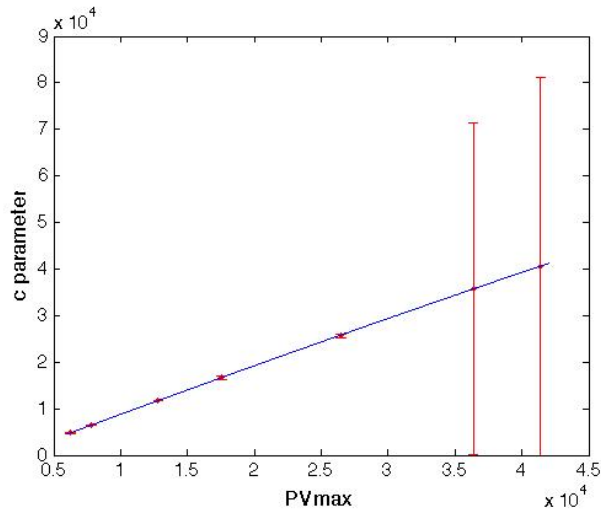
(b) Fit of the parameter c with the function $f(z) = p_1 z^2 + p_2 z + p_3$.

Figure 2.13: Fit of the parameter a and c of the parabola versus the maximum PV at various dose levels.

value. Then, a way to reduce these little variations could be the application of a filter on the pixel values with the aim of reducing the noise.
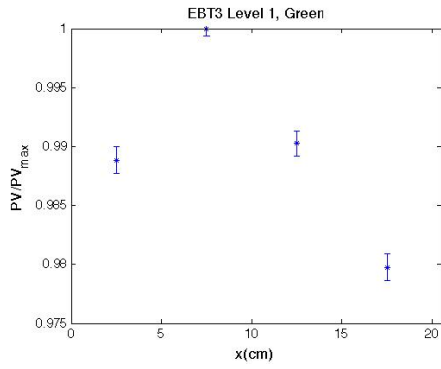
(a) Green PV versus x position, OD level 1.
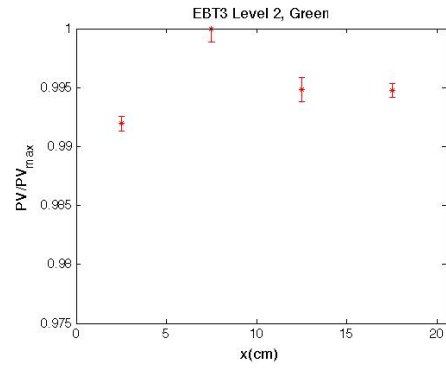
(b) Green PV versus x position, OD level 2.
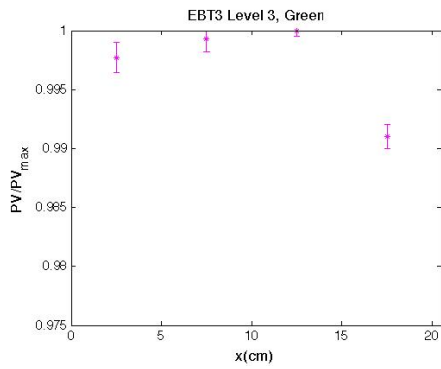
(c) Green PV versus x position, OD level 3.
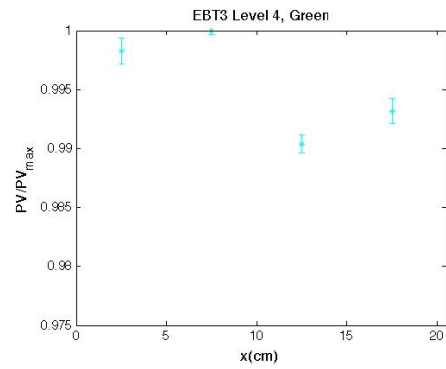
(d) Green PV versus x position, OD level 4.
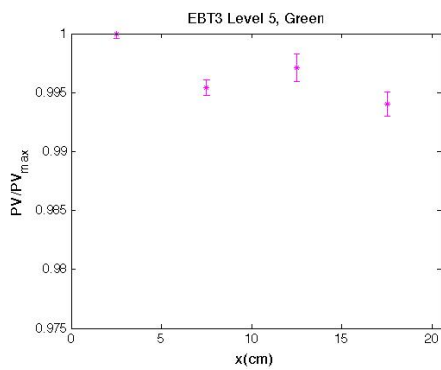
(e) Green PV versus x position, OD level 5.
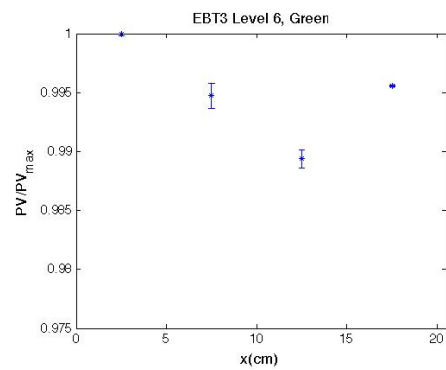
(f) Green PV versus x position, OD level 6.
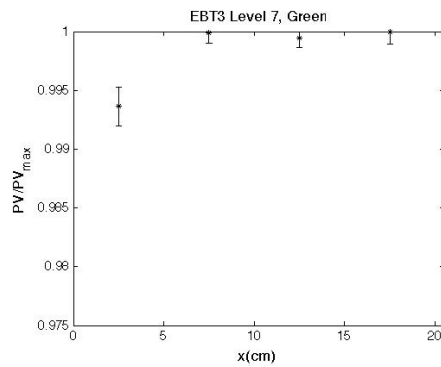
(g) Green PV versus x position, OD level 7.

Figure 2.14: Mean PV in the green channel along the x axis for different OD levels. The PV is normalized to its maximum value.
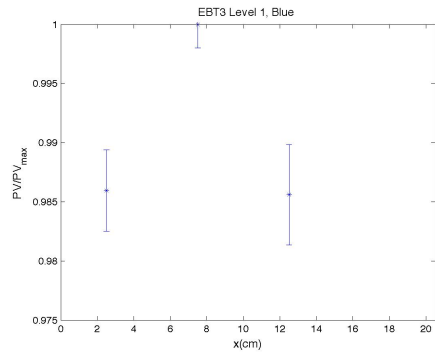
(a) Blue PV versus x position, OD level 1.
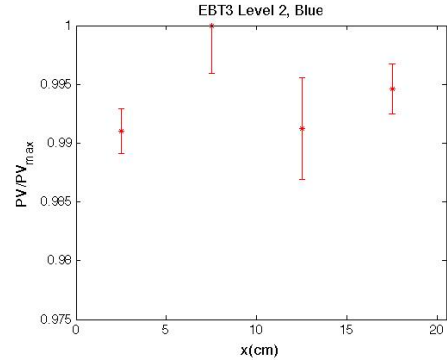
(b) Blue PV versus x position, OD level 2.
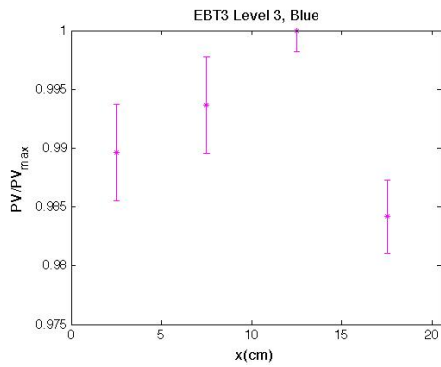
(c) Blue PV versus x position, OD level 3.
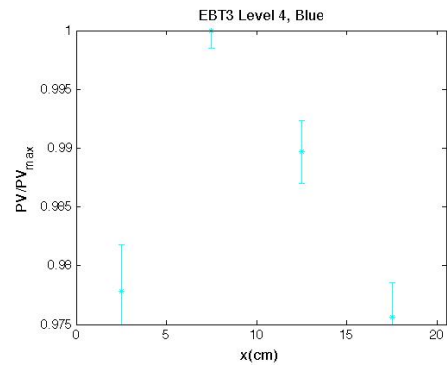
(d) Blue PV versus x position, OD level 4.
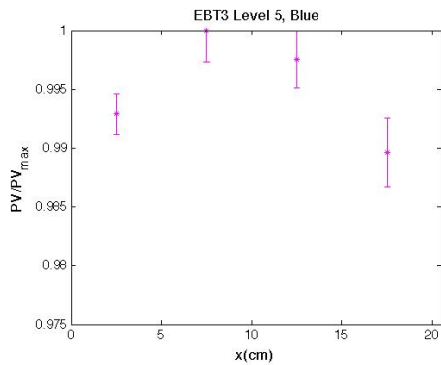
(e) Blue PV versus x position, OD level 5.
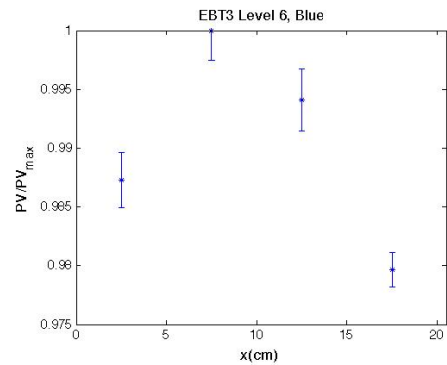
(f) Blue PV versus x position, OD level 6.
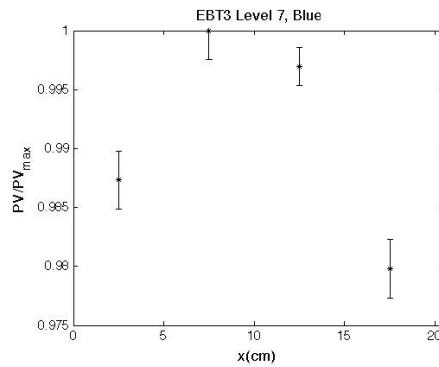
(g) Blue PV versus x position, OD level 7.

Figure 2.15: Mean PV in the blue channel along the x axis for different OD levels. The PV is normalized to its maximum value.

Chapter 3

EBT3 calibration

In this chapter the calibration procedures applied in Plesio-Röntgen therapy and at Linac are described. The necessity of two procedures comes from the reported energy dependence of EBT3 in the KV range [26,27]. Instead, since it has been demonstrated the EBT3 energy independence in the MV range in radiotherapy [25–27], a unique calibration has been used both for Linac and Tomotherapy, which uses a 6 MV Flattened Filter Free (FFF) beam. The first calibration has been set up because of the use of EBT3 for in vivo measurements in patients treated with Plesio-Röntgen therapy. In second place, the EBT3 calibration with a 6 MV photon beam from Linac has been necessary to use and analyze the EBT3 for pre-treatment QA and in vivo measurements both at Linac and in Tomotherapy.

As reported in many studies, the answer to the question of what is the best channel for dosimetry depends on the range of doses to be analyzed: the red channel gives good results in the range of doses between 0 and 5 Gy, between 5 and 50 Gy the green channel is preferred. Nevertheless, in general the red channel is the most used in clinical radiotherapy for EBT3 calibration because it provides the better results in terms of signal to noise ratio (SNR) [5,41,56,57]. For these reasons, the red channel calibration have been made both in Plesio-Röntgen therapy and at the Linac. Furthermore, since the pre-treatment QA dose maps obtained in radiotherapy are often complicated and contain high dose gradients, it has been necessary to set up and try other calibration methods with data acquired at Linac. During the last two decades, many studies have been published on how to extract, combine and use the informations contained in all the three color channels setting up multichannel dosimetry methods [5, 7, 49, 58–61]. Then, it has been decided to use a combination of the green and blue channels with the method proposed by McCaw et al. in 2011 [4] and applied also by Fiandra et al. in 2013 [3]. Moreover, the method for multichannel dosimetry described by Peréz Azorín et al. [5] has been applied.

3.1   Calibration in Plesio-Röntgen therapy

Film pieces of 4x5 cm^2 were cut from the same EBT3 film to perform some preliminary measurements and then the calibration. EBT3 films are known to not perturb an incident radiation beam, but in this case it was decided to investigate if a little attenuation of the beam occurred at the energies used in Plesio-Röntgen therapy (60-100 kV in Plesio therapy and 180-300 kV in Röntgen therapy). A ionizing chamber was placed in a block of solid water to measure the ratio between the dose measured in presence and in absence of the film sample. This attenuation measurement was made both in Plesio and in Röntgen therapy.

In the first case, a plan parallel ionizing chamber (PTW 23342) was located in a block of solid water with a thick of 5 cm below the chamber. A circular applicator with a diameter of 5 cm was employed and the film was fixed on the surface of the phantom, and at direct contact with the applicator and the sensitive part of the chamber (see Fig. 3.1). This

Figure 3.1: Experimental setup used during the preliminary measurements and the calibration in Plesio therapy. For the measurements made before the calibration, the dose was read by a plan parallel ionizing chamber with and without the film piece. When present, the film sample was located at direct contact with the chamber and with a circular applicator (5 cm diameter) during the measurements.

experimental setup was motivated by the fact that in Plesio therapy the MU are calibrated such that 1 MU corresponds to 1 cGy on the skin, and it was decided to irradiate the film under reference conditions. In this case the attenuation percentages were of 1.22% for filter 1 (60 KV) and of 0.7% for filters 2 and 3 (80 and 100 KV respectively).

The attenuation measurement was repeated in Röntgen therapy with 5 cm of solid water below the chamber (Farmer PTW 30013) and 2 cm above, because here the MU are calibrated such that 1 MU corresponds to 1 cGy at 2 cm of depth. The film was placed at 1 cm above the chamber, at 1 cm of depth in the phantom with respect to the radiation source (see Fig. 3.2) and a square applicator with a dimension of 10x10 cm^2 was used. Here, the measurement was made for the filter 9, which corresponds to 300 kV. In this case the attenuation percentage was of 0.04% in presence of the film, confirming that with the increase of radiation energy the film becomes more transparent to the incident beam. However, the attenuation at the energies used in Plesio therapy are low but not negligible, hence they will be taken into account during the calibration measurements. For the sake of clarity, the attenuation measurements are summarized in Table 3.1.

The calibration measurements have been set up for filters 1, 3 and 9, that correspond to 60, 100 and 300 kV. Film pieces of 4x5 cm^2 were irradiated with the same experimental setup described above. The dose in correspondence of the film was measured during the

(a) **(b)**
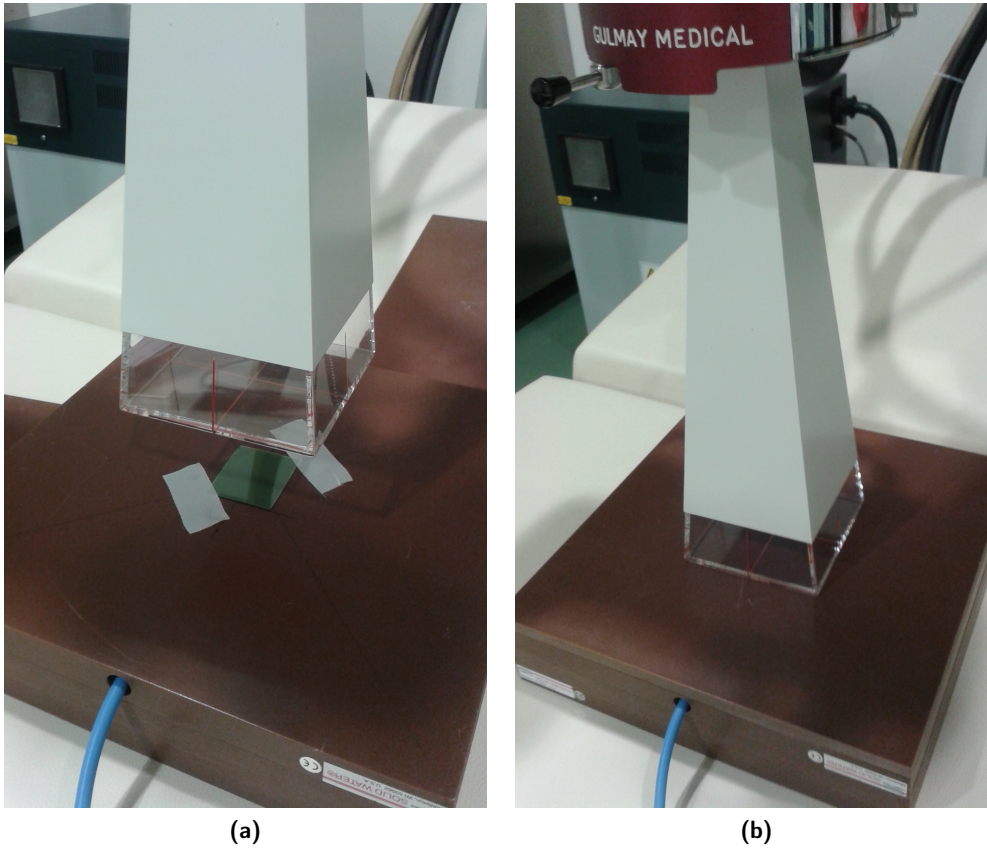
Figure 3.2: Experimental setup used during the preliminary measurements and the calibration in Röntgen therapy. For the measurements made before the calibration, the dose was read by the ionizing chamber with and without the film piece. When present, the film sample was located at 1 cm of distance above the chamber (3.2a) and then covered by another slab of solid water thick 1 cm (3.2b). The square applicator (10 cm dimension) was placed in direct contact with the slabs during the measurements (3.2b).

Table 3.1: Resume of film attenuation measurements in Plesio-Röntgen therapy.

	filter	applicator	k voltage	percentage attenuation
Plesio therapy	1	circular (diameter 5 cm)	60	1.22%
	2	circular (diameter 5 cm)	80	0.7%
	3	circular (diameter 5 cm)	100	0.7%
Röntgen therapy	9	square 10x10 cm^2	300	0.04%

irradiation and reported at the depth of the film. For each calibration, 5 irradiation points at different MU values were chosen (see table 3.2). Each film piece was read two times, one before and one after the irradiation, according to the scanning protocol that has been described previously. Moreover, in this case there was a further reading of the zero-light transmitted image of an opaque sheet, taken after the scans of the unexposed ($PV_{0,unexp}$) and exposed ($PV_{0,exp}$) films, respectively. This variation in the calculation of the net OD, used for example by Fiandra et al. [3], has been implemented in order to investigate the impact of this kind of correction on the estimated dose. According to this approach the net OD in channel k corrected for the black becomes:

$$netOD_{k,corr} = \log_{10} \frac{PV_{unexp,k} - PV_{0,unexp,k}}{PV_{exp,k} - PV_{0,exp,k}} \tag{3.1}$$

Another variant has been introduced: the exposed films were read both at 3 h and at 22 h after the irradiation, with the aim of comparing the readings with different post-irradiation times.

In all the cases taken into account, dose has been fitted with respect to the net OD in the red channel with a parabolic function ($f(x) = p_1 x^2 + p_2 x + p_3$) and the results are summarized in Table 3.3. This choice has been motivated by the fact that the dose distributions prescribed in this type of therapy are much simpler than those performed in Linac and in Tomotherapy. Hence, the use of EBT3 films in Plesio-Röntgen therapy in this work has been limited to the verification of in vivo skin dose. For this application, the simplest and effective calibration in the red channel seems to be sufficient. Instead, the use of more complicated methods to analyse calibration data, which combine more than one channel together, will be motivated in the calculation of the dose matrix in pre-treatment QA.

As can be appreciated from Figs. 3.3b, 3.4b and 3.5b, the differences between fits are more accentuated when the dose decreases. Moreover, the absolute values of the percentage differences between the fitted dose and the expected dose (measured with the ionizing chamber) decrease with the increasing dose. As can be noticed, at doses lower than 150 cGy the percentage error is higher for filter 1 (about 9 %), then it decreases for filters 3 (about 2-3 %) and 9 (0.5-2.5 %). As can be seen from the last column of Table 3.3 the mean percentage errors in the entire range of doses are less than 1 % for filters 3 and 9 and bit higher for filter 1, due to the larger deviation at very low doses in the latter case. The doses commonly prescribed in clinic are 300-500 cGy, hence errors committed in practice are lower 0.5 %. If comparing 3 h and 22 h readings, the results are quite well comparable for the first two filters, but the average percentage error decreases of one order of magnitude for filter 9, leading to prefer the 22 h reading. A final consideration regards the correction for the black reading. In this case results are always better or equal to the not corrected ones, leading to prefer this kind of approach if possible. However, this method requires two additive readings to involve an improvement in the dose estimation less than 0.1%, thus probably the complication introduced does not worth it.

3.2 Calibration in Linac

Film samples were cut (5x5 cm^2) and irradiated with a 6 MV photon beam from a Linac Synergy Agility, Elekta. They were placed at the isocenter of the accelerator at a source-axis distance (SAD) of 100 cm and the field size at the isocenter was of 10x10 cm^2. The films were centered in a block of solid water thick 5 cm over and 5 cm below the film. Moreover, a ionizing chamber (Farmer PTW 30013) placed at a depth of 6 cm was used to measure the dose delivered to the film during the irradiation (see Fig. 3.6). To obtain a calibration curve, the samples were exposed perpendicularly to the radiation beam in a dose range of

Table 3.2: Calibration table in the Plesio-Röntgen calibration. The MU supplied during the calibrations and the dose in correspondence of the film (measured through the ionizing chamber) and corrected for its attenuation are reported.

filter 1	MU	73	146	300	500	1000
	dose (cGy)	78.1	155.8	320.2	533.5	1178.9
filter 3	MU	100	200	300	500	1000
	dose (cGy)	110.0	219.7	329.7	549.6	1099.9
filter 9	MU	70	200	300	500	700
	dose (cGy)	73.5	209.9	315.0	526.1	735.9

Table 3.3: Results of the parabolic fits made in the Plesio-Röntgen calibrations. The estimated parameters (p_1, p_2 and p_3) and the R-square of the fit are reported. Moreover, the last column shows the average percentage errors of the estimated dose with respect to its expected value (measured with the ionizing chamber).

calibration data		p_1	p_2	p_3	R-square	$\delta_{dose}(\%)$
filter 1	3h	7569	-1200	1112	0.9998	1.26
		(2694, 1.244×10^4)	(-4668, 2268)	(542.2, 1682)		
	3h - black	6678	-1007	1082	0.9998	1.23
		(2369, 1.099×10^4)	(-4161, 2148)	(549.5, 1615)		
	22h	7432	-1123	1064	0.9997	1.29
		(2340, 1.252×10^4)	(-4775, 2529)	(458.6, 1669)		
	22h - black	6489	-903.1	1032	0.9998	1.23
		(2241, 1.074×10^4)	(-4043, 2236)	(496.3, 1567)		
filter 3	3h	3973	454.9	975.8	1	0.25
		(2565, 5381)	(-559.4, 1469)	(808.9, 1143)		
	3h - black	3416	526.5	954.2	1	0.22
		(2278, 4555)	(-317.2, 1370)	(811.6, 1097)		
	22h	3889	431.3	941.6	0.9999	0.38
		(1690, 6087)	(-1177, 2040)	(672.5, 1211)		
	22h - black	3295	531.9	916.3	1	0.34
		(1561, 5029)	(-775, 1839)	(691.5, 1141)		
filter 9	3h	2913	932.6	923.6	0.9999	0.37
		(181.4, 5645)	(-697.6, 2563)	(694, 1153)		
	3h - black	2490	953.8	908.5	1	0.32
		(359.1, 4622)	(-350.4, 2258)	(720.2, 1097)		
	22h	1892	1472	823.3	1	0.07
		(1153, 2631)	(1023, 1921)	(758.7, 887.9)		
	22h - black	1555	1458	807.2	1	0.05
		(887.9, 2221)	(1042, 1875)	(745.7, 868.7)		

(a)

(b)

Figure 3.3: Calibration curves (3.3a) and percentage errors (3.3b) in the red channel for filter 1 in Plesio therapy.
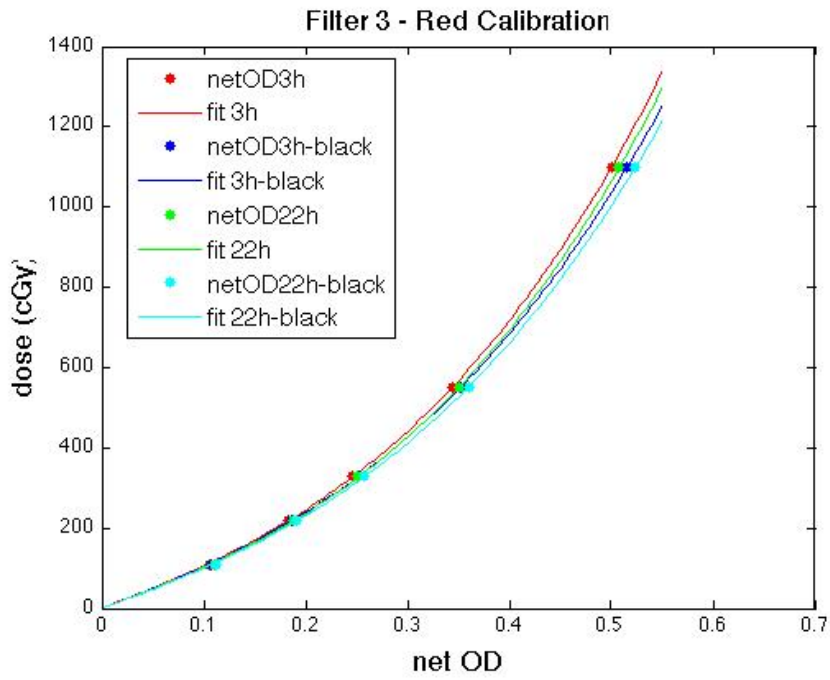
(a)
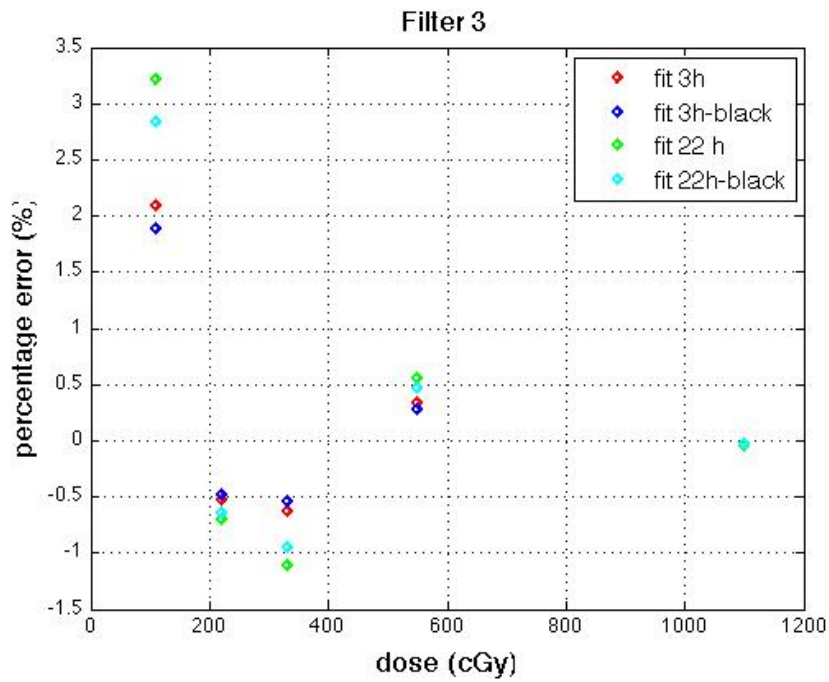
(b)

Figure 3.4: Calibration curves (3.4a) and percentage errors (3.4b) in the red channel for filter 3 (100 kV) in Plesio therapy.
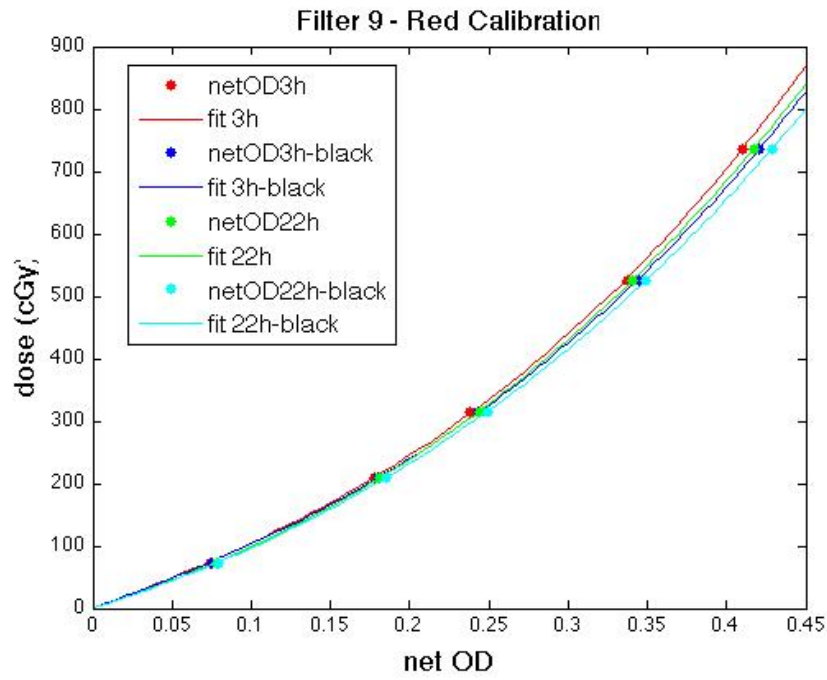
(a)
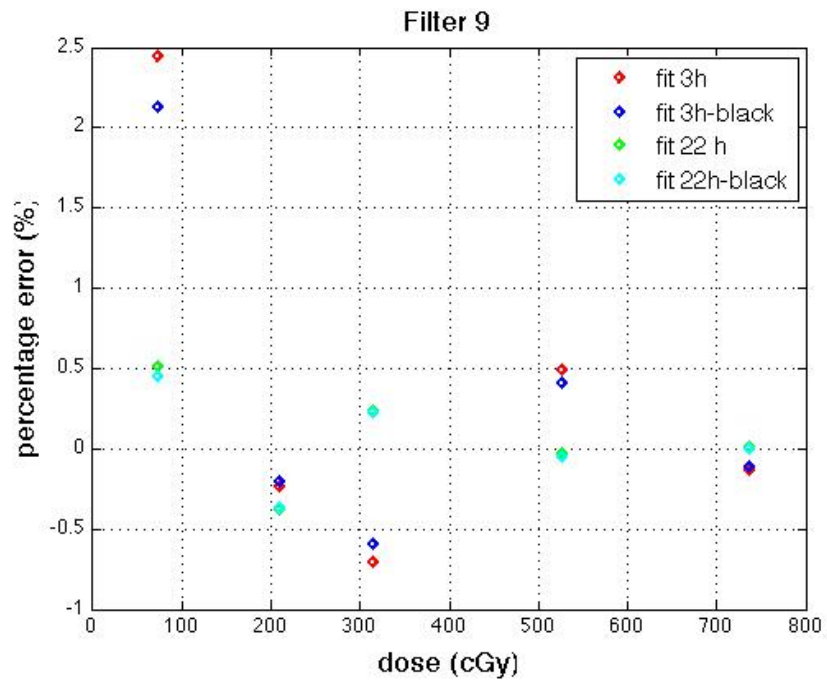
(b)

Figure 3.5: Calibration curves (3.5a) and percentage errors (3.5b) in the red channel for filter 9 (300 kV) in Röntgen therapy.
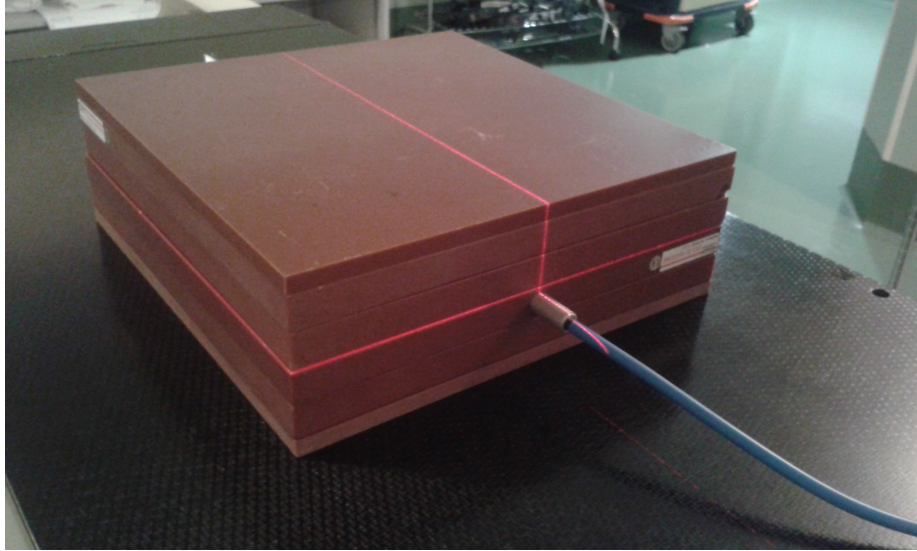
Figure 3.6: Experimental setup used during the calibration measurements in Linac. The film sample is located at the isocenter of the accelerator with 5 cm of solid water above and below. A ionizing chamber is placed at 1 cm below the film.

Table 3.4: Calibration table in Linac calibration. The MU supplied during calibration measurements and the dose in correspondence of the film are reported.

MU	0	10	20	30	50	80	130	210	340	550	1000	1450	2350	3800
dose (cGy)	0.00	9.63	19.25	28.88	48.41	77.29	125.70	202.99	328.98	532.26	968.83	1402.56	2276.26	3683.92

0-40 Gy with 14 values. The absolute doses were determined according to the AAPM TG-51 protocol [63] and are summarized in Table 3.4 .

The film pieces were scanned before and after the irradiation, in order to have an offset measurement to correct for film inhomogeneities. The post-irradiation reading was made after 22 h from the exposure, in order to guarantee a stabilization of the film reading output. They were read in the center of the scanner to avoid lateral artifacts of the scanner. Moreover, with the aim of reducing the noise, each scan was repeated for three times and readings were averaged at the end, obtaining a mean PV for each exposed film (PV_{exp}) and an average value for the correspondent offset (PV_{unexp}). The ROI analyzed was a 5x5 mm^2 square placed in the center of the film piece, obtaining for each film piece and for each channel the mean signals exposed and unexposed. Then, for each channel k the net OD has been estimated:

$$netOD_k = \log_{10} \frac{PV_{unexp,k}}{PV_{exp,k}} \tag{3.2}$$

3.2.1 Red channel calibration

The dose points used for the calibration have been fitted with respect to the net OD estimated in the red channel. With the aim of obtaining the best agreement between the fitted points and the experimental data, a number of functions have been tried. These were polynomial, exponential, and power functions. Finally, the best compromise was to fit the experimental points with two functions: a quadratic polynomial at low doses (<200 cGy), and a fourth degree polynomial ad higher doses (≥200 cGy). The zero degree parameter of the low dose curve was set equal to zero in order to have null dose when the net OD is zero.

$$y = \begin{cases} a_1 x^2 + a_2 x, & \text{x<200 cGy,} \\ b_1 x^4 + b_2 x^3 + b_3 x^2 + b_4 x + b_5, & \text{x≥200 cGy.} \end{cases} \tag{3.3}$$

Table 3.5: Results of the fit in the red channel calibration.

	fit function	fitted parameters			R-square
low doses (<200cGy)	$f(x) = a_1 x^2 + a_2 x$	a_1	979.1	(113.2, 1845)	0.9926
		a_2	901.4	(697.7, 1105)	
high doses (≥ 200cGy)	$f(x) = b_1 x^4 + b_2 x^3 + b_3 x^2 + b_4 x + b_5$	b_1	3.818×10^4	(5915, 7.044×10^4)	0.9994
		b_2	-5.655×10^4	(-1.171×10^4, 4048)	
		b_3	3.264×10^4	(-6302, 7.158e+04)	
		b_4	-5975	(-1.581×10^4, 3858)	
		b_5	473	(-320, 1266)	

Figure 3.7: Fit of the dose with respect to the net OD in the red channel. The experimental points are represented in red, the low dose curve in pink ($a_1 x^2 + a_2 x$), the high dose fit in green ($b_1 x^4 + b_2 x^3 + b_3 x^2 + b_4 x + b_5$) and the intermediate region average between the two curves in black.

Furthermore, in the the transition region between the two functions, the curves were substituted by their means (in the region 120-330 cGy), as can be seen in Fig. 3.7. The results of the fits have been summarized in Table 3.6. Moreover, the percentage differences between experimental data and fitted points are reported in Fig. 3.8. As can be seen, the percentage error for doses lower than 50 cGy is not negligible, having values sometimes much higher than 10% and on average of 12%. Moreover, it decreases for higher doses, reaching an average value of 0.2% for doses higher than 50 cGy. If considering the range of doses 0-200 cGy, the mean deviation is equal to 9%, and 0.48% above 200 cGy.

3.2.2 Green-blue channels calibration

The dose points used for the calibration have been fitted with respect to the net OD estimated in the green/blue color channel. The approach used by Fiandra et al. in 2013 [3, 4] has been employed considering the PV of the exposed and the unexposed images. This method uses the blue channel to measure marker-dye corrections from unexposed film, and the green channel to obtain desired dose values. The net OD measured both in the green and blue channels is used with the aim of minimize response differences caused by anomalies by means of the marker-dye correction. The optical density in the green and blue color

Table 3.6: Results of the fit in the red channel calibration.

	fit function	fitted parameters			R-square
low doses ($<$200cGy)	$f(x) = a_1x^2 + a_2x$	a_1	979.1	(113.2, 1845)	0.9926
		a_2	901.4	(697.7, 1105)	
high doses ($\geq$200cGy)	$f(x) = b_1x^4 + b_2x^3 + b_3x^2 + b_4x + b_5$	b_1	3.818×10^4	$(5915, 7.044 \times10^4)$	0.9994
		b_2	-5.655×10^4	$(-1.171\times10^4, 4048)$	
		b_3	3.264×10^4	(-6302, 7.158e+04)	
		b_4	-5975	$(-1.581\times10^4, 3858)$	
		b_5	473	(-320, 1266)	

Figure 3.8: Percentage differences between fitted points and reference dose values (measured with the ionizing chamber) in the red channel calibration.
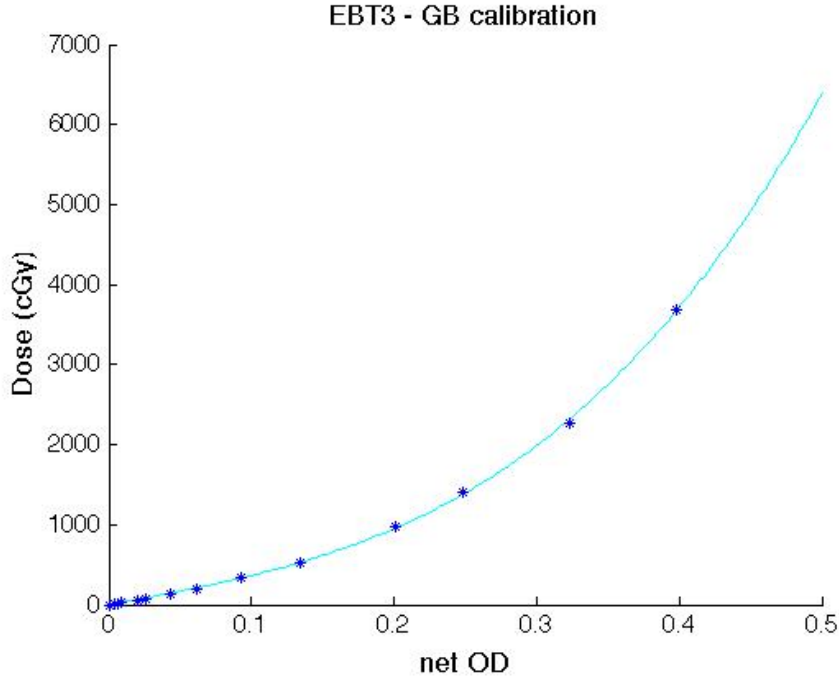
Figure 3.9: Fit of the dose with respect to the net OD in the green-blue channels. The experimental points are represented in blue and the fitted curve in cyan ($ax + bx^n$).

channels are firstly converted in OD both in the exposed and unexposed images:

$$OD_{gb} = \log_{10} \frac{2^{16}}{\frac{PV_{green}}{PV_{blue}}} = \log_{10} \frac{2^{16}}{PV_{gb}}, \tag{3.4}$$

where the PV are averaged in a ROI of 5x5 mm^2 placed at the centre of the film piece for each point of dose and for each color channel. The net OD mesured in the green/blue color channel was defined by McCaw et al. [4]:

$$netOD_{gb} = OD_{exp,gb} - OD_{unexp,gb} = \log_{10} \frac{PV_{unexp,gb}}{PV_{exp,gb}}. \tag{3.5}$$

Then, the function $ax + bx^n$ was fit to dose as a function of the netOD$_{gb}$ (see Fig. 3.9 and Table 3.7). As can be seen in Fig. 3.10 the percentage differences between fitted values and reference dose values (measured with the ionizing chamber during the irradiation) are on average 22% under 200 cGy, reaching differences of about 50% for very low doses. Instead, for doses higher than 200 cGy the percentage errors are on average 0.4%. If compared with the errors committed in the red channel fit, the results in the green/blue calibration are worse for doses lower than 200 cGy (on average 22% versus 9%). However the mean deviations become comparable above 200 cGy: 0.48% for the red fit and 0.43% for the green/blue color channels. It is evident that both the fits are not perfect, therefore a reasonable approach to calculate the final dose from an OD map could be to average the two calibration curves. In the pre-treatment QA the dose calculated from the red and the green/blue calibrations will be compared with the dose computed by a mean of the two calibrations, hence taking into account the informations from all the three color channels.

3.2.3 Multichannel film dosimetry

Recently, a number of studies have been carried out on multichannel dosimetry methods using all the color channels to calculate the final dose matrix [5,7,49,58–62]. As reported in

Table 3.7: Results of the fit in the green-blue channels calibration.

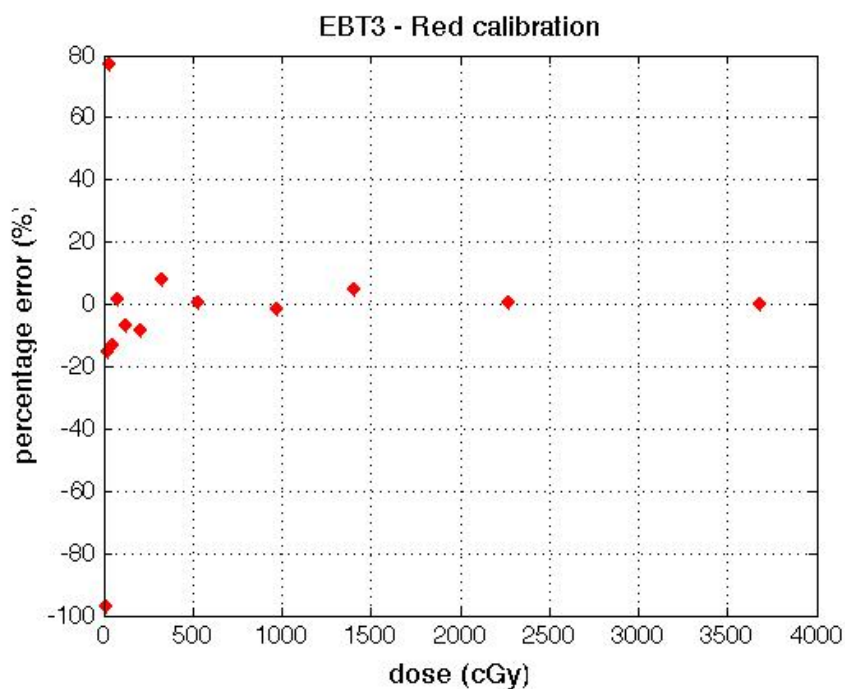| fit function	fitted parameters			R-square
$f(x) = ax + bx^n$	a	3293	(2991, 3596)	0.9998
	b	3.93×10^4	$(3.289 \times 10^4, 4.572 \times 10^4)$	
	n	3.05	(2.833, 3.267)	
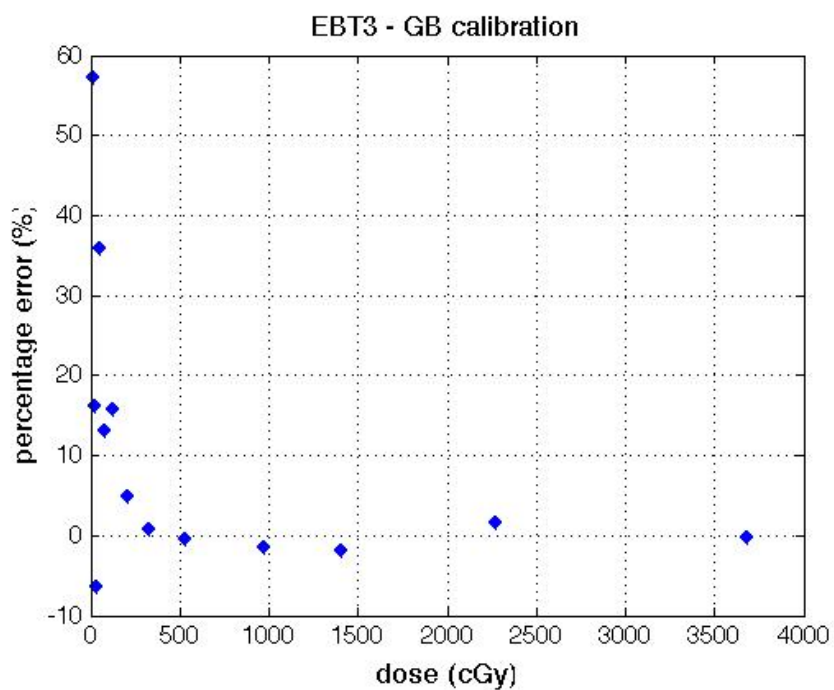
Figure 3.10: Percentage differences between fitted points and reference dose values (measured with the ionizing chamber) in the green-blue channels calibration.

Table 3.8: Results of the fits in the multichannel calibration. For each channel the fitted curve was: $D = \frac{p_{1,k} - p_{2,k}X_k}{X_k - p_{3,k}}$.

color channel	fitted parameters			R-square
	p_1	p_2	p_3	
red	1.391×10^7	325.3	3039	0.9998
	$(1.332 \times 10^7,\ 1.449 \times 10^7)$	(299, 351.6)	(2903, 3176)	
green	2.785×10^7	671.3	-1108	0.9997
	$(2.649 \times 10^7,\ 2.922 \times 10^7)$	(624.5, 718.1)	(-1453, -763)	
blue	3.783×10^7	1528	1310	0.9992
	$(3.408 \times 10^7,\ 4.159 \times 10^7)$	(1358, 1699)	(595.7, 2025)	

literature, the application of a multichannel optimization method strongly improves the results in patient specific QA in terms of gamma passing rates. This conclusion has been drawn both for the Linac plans and the TomoTherapy irradiations, and the standard deviations over repeated measurements indicate a larger variability when the single channel dosimetry is employed, thus suggesting that the multichannel approach also impacts on measurement repeatability [7]. Among the methods employed, the procedure developed by Pérez Azorín et al. [5], which refines the Mayer et al. method [61] and explicitly takes the information of unexposed film into account, shows some improvements compared to other approaches. Very good results have also been obtained by Mendez et al. [58], who developed a generalized channel-independent perturbation framework. Up to now, the method implemented by Micke and Lewis [59, 60] is the only one commercially accessible (FilmQA^{TM}Pro software, Ashland Inc., Wayne, N.J. and at www.filmqapro.com). For this reason it is spreading in many routine patient specific QA activities, but it has the disadvantage of being not freely available. Hence, it has been decided to implement the method introduced by Pérez Azorín et al. [5], motivated by its great results in terms of gamma passing rates and its improvements compared with other multichannel methods. Moreover, the clarity and completeness of the description of the method have allowed the writing of the correspondent Matlab code (The MathWorks, Inc.).

The calibration data were fitted using the following calibration curve:

$$D = \frac{p_{1,k} - p_{2,k}X_k}{X_k - p_{3,k}}, \tag{3.6}$$

where X_k is the pixel value for each color channel (k=R, G, B), D is the dose, and $p_{i,k}$ are the fitting parameters. This function has the advantage of being analytically invertible that entails a considerable numerical advantage in this method. To perform the calibration, X_k was evaluated from the exposed films in a central ROI of 5x5 mm^2, the same that has been used for the calibration in the red and in the green/blue channels. The results of the three fits are shown in Fig. 3.11 and in Table 3.8.

According to this multichannel dosimetry method, ideally, the dose measurement for each channel should be the same. Nevertheless, due to different response of the color channel to inhomogeneities and uncertainties in the calibration curves itself, there are differences in the dose response between the three channels. Following this reasonable assumption, the scanned dose could be expressed as a function of the real dose applying a first order Taylor expansion from the expected dose:

$$D_k^{scan}(i,j) = D(i,j) + \alpha_k(i,j)\Delta X_k(i,j), \tag{3.7}$$

where i and j are the coordinate in the dose matrix, D_k^{scan} are the scanned dose matrices
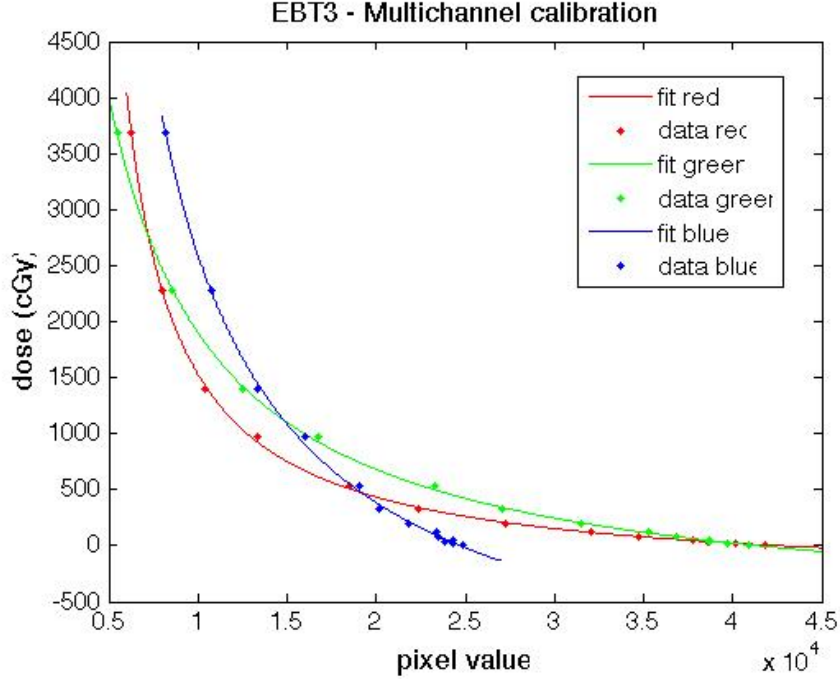
Figure 3.11: Fitted curves in the multichannel calibration. The fitted curve is represented with a continuous line superimposed to experimental points.

for each channel k and the α_k terms are defined as:

$$\alpha_k(i,j) = \frac{\partial D}{\partial X_k}\bigg|_{D(i,j)}(i,j). \tag{3.8}$$

These terms can be analytically calculated from Eq. 3.6 and evaluated in the expected dose D(i,j), hence obtaining:

$$\alpha_k(i,j) = \frac{(p_{2,k} + D(i,j))^2}{p_{2,k}p_{3,k} - p_{1,k}}. \tag{3.9}$$

The perturbation term ΔX_k can be expressed as the sum of two terms, one of which depends on the color channel (β_k) and the other is independent on the color channel and it takes into account the perturbation sources that are common to the three channels (Δ):

$$\Delta X_k(i,j) = \Delta(i,j) - \beta_k(i,j). \tag{3.10}$$

In the above equation the minus sign is used for convenience. In this method it is assumed that the β_k correction term is independent on dose, hence it does not depend on the pixel value and can be calculated from the unexposed film. Using Eq. 3.7 and 3.10, the final expression of the expected dose becomes:

$$D(i,j) = D_k^{scan}(i,j) + \alpha_k(i,j)\beta_k(i,j) - \alpha_k(i,j)\Delta(i,j) \tag{3.11}$$

From now on, the pixel coordinate (i,j) will be implied in the equations. Ideally, Eq. 3.11 gives the real dose using any of the color channels if the perturbation terms are known. The aim of the method is to estimate the dose by minimizing the difference between right- and left-hand sides of the above equation using the least square method, then to find the values of D and Δ which minimize the functional $\Phi(D, \Delta)$:

$$\Phi(D, \Delta) = \sum_{k=1}^{3}[D_k^{scan} + \alpha_k\beta_k - \alpha_k\Delta - D]^2. \tag{3.12}$$

47

Deriving this functional with respect to the variables D and Δ and equating the derivatives to zero, there will be a pair of nonlinear equation to solve:

$$
\begin{aligned}
F_1(D, \Delta) = \frac{\partial \Phi(D, \Delta)}{\partial D} = & \left(3 - \sum_{k=1}^{3} \beta_k \frac{\partial \alpha_k}{\partial D} \right) D \\
& + \sum_{k=1}^{3} \left(\alpha_k - D_k^{scan} \frac{\partial \alpha_k}{\partial D} - 2\alpha_k \beta_k \frac{\partial \alpha_k}{\partial D} \right) \Delta \\
& + D\Delta \left(\sum_{k=1}^{3} \frac{\partial \alpha_k}{\partial D} \right) + \Delta^2 \left(\sum_{k=1}^{3} \alpha_k \frac{\partial \alpha_k}{\partial D} \right) \\
& + \sum_{k=1}^{3} (D_k^{scan} + \alpha_k \beta_k) \left(\beta_k \frac{\partial \alpha_k}{\partial D} - 1 \right) = 0,
\end{aligned}
$$

(3.13)

$$
\begin{aligned}
F_2(D, \Delta) = \frac{\partial \Phi(D, \Delta)}{\partial \Delta} = & D \left(\sum_{k=1}^{3} \alpha_k \right) + \Delta \left(\sum_{k=1}^{3} \alpha_k^2 \right) \\
& - \left(\sum_{k=1}^{3} \alpha_k (D_k^{scan} + \alpha_k \beta_k) \right) = 0.
\end{aligned}
$$

(3.14)

The terms α_k and β_k need to be estimated in order to solve the system of equations.
The β_k terms are assumed to be independent on dose, hence they can be calculated at the beginning from the unexposed films and they will remain constant for the rest of the multichannel analysis. To calculate the β_k terms, an iterative scheme is used. Since the dose for the unexposed films must be zero, the Eq. 3.11 can be solved imposing D=0 to calculate β_k for each channel at the iteration n:

$$
\beta_k^{(n)} = \begin{cases} -\frac{D_{k,D=0}^{scan}}{\alpha_{k,D=0}} + \Delta_{D=0}^{(n-1)} & (n>0), \\ \\ -\frac{D_{k,D=0}^{scan}}{\alpha_{k,D=0}} & (n=0). \end{cases}
$$

(3.15)

The starting values for the first iteration (n=0) assume $\Delta_{D=0}^{(0)}$ equal to zero and at each new step this term is calculated through equations 3.13 and 3.14, substituting D=0 and where:

$$
\alpha_{k,D=0} = \frac{p_{2,k}^2}{p_{2,k} p_{3,k} - p_{1,k}}.
$$

(3.16)

The iterations proceede until convergence, i.e. up to the difference between β_k^n and $\beta_k^{(n-1)}$ becomes lower than a prefixed value.
The system of nonlinear equations (3.13 and 3.14) can be efficiently solved iteratively using the Newton algorithm [64]. In order to begin the procedure, an initialization at the iteration m=0 of D, Δ and of the α_k terms is needed. These terms are calculated in the approximation in which α_k is independent on dose, hence it is $\alpha_k^{(m=0)} = \alpha_{k,D=0}$, and its derivative with respect to D is null. In this condition the Eq. 3.13 and 3.14 become:

$$
D^{(m=0)} = \frac{\sum_{k=1}^{3} D_k'^{scan} - W \cdot (\sum_{k=1}^{3} \alpha_{k,D=0} D_k'^{scan})}{3 - W \cdot \sum_{k=1}^{3} \alpha_{k,D=0}},
$$

(3.17)

$$
\Delta^{(m=0)} = \frac{\sum_{k=1}^{3} \alpha_{k,D=0} (D_k'^{scan} - D^{(m=0)})}{\sum_{k=1}^{3} \alpha_{k,D=0}^2},
$$

(3.18)

where in the above equations $D_k^{'scan}$ and W are defined:

$$D_k^{'scan} = D_k^{scan} + \alpha_{k,D=0}\beta_k, \tag{3.19}$$

$$W = \frac{\sum_{k=1}^{3} \alpha_{k,D=0}}{\sum_{k=1}^{3} \alpha_{k,D=0}^2}. \tag{3.20}$$

As can be verified, the approach employed by Mayer et al. [61] can be obtained from the equations above by neglecting the β_k correction terms.

Having obtained the initial values of the parameters α_k and β_k and of D and Δ, the equations 3.13 and 3.14 can be solved using the following iterations until convergence:

$$\begin{pmatrix} D_m \\ \Delta_m \end{pmatrix} = \begin{pmatrix} D_{m-1} \\ \Delta_{m-1} \end{pmatrix} + \begin{pmatrix} \frac{\partial F_1}{\partial D} & \frac{\partial F_1}{\partial \Delta} \\ \frac{\partial F_2}{\partial D} & \frac{\partial F_2}{\partial \Delta} \end{pmatrix}^{-1} \cdot \begin{pmatrix} F_1(D_{m-1}, \Delta_{m-1}) \\ F_2(D_{m-1}, \Delta_{m-1}) \end{pmatrix}. \tag{3.21}$$

The second order derivatives of $\Phi(D, \Delta)$ can be calculated from the Eq. 3.13 and 3.14:

$$\begin{aligned}
\frac{\partial F_1}{\partial D} = & -D \sum_{k=1}^{3} \beta_k \frac{\partial^2 \alpha_k}{\partial D^2} \\
& + \Delta \sum_{k=1}^{3} \left\{ 2\frac{\partial \alpha_k}{\partial D} - 2\beta_k \left[\left(\frac{\partial \alpha_k}{\partial D}\right)^2 + \alpha_k \frac{\partial^2 \alpha_k}{\partial D^2} \right] - D_k^{scan} \frac{\partial^2 \alpha_k}{\partial D^2} \right\} \\
& + D\Delta \sum_{k=1}^{3} \frac{\partial^2 \alpha_k}{\partial D^2} + \Delta^2 \sum_{k=1}^{3} \left\{ \left(\frac{\partial \alpha_k}{\partial D}\right)^2 + \alpha_k \frac{\partial^2 \alpha_k}{\partial D^2} \right\} + 3 \\
& + \sum_{k=1}^{3} \left\{ \beta_k \left[D_k^{scan} \frac{\partial^2 \alpha_k}{\partial D^2} - 2\frac{\partial \alpha_k}{\partial D} \right] + \beta_k^2 \left[\left(\frac{\partial \alpha_k}{\partial D}\right)^2 + \alpha_k \frac{\partial^2 \alpha_k}{\partial D^2} \right] \right\},
\end{aligned} \tag{3.22}$$

$$\frac{\partial F_2}{\partial \Delta} = D \sum_{k=1}^{3} \frac{\partial \alpha_k}{\partial D} + 2\Delta \sum_{k=1}^{3} \alpha_k \frac{\partial \alpha_k}{\partial D} + \sum_{k=1}^{3} \left\{ \alpha_k \left(1 - 2\beta_k \frac{\partial \alpha_k}{\partial D} \right) - D_k^{scan} \frac{\partial \alpha_k}{\partial D} \right\}, \tag{3.23}$$

$$\frac{\partial F_2}{\partial D} = \frac{\partial F_1}{\partial \Delta}, \tag{3.24}$$

$$\frac{\partial F_2}{\partial \Delta} = \sum_{k=1}^{3} \alpha_k^2, \tag{3.25}$$

where $\frac{\partial \alpha_k}{\partial D}$ and $\frac{\partial^2 \alpha_k}{\partial D^2}$ can be easily calculated from Eq. 3.9:

$$\frac{\partial \alpha_k}{\partial D} = \frac{2(p_{1,k} + D)}{p_{2,k}p_{3,k} - p_{1,k}}, \tag{3.26}$$

$$\frac{\partial^2 \alpha_k}{\partial D^2} = \frac{2}{p_{2,k}p_{3,k} - p_{1,k}}. \tag{3.27}$$

It must be noticed that this method corrects the light scattering phenomena through β_k terms, which describe the inhomogeneities of film-scanner assembly, but it consider that these channel dependent inhomogeneities are independent on dose, which in principle is not true [35, 51, 65]. Therefore, the dose matrix computed through the multichannel method needs a parabolic correction as well as it is necessary when the red channel calibration is employed. In fact, as it has been explained in the previous chapter, the need of a correction for the light scattering phenomena becomes more important when the dose increase.

Chapter 4

Pre-Treatment QA

In this chapter, with the purpose of validating GafChromic film dosimetry method and understanding which of the EBT3 calibration approaches better responded to the range of doses commonly used in radiotherapy, some films irradiated at Linac with different standard fields have been compared with data measured through PTW 2D-Array 729 (http://www.ptw.de/3099.html) at Linac. Moreover, pre-treatment QA measurements have been performed with EBT3, and absolute dose maps have been compared with TPS calculations using γ-analysis [6], applied through VeriSoft Patient Plan Verification Software (http://www.ptw.de/2406.html). Furthermore, the scanner parabolic correction was implemented, tested through comparison between array measurements and film analysis, then implemented in pre-treatment QA if necessary.

The film dosimetry method was developed and applied using a homemade Matlab code (http://it.mathworks.com/) which provides for:

- opening the scans of exposed and unexposed images and averaging each group (see Fig. 4.1a);

- if required by the user the average exposed and unexposed images are filtered and/or corrected for the parabola effect;

- the OD map is centred at the isocenter by the user led by the laser markers signed at the film edges (see Fig. 4.1b);

- the OD computed for each color channel is analysed using one of the film dosimetry method to calculate an absolute dose map (see Fig. 4.1c).

4.1 Validation measurements

In the first part of this chapter, some preliminary measurements made to assess the performances of GafChromic film dosimetry method at various dose levels have been set up. The exposed films and their offsets have been scanned using the reading protocol described in Chapter 2 and analysed through red channel calibration, green-blue channel approach and using multichannel dosimetry method (see Chapter 3). Moreover an average of single and double channels output has been computed (Mean R-GB) and the scanner parabolic correction method has been implemented and tested.

During the validation measurements performed at Linac each film was located at the isocenter of the accelerator (SAD 100 cm), centred in a block of solid water thick 10 cm (SSD 95 cm). Then, each exposure was repeated on a PTW 2D-Array 729 placed such that its effective point of measurement was at the isocenter. Since the array thickness was 2 cm and being the effective layer of measurement of the chambers at 0.75 cm of depth, a block

of 4.2 cm of solid water (SSD 95 cm) and a block thick 4 cm were positioned above and below respectively (see Fig. 5.2).

4.1.1 Square field test

In first place, both the PTW array and EBT3 film were irradiated under same conditions using a square field of 15x15 cm^2 with 6 MV and 200 MU. The dose maps were generated for the red channel calibration, the green-blue method, mean R-GB and for multichannel method. With the aim of evaluating the general behaviours of these calibrations independently on the particular dose value reached with this irradiation field, the simplest approach was to normalize each dose map to its central value. Hence, the in-plane normalized dose profiles are compared in Fig. 4.3. As can be noticed, all the methods present a good agreement with experimental points. However, the multichannel approach and the red channel seem to follow better measured data. If considering green-blue and Mean R-GB, there is a soft underestimation. Nevertheless, when considering the cross-plane profiles at the isocenter, there seems to be a worse accordance at the edges, probably for the light scattering effect (see Fig. 4.4).

4.1.2 Low doses test (0-6 Gy)

A second test has been made to evaluate the film dosimetry method behaviour at various doses in the range 0-6 Gy. The irradiaton was performed using a field dimension of 3x25 cm^2, 6 MV and 1000 MU at Linac. Moreover, a wedge of 60° was employed with the purpose of obtaining a wide range of doses during the same irradiation. The absolute dose maps were compared to measurements performed using the PTW array through γ analysis. Results were computed using local $\gamma_{2D}(3\%,3mm)$ analysis (see Fig. 4.5). As can be seen in Fig. 4.6, all the approaches have a great behaviour in the range of doses under study. Nevertheless, if considering the overall behaviour of the profile, the green-blue shows the best trend, as confirmed by the greater value of γ_{2D} (see Table 4.1). Even if this strip was read along the central axis of the scanner, for further information, Table 4.1 also reports the γ_{2D} results for the dose maps corrected for the parabola effect. As can be noticed, it does not involve an improvement, with the exception of the multichannel, which reaches the 92 % of γ_{2D} pass rate.

4.1.3 High doses test (2-10 Gy)

Another test was set up with the aim of assessing film dosimetry protocols responses both in a higher dose range and in presence of a more extended field. In the first pair of tests the parabolic correction was not necessary, especially in the second case, where a narrow strip was read along the central axis of the scan. Nevertheless, in the cross-plane profiles, parallel to the x axis of the scanner, obtained for the 15x15 field an overestimation of the dose at the borders became to be noticed. As discussed in Chapter 2, till the doses remain low the parabolic effect is negligible, and a correction would only introduce noise. Instead, with increasing doses and when they are read far from the central axis, a correction for this effect is needed both for the red channel and for the multichannel method, which only computes a perturbation maps from the unexposed images.

Then, the PTW array was irradiated with 1600 MU, with a field 30x40 cm^2 and using a wedge of 60° to obtain a wide range of doses between 2 and 10 Gy. The EBT3 film, exposed in the same conditions, was read through all the protocols both with and without parabolic correction, with the aim of investigating on its efficacy. The results, expressed in terms of $\gamma(3\%,3mm)$ are summarized in Table 4.1, showing a great improvement for the mean R-GB

(a)

(b)

(c)
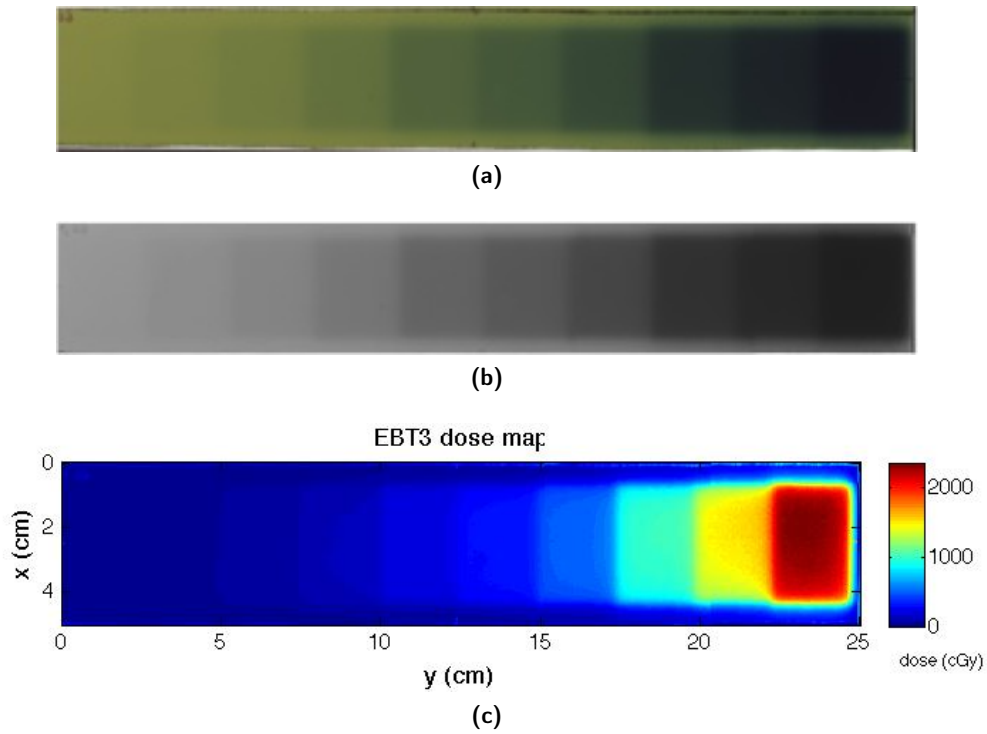
Figure 4.1: An example of the phases of the film dosimetry protocol. The scanned films are open (4.1a) and averaged between multiple scans. The OD is computed (4.1b) and analysed using a specific calibration method to obtain an absolute dose map (4.1c).

Figure 4.2: Measurement setup during validation measurements performed with PTW 2D-Array 729 at Linac.
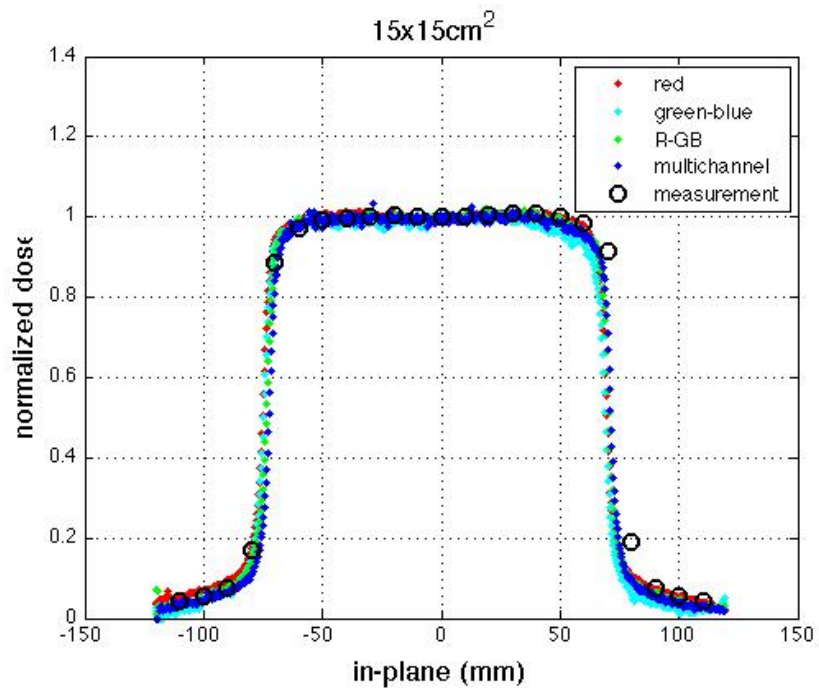
Figure 4.3: In-plane profile for 15x15 ^{2} field, normalized to the central dose value.
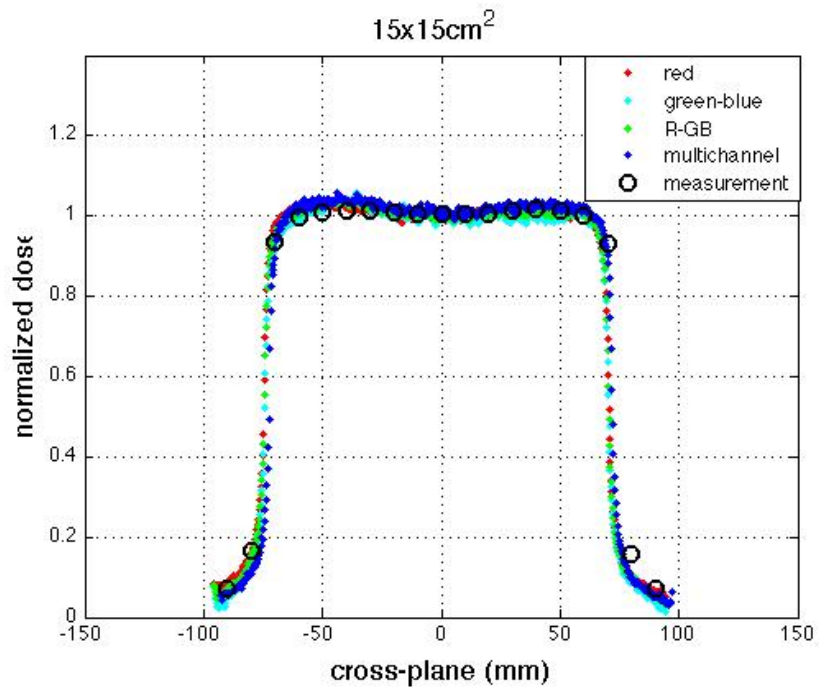
Figure 4.4: Cross-plane profile of 15x15 ^{2} field, normalized to the central dose value.

and for the multichannel methods but not for the red channel. As can be seen in Figures 4.7-4.10, the latter has a bad response to this test, hence it does not get better with a correction that is based on some preliminary assumptions. If the pixel values are very far from the real values that they had had if they would have read along the central axis, the parabolic method combined with a fit that is weak in that range of doses fails. Instead, a more robust approach, such as the multichannel method can benefit from a pixel value correction at the border of the scanner, because it is performed before the optimization procedure provided by this approach. Finally, the dose maps obtained through the multichannel approach both without and with the parabolic effect correction are shown in Figures 4.12 and 4.11. As can be noticed, they give an immediate idea of the presence of this effect, and on how it increases with dose. Even if using a method that undoubtedly could be improved, it can be appreciated the benefits resulted from its application.

4.1.4   10 fields test (0-24 Gy)

In this case a very large range of doses has been tested (0.2-24 Gy). This choice was motivated by the objective to appraise the behaviour of the EBT3 dosimetric protocols with a film containing at the same time very different optical densities (see Fig. 4.1b). Firstly, an irradiation field with a dimension of 3x25 cm^2 was used with a low number of MU, then the field was reduced by 2.5 cm in the in-plane direction with a major number of MU. This procedure was repeated for ten times, each of them with a field reduction of 2.5 cm, hence obtaining 10 squares with different doses. The MU were chosen to have very different dose values in the various squares of 3x2.5 cm^2. The plane in transversal and coronal views is reported in Fig. 4.13 and the prescribed doses were: 10, 25, 50, 100, 200, 300, 500, 1000, 1500, 2347.8 cGy.

Moreover, to stress the method, the film strip was not read in the central axis of the scanner, instead it was scanned along a direction parallel to it but far about 5 cm. Hence, the dose map was obtained for red, mean R-GB and multichannel methods correcting before the pixel values for the parabolic effect.

The analysed films dose maps and the array measurements were compared through γ-analysis, whose distributions are shown in Fig. 4.14 and the in-plane absolute dose profiles are superimposed in Fig. 4.15. Despite a failure at doses lower than 1 Gy and at the end of the dose range under study, the behaviour of all the approaches seems to be quite good taking into account the large range of doses that was tested. Nevertheless, the multichannel method seems to confirm to follow better than the other techniques the array measurements in the entire range of doses, especially when corrected for the parabola, which is really necessary in this case. This conclusion is also evident from an inspection to the γ distribution (Fig. 4.14d) and to the results expressed in terms of local $\gamma(3\%,3mm)$ passing rates (Table 4.1). To sake of completeness, in Table 4.1 are also reported the γ analysis results of the dose maps without parabolic correction. As can be noticed, the correction does not involve an improvement in the red channel, hence leading to worse results also in the mean R-GB. This is probably because an underestimation of the red channel calibration at higher doses is enhanced when correcting for the parabola, which has the effect of decrease the higher doses when not read along the central axis.

Finally, from these validation tests it can be concluded that the multichannel method is the one that best responses within an extended range of doses, and that the parabola correction acts is effective in this approach when it needs to be applied (see mean results in Table 4.1).

(a) OD map

(b) dose map

(c) red channel

(d) green-blue channels

(e) mean R-GB
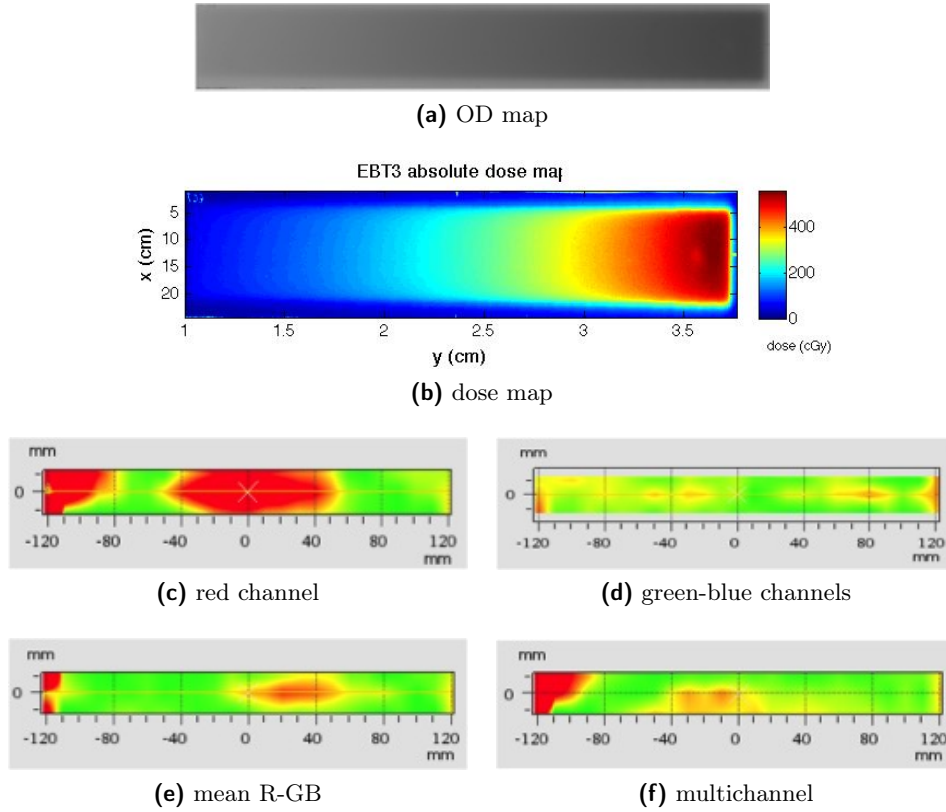
(f) multichannel

Figure 4.5: γ-analyses to compare films exposes at low doses with array measurements (4.5c-4.5f) without parabolic correction. The OD map for the red channel (4.5a) and the dose map computed with the multichannel method (4.5b) are also reported.

Table 4.1: Results of the local $\gamma_{2D}(3\%,3mm)$ without low dose suppressions for the various film dosimetry protocols in comparison with array measurements.

Validation test	$\gamma_{2D}(3\%,3mm)$						
	Red	Red-corr	Green-Blue	Mean R-GB	Mean R-GB-corr	Multichannel	Multichannel-corr
Low doses - centred (0-6 Gy)	60.0	60.0	96.0	92.0	92.0	89.3	92.0
High doses - extended (2-10 Gy)	51.5	26.5	55.6	79.2	83.8	53.3	86.5
10 field - off-axis (0-24 Gy)	68.0	62.7	81.3	77.3	77.3	85.3	87.0
Mean	59.8	49.7	77.6	82.8	84.4	76.0	88.5
SD	8.3	20.2	20.4	8.0	7.4	19.7	3.0
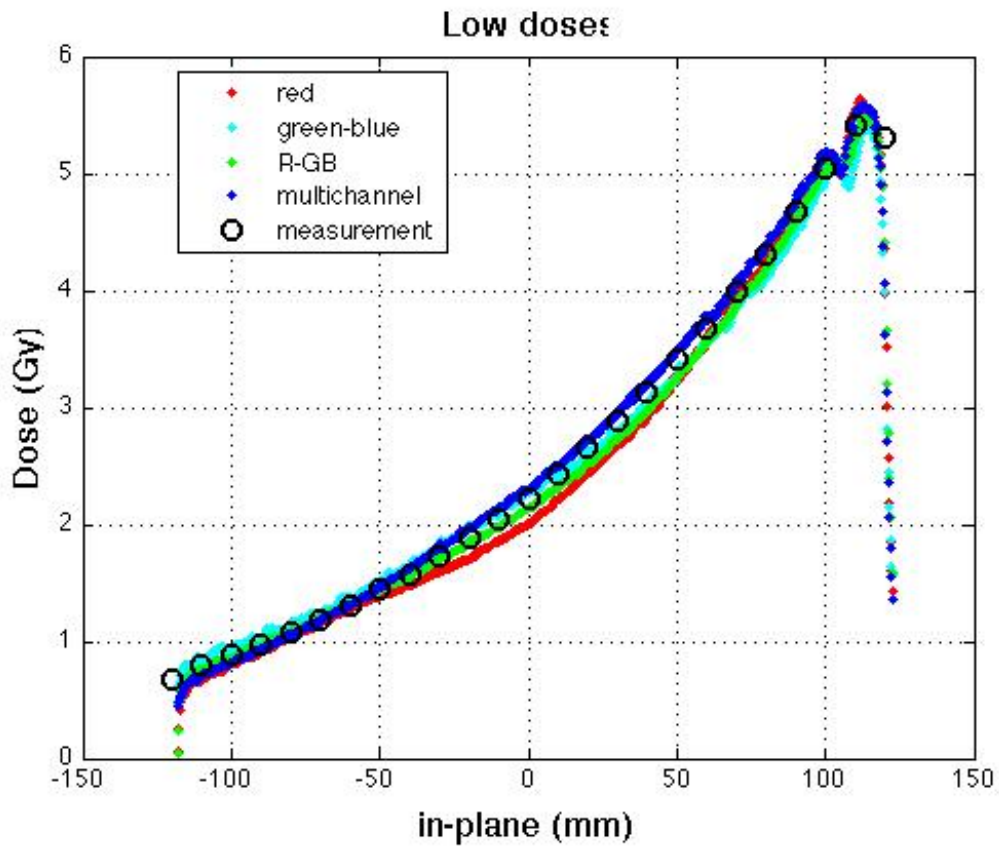
Figure 4.6: Comparison of dose profiles between film dosimetry methods and array measurements in the low doses test (0-6 Gy) without parabolic correction.

(a) Red

(b) Red corrected
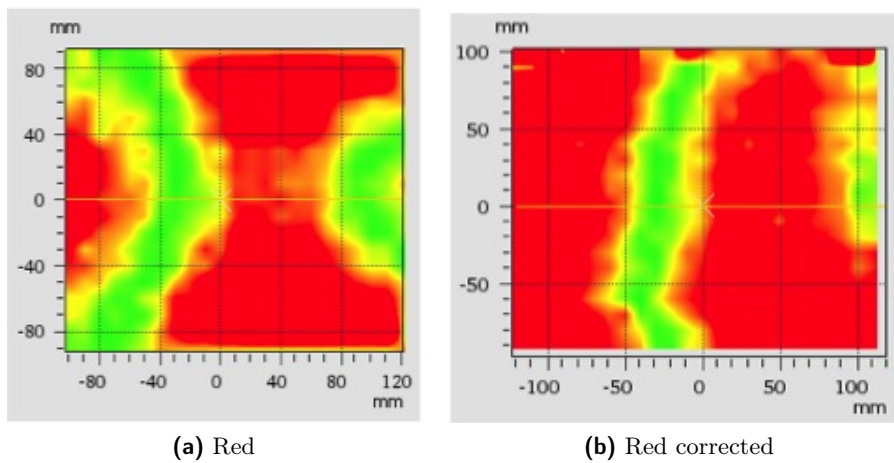
Figure 4.7: Local γ_{2D}(3%,3mm) distribution for red channel method without (4.7a) and with (4.7b) parabolic correction applied to the high dose test.
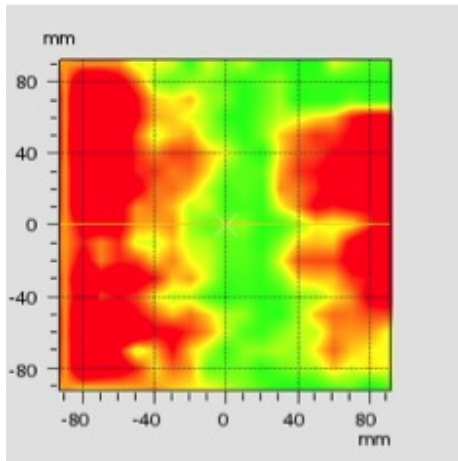
Figure 4.8: Local $\gamma_{2D}(3\%,3\text{mm})$ distribution for green-blue analysis applied to the high dose test.

(a) Mean R-GB

(b) Mean R-GB corrected
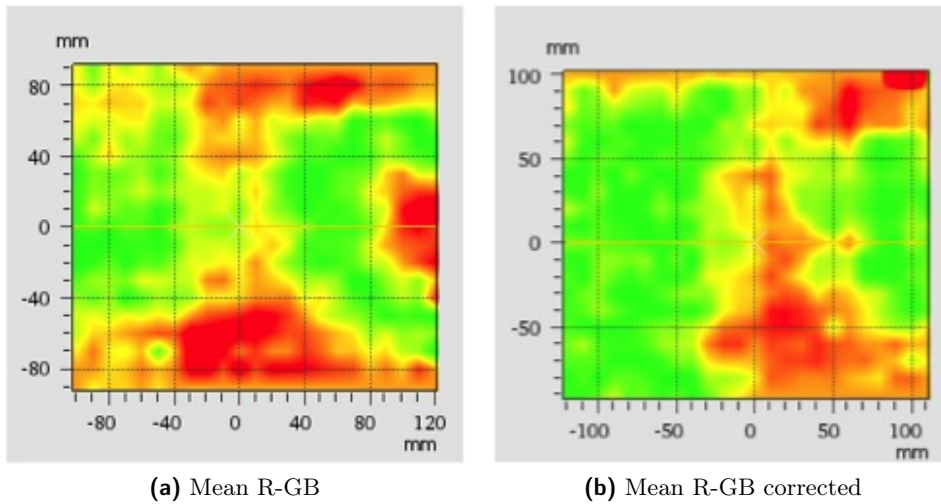
Figure 4.9: Local $\gamma_{2D}(3\%,3\text{mm})$ distribution for mean R-GB analysis without (4.9a) and with (4.9b) parabolic correction applied to the high dose test.

(a) Multichannel

(b) Multichannel corrected
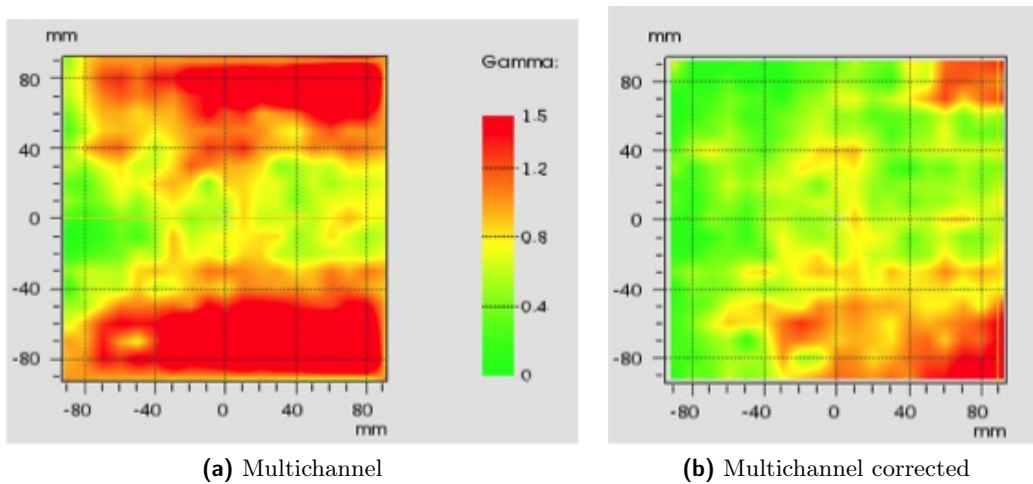
Figure 4.10: Local $\gamma_{2D}(3\%,3\text{mm})$ distribution for multichannel without (4.10a) and with (4.10b) parabolic correction applied to the high dose test.

57
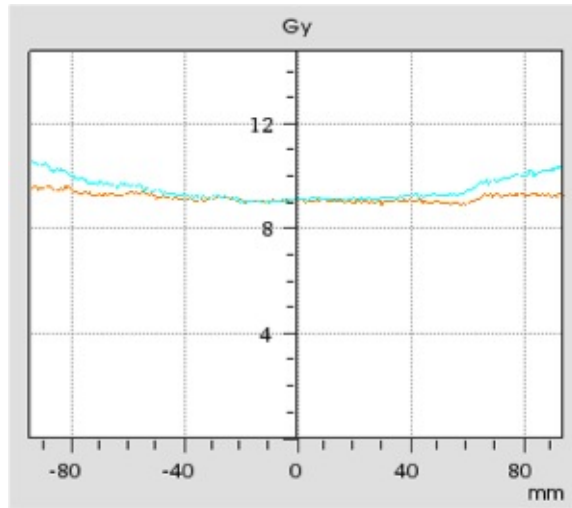
(a) Cross-plane profiles of corrected (red curve) and uncorrected (cian curve) multichannel dose maps.
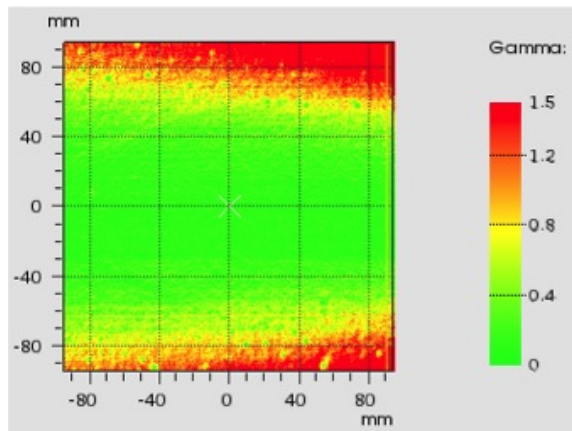
(b) γ_{2D} to achieve a visual comparison between corrected and uncorrected multichannel dose maps.

Figure 4.11
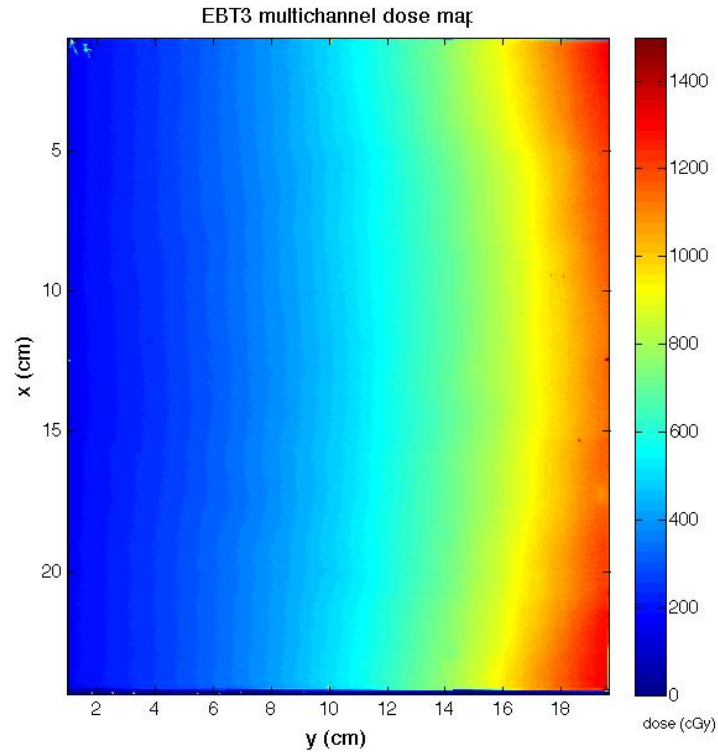
(a) Multichannel dose map.
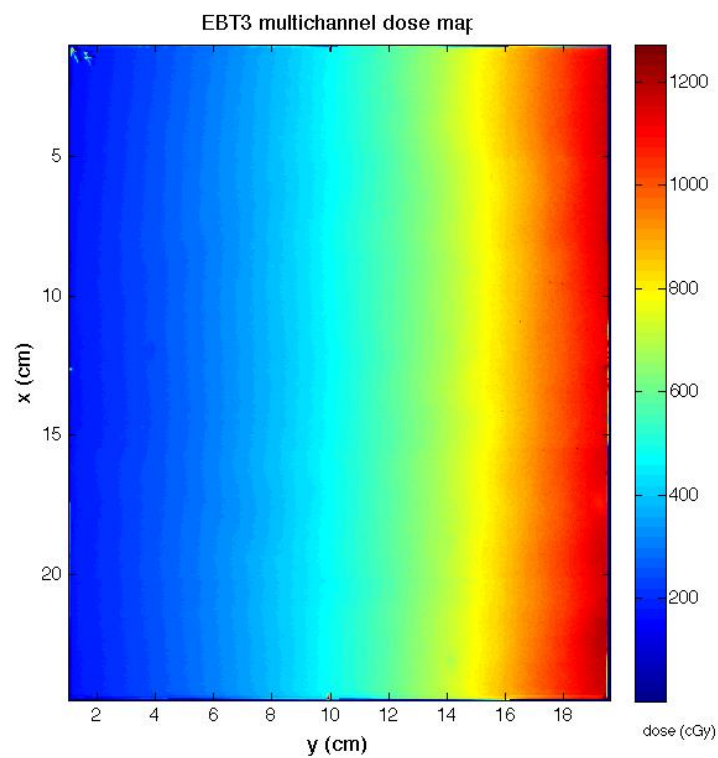
(b) Multichannel dose map corrected for parabolic effect of the scanner.

Figure 4.12: Comparison between multichannel dose maps with and without parabolic correction.
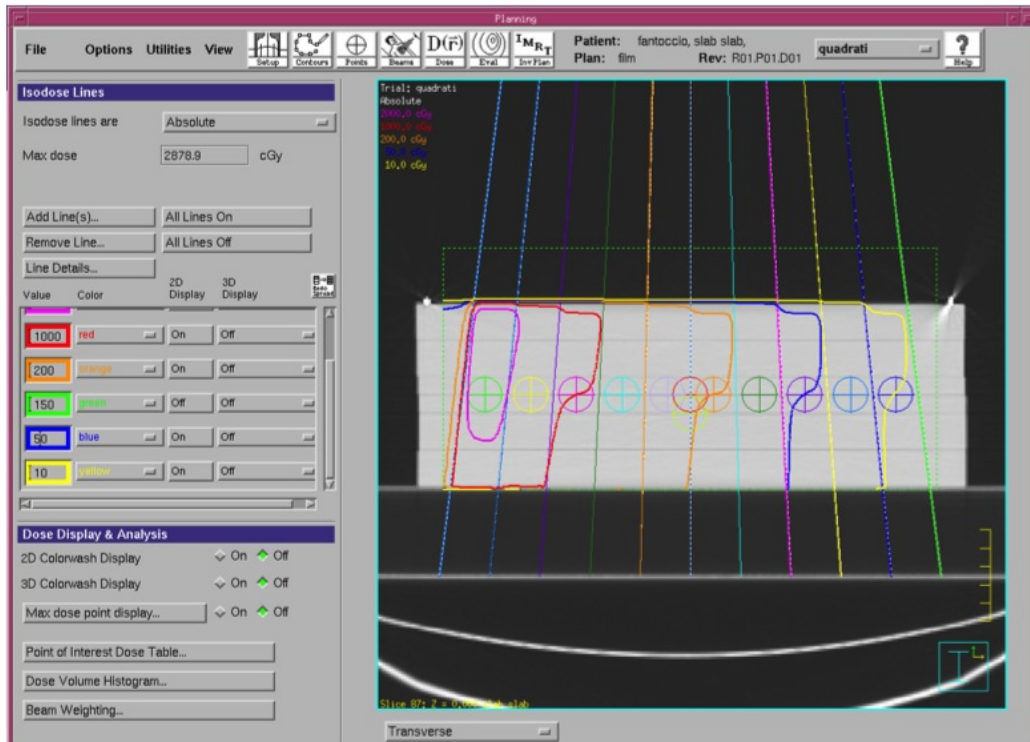
(a) Transversal view in Pinnacle.
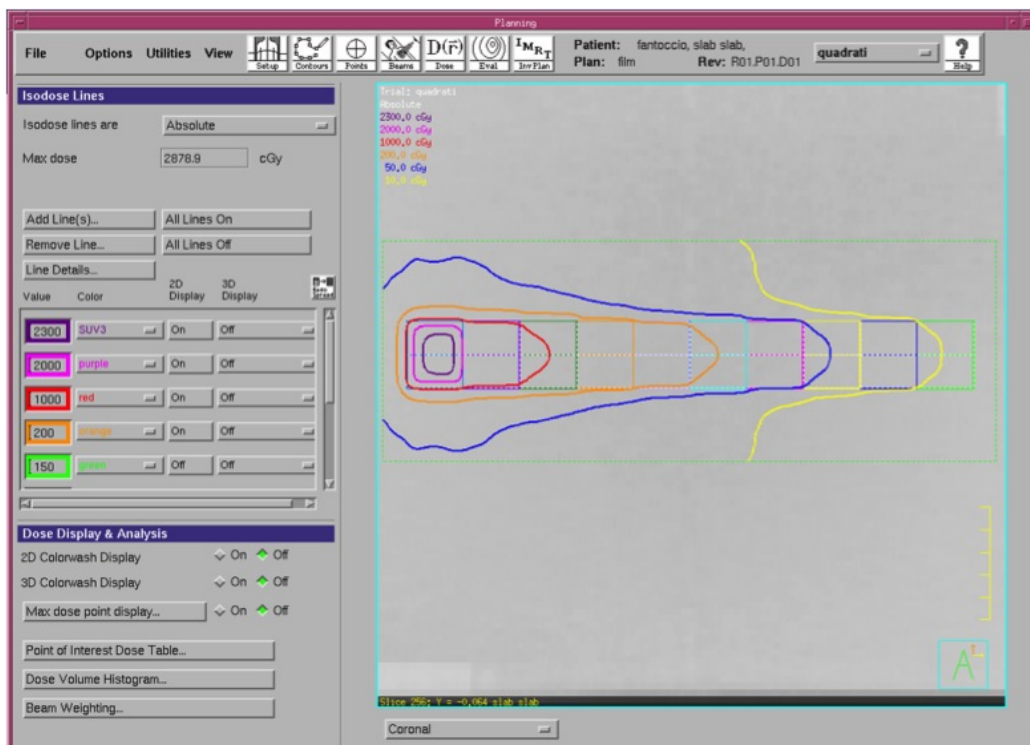
(b) Coronal view in Pinnacle.

Figure 4.13: Plan set up in Pinnacle to obtain 10 squares with different doses in the range 0.2-24 Gy. The prescribed doses in the center of each square were: 10, 25, 50, 100, 200, 300, 500, 1000, 1500, 2347.8 cGy. Fig. 4.13a reports the transversal view, instead Fig. 4.13b reports the coronal perspective.

4.2 Pre-treatment QA verifications

After the investigation on the reliability of the four dosimetric methods, made by comparing the film analysis with an accurate measurement system such as the array of ionizing chambers, they have been employed to analyse a collection of pre-treatment QA. In particular, thirteen verifications were performed in tomotherapy, conformal arc planned both in Pinnacle and in Monaco, and in VMAT planned in Monaco.

The differences between film readings and dose distributions computed by the TPS were compared in terms of local $\gamma_{2D}(3\%,3mm)$ analysis, suppressing points under 10% of maximum dose. Table 4.2 shows the γ_{2D} results for the four dosimetric methods for the various QA and compares the means and the standard deviations (SD) for all the QA verifications subdividing them according to the planning technique employed. As can be noticed, the multichannel method allows to achieve the best results, reaching an average γ_{2D} pass rate of 94.9 %. The mean R-GB also gives good performances, followed by green-blue and red channels techniques. It is evident that more robust methods are able to achieve good results in different treatment situations and with dissimilar software plannings. If considering different TPSs, from these observations it can be noticed that Monaco seems to be more accurate, even if only two cases have been taken into account. Instead, with conformal arc in Pinnacle quite worse results are obtained. To take a couple of examples, the γ_{2D} distribution of a plan made in tomotherapy (patient 2) and a conformal arc in Monaco are shown in Figures 4.16 and 4.17 respectively.

In addition, the same pre-treatment QA films were analysed employing the parabolic correction for the red, the mean R-GB and the multichannel methods. In these types of dose distributions the higher doses are usually located in the central part of the film, otherwise, if the dose distributions are more extended they often contain low dose values. Hence, the parabolic correction seems to be not necessary, excepted for those situations in which films are read in a decentralized position on the scanbed. However, the effectiveness of this correction in pre-treatment QA has been studied and the results are reported in Table 4.2. As can be observed from the mean results of γ_{2D}, there is not an overall improvement in any of the dosimetric protocols. However, if considering the trends in the subgroups, the multichannel method and the mean R-GB take some benefits from the correction in conformal arc, where also the red channel take some improvements, especially in Pinnacle. Moreover, the tomotherapy plans, that are the more extended but with lower doses in this case take no benefits from this correction.

(a) red channel   **(b)** green-blue channels

(c) mean R-GB   **(d)** multichannel
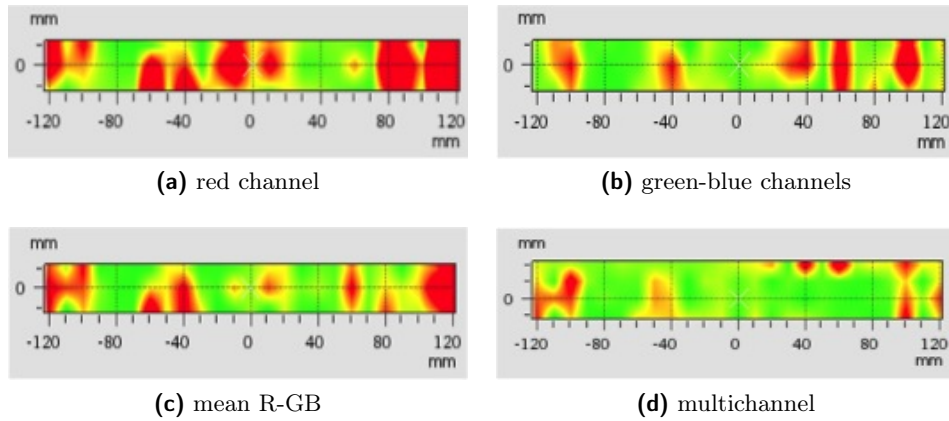
Figure 4.14: 2D-γ distributions in the 10 fields tests, comparing different film analyses with different protocols corrected for the scanner with array measurements.

Table 4.2: QA results in terms of local γ_{2D}(3%,3mm) distribution, suppressing points under 10% of maximum dose. Passing rates are compared for the red, green-blue, mean R-GB and multichannel methods and the mean and the standard deviation (SD) of the results are reported.

Planning technique	Patient	Site of treatment	γ_{2D}(3%,3mm)			
			Red	Green-Blue	Mean R-GB	Multichannel
Tomotherapy						
	1	H&N	95.9	92.7	96.8	98.0
	2	H&N	82.7	71.7	97.9	94.4
	3	H&N	82.8	84.3	93.2	87.1
	4	H&N	95.4	84.8	98.1	99.4
mean			89.2	83.4	96.5	94.7
SD			7.5	8.7	2.3	5.5
Conformal Arc (Pinnacle)						
	5	SBRT brain	62.8	91.2	93	99.7
	6	SBRT brain	82.6	70.8	80.1	83.7
	7	SBRT lung	42.1	66.5	56.5	81.8
mean			62.5	76.2	76.5	88.4
SD			20.3	13.2	18.5	9.8
Conformal Arc (Monaco)						
	8	SBRT brain	97.3	76.7	93.7	98.3
	9	SBRT brain	95.1	66.8	85.4	98.1
	10	SBRT brain	85.5	98.1	93.6	99.6
	11	SBRT brain	94.0	98.3	98.6	98.3
mean			93.0	85.0	92.8	98.6
SD			5.2	15.8	5.5	0.7
VMAT (Monaco)						
	12	SBRT brain	88.4	93.1	97.5	98.1
	13	bladder	59.4	85.6	88.9	97.5
mean			73.9	89.4	93.2	97.8
SD			20.5	5.3	6.1	0.4
mean			81.8	83.1	90.3	94.9
SD			17.0	11.5	11.5	6.3
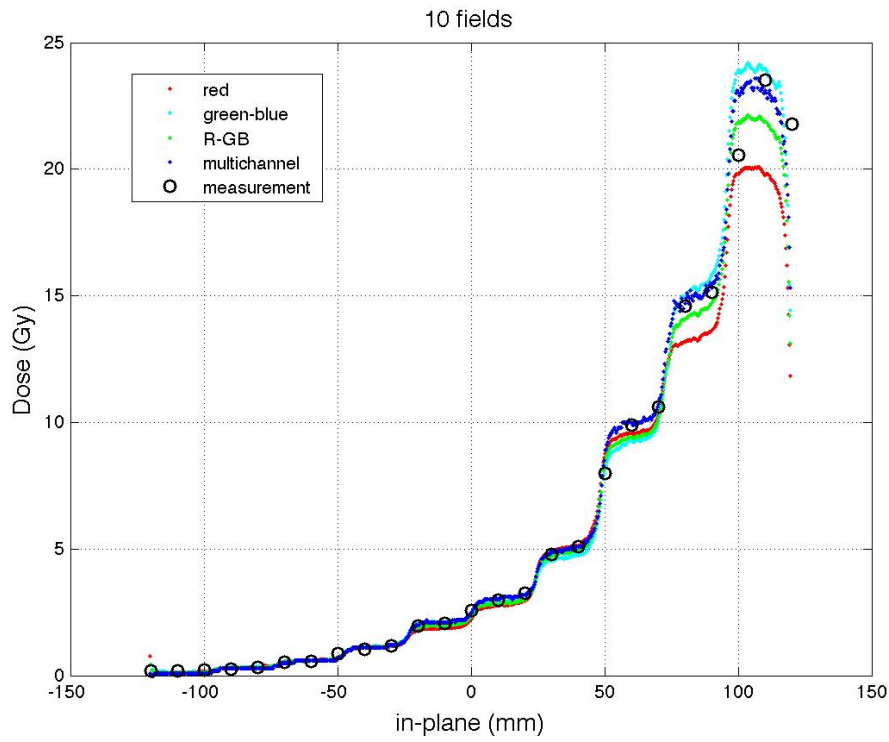
(a)
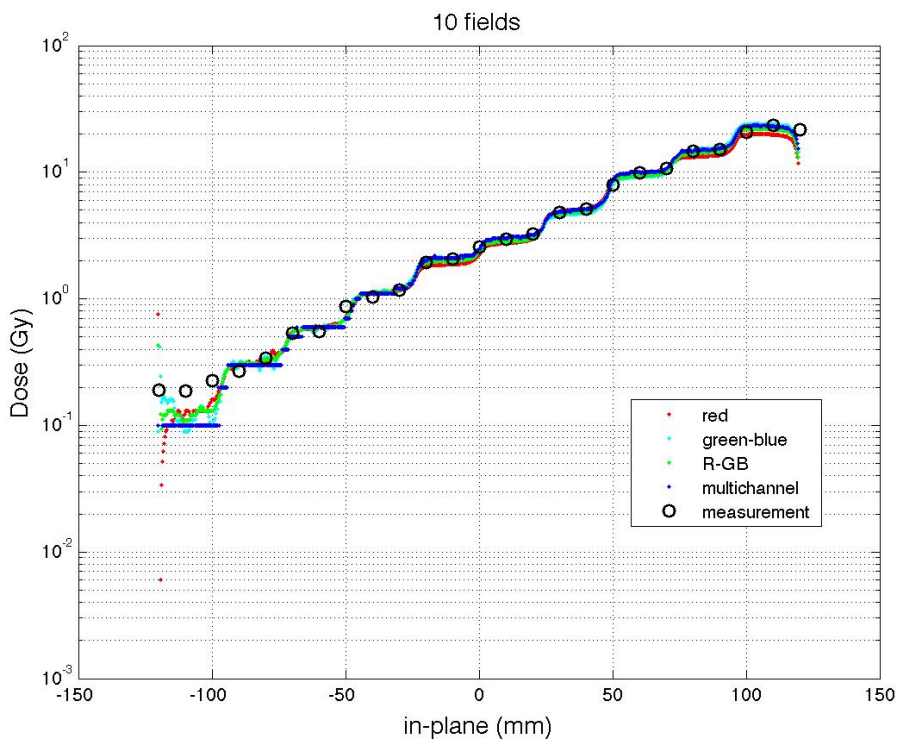
(b)

Figure 4.15: Dose profiles comparison in the 10 fields test. The measurement superimposition was performed both in linear scale (4.15a) and in semilogarithmic scale (4.15b), in order to appreciate the discrepancies between different approaches both at low and high doses. Here, the red, mean R-GB and multichannel are corrected for the scanner parabola effect.

Table 4.3: QA results in terms of local $\gamma_{2D}(3\%,3\text{mm})$ distribution, suppressing points under 10% of maximum dose. Passing rates are compared for the red, mean R-GB and multichannel methods, all applying parabolic correction to the exposed images. Moreover, the mean and the standard deviation (SD) of the results are reported.

Planning technique	Patient	Site of treatment	$\gamma_{2D}(3\%,3\text{mm})$		
			Red-corr	Mean R-GB-corr	Multichannel-corr
Tomotherapy					
	1	H&N	90.5	91.1	98.1
	2	H&N	60.4	81.3	89.6
	3	H&N	79.2	82.3	87.8
	4	H&N	89.4	96.3	99.2
mean			79.9	87.8	93.7
SD			13.9	7.2	5.8
Conformal Arc (Pinnacle)					
	5	SBRT brain	66.6	93.4	99.5
	6	SBRT brain	86.8	84.7	94.8
	7	SBRT lung	56.0	54.6	85.9
mean			69.8	77.6	93.4
SD			15.6	20.4	6.9
Conformal Arc (Monaco)					
	8	SBRT brain	93.7	97.6	98.3
	9	SBRT brain	88.4	97.3	95.7
	10	SBRT brain	88.3	97.8	96.9
	11	SBRT brain	92.5	97.9	95
mean			90.7	97.7	96.5
SD			2.8	0.3	1.4
VMAT (Monaco)					
	12	SBRT brain	87.5	97.6	94.6
	13	bladder	61.2	88.5	97.3
mean			74.4	93.1	96.0
SD			18.6	6.4	1.9
mean			80.0	89.3	94.8
SD			13.8	12.1	4.4
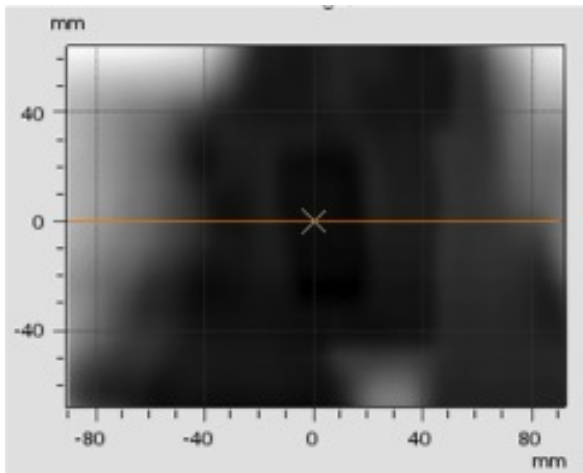
(a) TPS dose map.
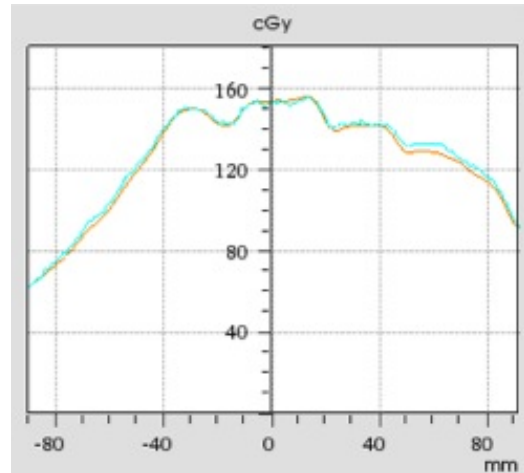
(b) In-plane dose profiles at the isocenter.
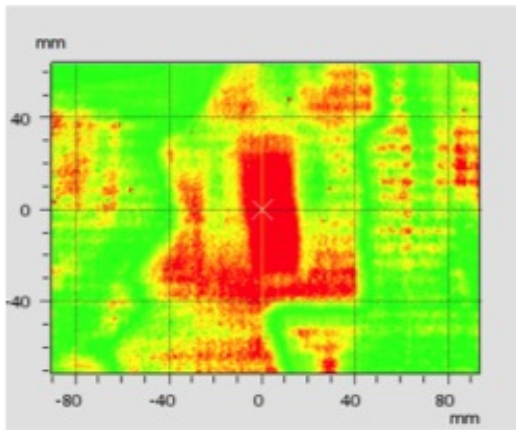
(c) γ_{2D} for red channel.
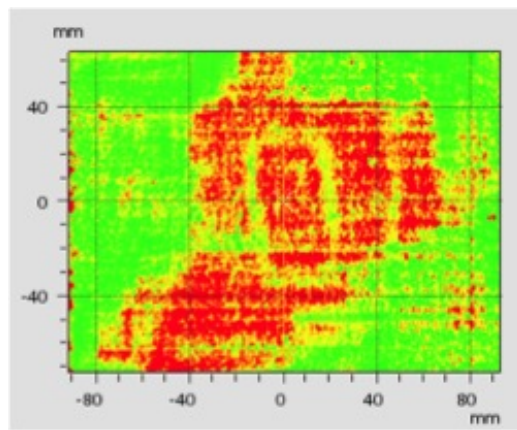
(d) γ_{2D} for green-blue channels.
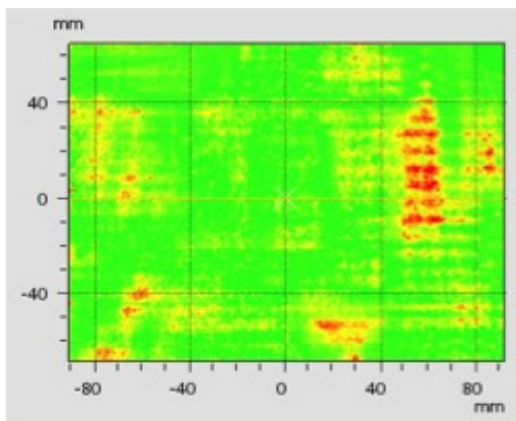
(e) γ_{2D} for mean R-GB.
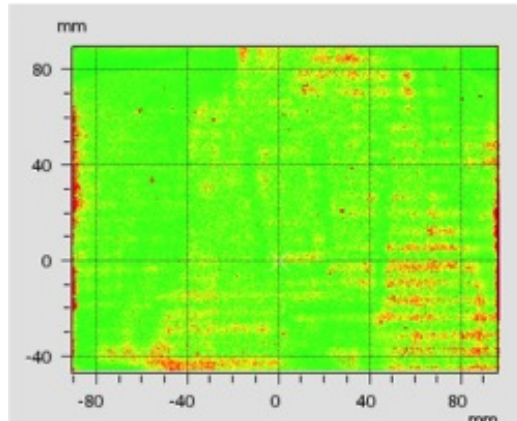
(f) γ_{2D} for multichannel.

Figure 4.16: Analysis of a QA OD map (4.16a) with different EBT3 dosimetric methods through $\gamma_{2D}(3\%,3mm)$ for patient 2 in tomotherapy (4.16c-4.16f). Moreover inplane profiles comparison of TPS dose (red curve) and EBT3 dose estimated with mean R-GB (cian curve) are shown (4.16b).
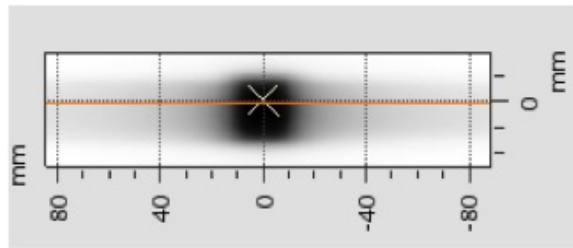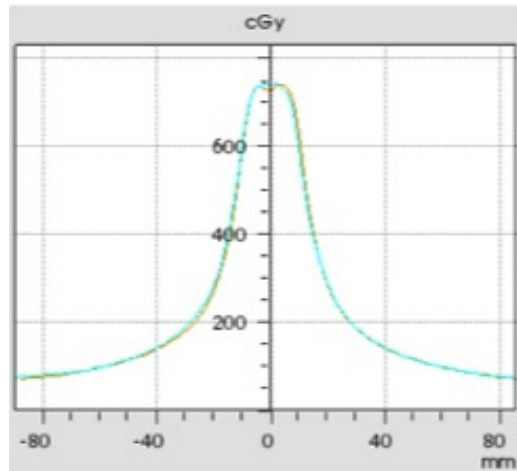
65

(a) TPS dose map.

(b) In-plane dose profiles at the isocenter.

(c) γ_{2D} for red channel.
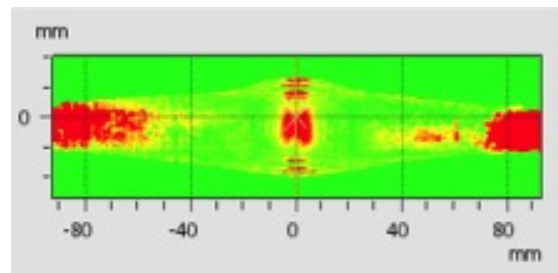
(d) γ_{2D} for green-blue channels.
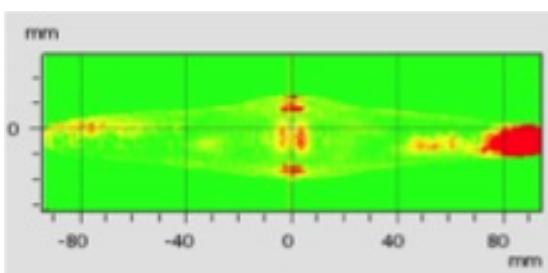
(e) γ_{2D} for mean R-GB.
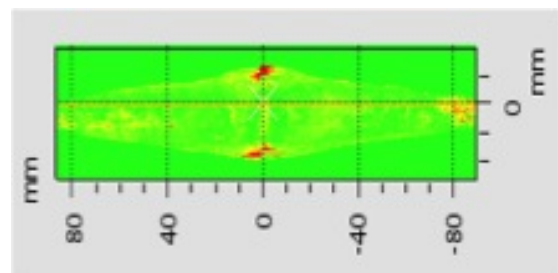
(f) γ_{2D} for multichannel.

Figure 4.17: Analysis of a QA OD map (4.17a) with different EBT3 dosimetric methods through $\gamma_{2D}(3\%,3\text{mm})$ for patient 8 planned with a conformal arc in Monaco (4.17c-4.17f). Moreover in-plane profiles comparison of TPS dose (red curve) and EBT3 dose estimated with multichannel (cian curve) are shown (4.17b).

Chapter 5

In vivo dosimetry

Clinical side effects to superficial structures are a major concern with radiotherapy patients during the treatment of malignant disease by radiation, and for radiological protection. The skin response to ionizing radiation limits the fully effective use of such radiation in cancer therapy where relatively large areas of skin are exposed to penetrating X or gamma rays. As a consequence, it becomes important to accurately determine the dose delivered to a patient skin during radiotherapy owing to complications that can arise [48]. Clinical side effects to superficial structures typically occur in 2-3 weeks after the beginning of radiotherapy treatment, and may cause, if they are not tolerated by the patient, a treatment break [66]. Moreover, incidences of toxicities to superficial structures, such as dermatitis and alopecia have been observed with IMRT treatments [67–69]. For these reasons, it is recommended to reduce dose to the skin in optimization of radiotherapy plans, especially in IMRT. The occurrence of complications in superficial structures as skin and mucosa in IMRT is possibly related to increasing number of tangential beams compared with 3D-CRT, resulting in more non-target tissues irradiated [67]. The dose to the skin could be higher in IMRT than in 3D-CRT also because, during the inverse planning, it is required to cover the planned target volume (PTV) with the prescribed dose even in areas where build-up effect occur [70].

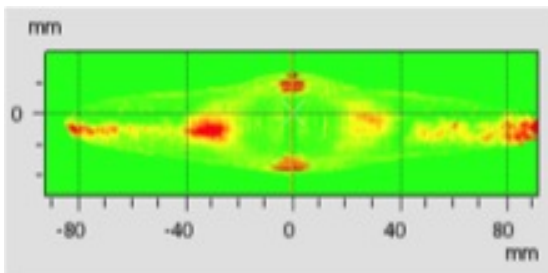However, TPSs do not accurately model skin dose. One reason is the fact that voxels sizes derived from patient CT images used in dose calculations are larger than skin dimensions. This makes it difficult to for the TPS to accurately define the skin, and consequently leads to inaccurate quantification of the skin dose. Another reason is the inability of most TPS to accurately account for electron contamination, that has been shown by many authors to contribute significant dose at the surface, therefore incorporation of this component in the TPS is extremely important [48]. The inefficiency of the TPS in estimating the dose to the skin or surface dose region has been subject of several studies. The build-up region dose comprises a primary component of photons and electrons, and contamination electrons from the treatment head and volume of air between the treatment head and patient. Excepted for the primary component, the magnitude and importance of the skin dose contributed from each of these components will vary with field size and shape. Therefore with the widespread use of multileaf collimator (MLC) for field shaping and conformal therapy, the dose contribution to the skin can vary significantly from one system to another depending on the complexity of the MLC system, the variation in the gantry components, dosimetric characteristics and modulation of the beams during delivery.

An overestimation of surface dose in phantom by the TPS of up to 14% has been reported for helical tomotherapy and several studies in vivo have also demonstrated that the TPS overestimate skin dose in tomotherapy treatments [72, 73, 77].

Dosimeters that have been used to evaluate superficial doses in vivo an in phantom for IMRT and tomotherapy include TLDs [71, 78], diodes [74], and MOSFETs [75–78]. Radiochromic EBT films have many attractive characteristics that make them candidates for

in vivo skin dosimetry such as high spatial resolution, near-tissue equivalence, and weak energy response. Moreover, the equivalent depth in water of the effective point of measurement for EBT radiochromic films has been determined as 153 μm [47], which is very close to the clinically relevant depth for skin of 70 μm recommended by ICRP [1] and ICRU [2].

The aim of this chapter is to report the results of in vivo measurements performed during radiotherapy treatments in tomotherapy, at Linac both with 3D-CRT and VMAT and in Plesio-Röntgen therapy. Then, skin dose measurements, analysed through GafChromic dosimetry, have been compared with TPS planned doses, investigating on factors possibly related to discrepancies between expected and measured doses.

5.1 Measurement protocol

In film handling and storing the recommendations of the AAPM TG-55 report were followed: gloves were used to avoid film soiling, exposure to light was minimized and films were kept together to avoid differences in thermal histories [79]. Films of the same batch were cut in pieces of 2x2 cm^2 and each of them was enveloped with plastic film to facilitate their using during in vivo measurements (see Fig. 5.2a).

The reading protocol adopted was the same described in Chapter 2, in particular each piece was read three times before and after the irradiation. A consistent orientation was maintained for all scans and the central axis was used for the reading in order to avoid a non-uniform response of the scanner (see Fig. 5.2b). The remaining area of the glass tray was covered by opaque radiographic films to reduce scattered light. The films were scanned with 75 dpi resolution with 48-bit in RGB with all filters turned off and read 22 h after the irradiation. The film readings were analysed using the red channel calibration because it is more performant than the green-blue at doses equal or lower than 200 cGy, that are the values commonly used for clinical fractions. Moreover, despite the multichannel method was demonstrated to be more accurate than the others, it is more suitable to analyse extended distribution of doses, then it seemed to be wasted to use an iterative method to read more than one hundred film pieces. In fact other studies performed in vivo with EBT3 adopt the same approach [46, 80].

In order to compare the measured doses with expected values, the dose computed by the TPS was used. In particular, given a point in the dose grid and a square centred on it with a dimension of about 1 cm^2, the expected dose in that point was computed averaging the central value, the vertex values and the middle points on the sides of the square, hence a mean of nine points of dose was computed. At the same time the mean PV of each film piece was computed with ImageJ using a ROI of 1 cm^2 centred in the film piece (see Fig. 5.1). This approach was used both for the measurements on phantom and in vivo. The comparison between EBT3 and TPS expected doses will be made as follows [46, 80]:

$$EBT3 - TPS(\%) = 100 \cdot \frac{EBT3_{dose} - TPS_{dose}}{TPS_{dose}}. \tag{5.1}$$

5.2 Preliminary measurements on phantom

With the aim of assessing the reproducibility of the measurements, the stability of the response of different film pieces exposed to the same radiation field, and to evaluate the agreement between film measurements and TPS expected doses, a set of measurements on the Cheese Phantom (www.accuray.com) were performed.

In first place, a tomotherapy test plan was optimized to give 10 Gy in 5 fractions to three circular superficial PTV in the Cheese. The plan was computed through a dose grid with a fine resolution, which in tomotherapy means having the same resolution of the the

Table 5.1: Summary of the results for preliminary tests on Cheese Phantom with EBT3 samples located on its surface (right, anterior and left in tomotherapy; anterior at Linac). Moreover the percentage deviations of the EBT3 readings with respect to the TPS values are reported.

Machine	Film position	EBT3 measured dose (cGy)	TPS dose (cGy)	EBT3-TPS (%)
Tomotherapy	Right	126.7 ± 2.9	134.5 ± 0.3	-5.8
	Anterior	127.8 ± 3.3	175.0 ± 0.2	-27.0
	Left	124.8 ± 2.6	161.0 ± 0.3	-22.5
Linac	Anterior	126.1	159.0 ± 3.9	-20.7

CT images used fot the planning, that was $0.16 \text{x} 0.3 \text{x} 0.16$ cm^3 in this case (see Fig. 5.3). This choice was motivated by the fact that thomotherapy plans are usually computed with a fine grid, hence it was decided to assume the same conditions that will be present in the in vivo case. Three superficial positions on the surface of the Cheese Phantom (see Fig. 5.4) were chosen to measure the film readings for five times. Then, the mean and standard deviation of the film readings were evaluated. In order to have a reference dose value during the film measurements, two ionizing chambers were used to measure the dose in two points of the phantom to control the stability of the experimental conditions and the accordance with the expected dose.

The results of these measurements are summarized in Table 5.1. As can be noticed, the mean deviations between film readings are of 3 cGy, corresponding to about the 2% of the absolute dose. Hence, it seems to be a good reproducibility between the measurements and a great accordance between the reading of different EBT3 samples exposed to the same plan fraction. Moreover, the TPS expected doses were estimated with the method described above, considering a square with a dimension of about 1 cm^2. In all the cases taken into account the TPS overestimates the measurements of about the 23%. This trend is in accordance with other results reported in literature.

Moreover, a measurement with an EBT3 film fixed on the Cheese surface was performed at Linac in order to compare the film reading with the TPS estimated value. A field 10x10 cm^2 with SSD 85 cm and energy of 6 MV was used. Even in this case an overestimation of the TPS occurs, as shown in Table 5.1.

Secondly, an estimation of the MVCT contribution in Tomotherapy and of the cone beam CT (CBCT) at Linac was performed using EBT3 pieces fixed on Cheese surface in the same three positions used above. The measurement of the dose contribution on surface of the CBCT was of 6.99 ± 0.09 cGy, instead the MVCT contribution was of 1.03 ± 0.03 cGy. These evaluations were necessary since treatment fractions are often supplied after MVCT or CBCT, hence some in vivo measurements contain this dose contribution. However, these preliminary measurements demonstrated that this dose is negligible with respect to the treatment componenct, which is of the order of 100 cGy, for Tomotherapy treatments, instead it will be subtracted for patients treated at Linac.

5.3 Skin dose measurements

An evaluation of skin dose for patients treated with three radiation therapy have been performed: Tomotherapy, 3D-CRT, VMAT and electron beams at Linac, and Plesio-Röntgen therapy. A total of 21 patients were recruited, selecting those plans regarding superficial lesions. In Plesio-Röntgen only cutaneous lesions are usually treated, instead in tomotherapy were chosen five head and neck (H&N) and two brain plans having tumour lesions very close to the skin and one patient with a sarcoma at the right thigh. Moreover, five breast cancers, four treated with 3D-CRT and one with VMAT and two cutaneous lesions treated

with electron beams were considered. Finally EBT3 measurements were made on a patient treated with 180 kV in Röntgen therapy and on five irradiated with 60 kV in Plesio therapy.

Both in tomotherapy for superficial and cutaneous lesions and in kV range treatments, an in vivo monitoring of skin dose could be important to prevent overdosage effects during the treatment. In fact, in Plesio-Röntgen therapy the prescribed dose and MU can easily be modified during therapy if necessary, and in tomotherapy it would be possible to readapt the plan to avoid undesired effects such as alopecia and dermatitis. Moreover, if considering breast tumours, the effect that usually occur is a cutaneous redding in the very last fractions of the plan, hence the utility of EBT3 in adaptive plans is more limited. Nevertheless, it was chosen to consider such cases in this study with the aim of having the possibility to compare in vivo measurements with EBT3 between different types of plans and irradiation techniques, and tanking into account varying positioning conditions.

In H&N and brain plans the film measurements were performed locating the EBT3 pieces in fixed positions in the inner part of thermoplastic masks (see Fig. 5.5). Conversely, at Linac and for cutaneous lesions both in tomotherapy and in kV treatments, the film pieces were positioned directly on the skin of the patients, helped by laser position or using other reproducibles points, such as scars of tatoos (see Fig. 5.6). Regarding breast lesions treated with 3D-CRT, films were positioned at the isocenter, at the border of the light field and in correspondence of the medial tatoo. In the case of VMAT treatment, dose was also monitored in correspondence of the collarbone.

The measurements were compared with expected dose estimated with the method previously described from the TPS dose grid for thomoterapy and Linac plans (see Figures. 5.7 and 5.8). Instead, the comparison in Plesio-Röntgen therapy was performed with prescribed doses at the center of the lesions.

The results of in vivo measurements are reported in Tables 5.2-5.4. Looking at the overall results, the average deviations of EBT3 measurements from expected values of TPS range from 17.7% for Linac treatments to 3.8% for Plesio-Röntgen therapy. Instead Tomotherapy is located at an intermediate position, reaching a mean of 11.6%. Moreover the mean percentage error in EBT3 measurements are equal to 9.2% in Linac, 2.6 % in Tomotherapy and 1.3% in Plesio-Röntgen treatments. The last two results are in great accordance with the 2% of EBT3 variability estimated on phantom, confirming a good reproducibility also in vivo. Instead, the worse results obtained in Linac in vivo measurements are motivated by a more difficult positioning in these type of treatments, where thermoplastic masks are not employed, and remembering that these treatments regard an area sensible to breathing movements.

More in detail, if considering measurements on breasts treated with 3D-CRT, the deviations from the TPS are on average smaller for the measurements made at the isocenter, as expected. Instead, the edge and the median tatoo seem to be more uncertain to estimate skin dose. A motivation of this trend for the edge point is the more difficult repositioning of the film, being more affected by the re-positioning of the breast, and because it is at the border of the irradiating field. Instead the median point measurements, where the positioning has a good reproducibility, are probably effect by the effect of the edge fields. In these plans, there were some difficulties in re-positioning the film due to patient overweight, instead for patient n. 4, where this was not a problem, the measurements are quite better than the others. A better accordance there is for electron treatments, probably due to the presence of the bolus, which moves the EBT3 point of measurement more in depth, leading to a better accordance with the TPS, and for VMAT. Nevertheless, the number of patients taken into account is too small to conclude something about different TPS performances in calculating dose in the build-up region. In addition, the better agreement achieved in tomotherapy is problably motivated by the presence of thermoplastic masks, which aid the film re-positioning in each fraction very much. In addition, the best agreement with ex-

Table 5.2: In vivo measurements with EBT3 made in radiotherapy treatments at Linac. Here, the number of the patient (Pat.), the dose per fraction (dose/fx) and the number of measurements (N) reported.

Pat.	Treated site	Plan (TPS)	Dose/fx(cGy)	Point	N	EBT3 dose (cGy)	TPS dose (cGy)	TPS SD (%)	EBT3-TPS (%)
1	breast dx	3D-CRT(Pinnacle)	200	iso	4	141.5 ± 3.8	124.5 ± 20.1	16.1	13.7
				med	4	63.0 ± 22.1	41.6 ± 9.9	23.8	51.6
				edge	4	62.7 ± 37.1	129.3 ± 16	12.4	-51.5
2	breast dx	3D-CRT(Pinnacle)	200	iso	4	162.6 ± 4.9	151.7 ± 33.1	21.8	7.2
				med	4	129.0 ± 18.0	181.8 ± 20.5	11.3	-29.0
				edge	4	175.4 ± 7.1	150.9 ± 32.8	21.7	16.2
3	breast dx	3D-CRT(Pinnacle)	200	iso	3	108.2 ± 5.2	136.8 ± 12.6	9.2	-20.9
				med	3	66.0 ± 3.8	55.1 ± 8.1	14.7	19.9
				edge	3	142.9 ± 1.8	151.7 ± 14.7	9.7	-5.8
4	breast sx	3D-CRT(Pinnacle)	275	iso	3	136.8 ± 1.0	131.3 ± 18.2	13.9	4.2
				med	3	103.1 ± 1.2	102.2 ± 27.5	26.9	0.9
				edge	3	137.2 ± 2.0	127.8 ± 24.7	19.3	7.4
5	breast+collarbone dx	VMAT	200	iso	3	120.5 ± 12.7	116.0 ± 53.7	46.3	3.9
				dx	3	124.3 ± 6.1	138.0 ± 48.0	34.8	-9.9
				collarbone	3	59.1 ± 3.9	98.4 ± 25.0	25.4	-39.9
6	hip dx	electrons (Pinnacle)		iso	1	179.3	196.9 ± 3.9	2.0	-8.9
7	hip dx	electrons (Pinnacle)		iso	2	178.2 ±1.3	198.3 ± 3.9	2.0	-10.1
	Mean of the absolute values of EBT3-TPS (%)								17.7

pected measurements is reached for Plesio-Röntgen therapy, surely because it is the most simple type of treatment, which is not affected by many error sources that on contrary are present in the other in vivo measurements. Moreover, in Plesio therapy the calculation of prescribed dose is based on measurements that are directly performed on surface, hence the common TPS errors are not present in this type of treatment.

Moreover, opposite to the results reported in literature, according to which the TPS always overestimates the measured dose, in this study there is not a defined trend about the overestimation of the TPS. In fact, especially in Linac measurements, the measurements are sometimes lower and other times higher than calculated values. Instead, in Plesio-Röntgen therapy in general the measured dose is a bit lower than the prescribed one, and in tomotherapy in general the TPS underestimates the measurements, excepted for the unique treatment performed without a positioning mask.

Finally, the measurements of a couple of patients treated with Plesio therapy (patients 16 and 17) have been analysed using different calibrations, in order to make a comparison between the different readings. The calibration in Plesio-Röntgen therapy in the red channel was performed both at 3h and 22 h after the irradiation, with and without the use of a black reading(see Chapter 3). Hence, these calibration curves have been used to analyse the net ODs of the the film pieces exposed during Plesio treatments with filter 1 (patient 16) and with filter 3 (patient 17). The calibration performed for filter 9 was not used, since there were no patients recruited with this type of treatment. The measurements are reported in Table 5.5. Even if the 22 h calibration leads to a better accordance with prescribed dose with respect to the 3 h analyses, the results are quite comparable. Moreover, both for 3 h and for 22 h readings, the accordance is better using the black, but the improvement is really poor. These considerations lead to prefer an easier calibration after 3 h without black reading.

5.4 Final assessments

Motivated by the good agreement achieved in tomotherapy measurements with TPS estimated doses, and by the trend observed regarding an underestimation of the TPS skin dose, contrary to results reported in literature, a final test was set up. A thermoplastic mask was built ad hoc for the Cheese Phantom (see Fig. 5.9) and some measurements were made on the surface of the phantom both in presence and in absence of the mask both in tomotherapy and at Linac.
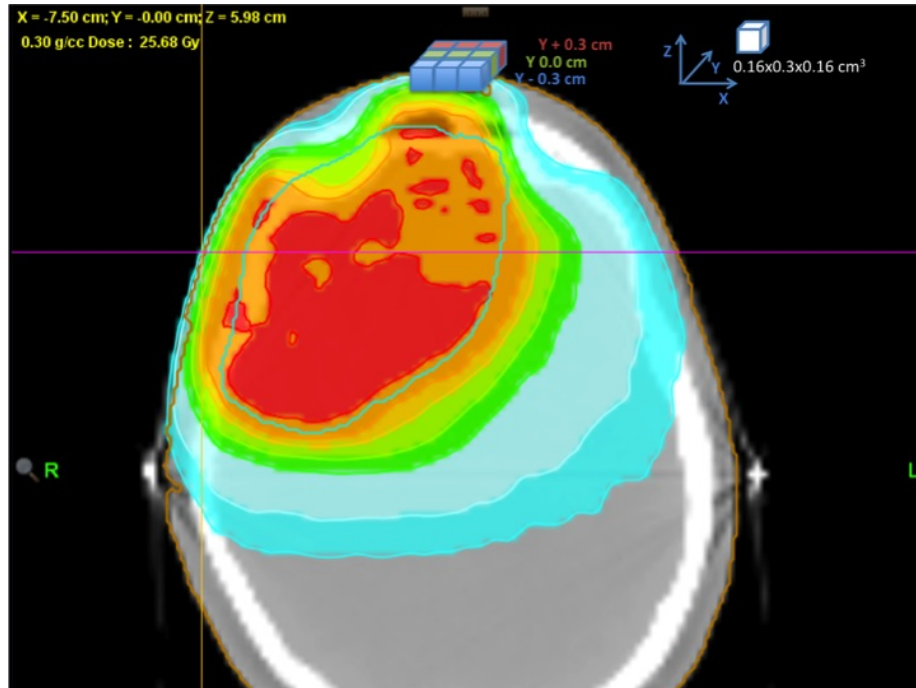
Figure 5.1: Schematic picture exemplifying the estimation of dose from the TPS dose grid. The central point value is averaged with the other eight points of doses around. The grid cubes are not in scale with respect to the CT image and its contours only for demonstrative reasons.

Table 5.3: Summary of in vivo measurements with EBT3 performed during tomotherapy treatments. Here, the number of the patient (Pat.), the dose per fraction (dose/fx) and the number of measurements (N) reported.

Pat.	Treated site	Plan (TPS)	Dose/fx (cGy)	Point	N	EBT3 dose (cGy)	TPS dose (cGy)	TPS SD (%)	EBT3-TPS (%)
8	H&N	IMRT (Tomo)	200	sx	1	107.3	90.9 ± 2.1	2.3	18.1
				dx	1	117.1	85.0 ± 0.1	0.1	37.8
9	H&N	IMRT (Tomo)	200	sx	1	94.3	92.2 ± 2.1	2.3	2.3
				dx	1	83.8	83.8 ± 0.1	0.1	0.0
10	H&N	IMRT (Tomo)	200	center	6	170.5 ± 4.8	168.6 ± 0.1	0.1	1.1
11	H&N	IMRT (Tomo)	200	sx	5	57.5 ± 4.9	53.3 ± 0.1	0.2	7.9
				dx	5	95.4 ± 5.6	93.2 ± 0.1	0.1	2.3
12	brain	IMRT (Tomo)	200	sx	4	64.4 ± 3.9	64.3 ± 0.9	1.4	0.2
				dx	4	149.3 ± 2.8	146.5 ± 5.1	3.5	1.9
13	H&N	IMRT (Tomo)	200	sx	1	133.0	124.8 ± 0.1	0.1	6.6
				center	1	140.6	174.1 ± 0.1	0.1	-19.3
14	brain	IMRT (Tomo)	200	center	3	119.1 ± 7.4	96.6 ± 0.2	0.2	23.3
				dx	3	144.3 ± 3.3	106.2 ± 0.2	0.2	35.9
15	sarcoma	IMRT (Tomo)	200	red dx	5	136.2 ± 3.7	135.3 ± 0.3	0.2	0.6
				scar dx	4	136.3 ± 1.2	155.2 ± 1.2	0.8	-12.2
				green dx	4	139.4 ± 6.7	165.9 ± 0.2	0.1	-16.0
	Mean of the absolute values of EBT3-TPS (%)								11.6

Table 5.4: Summary of in vivo measurements with EBT3 performed during Plesio-Röntgen treatments. Here, the number of the patient (Pat.) and the number of measurements (N) reported. [*]This prescribed dose value is referred to 5 mm of depth, and the measurement is affected to a further error due to the presence of a lead template that was not considered by the TPS.

Pat.	Treated site	Plan	Point	N	EBT3 dose (cGy)	Prescribed dose/fx (cGy)	EBT3-Prescribed (%)
16	head	Plesio-Filter 1 (60 kV)	iso	2	280.3± 1.7	300.0	-6.6
17	eye sx	Plesio-Filter 3 (100 kV)	iso	2	298.6 ±0.0	300.0	-0.5
18	head	Plesio-Filter 1 (60 kV)	iso	4	285.6 ±13.1	300.0	-4.8
19	foream	Plesio-Filter 1 (60 kV)	iso	4	298.7± 7.9	300.0	-0.4
20	ear dx	Röntgen-Filter 6 (180 kV)	iso	1	299.1	315.0[*]	-5.0
21	chest	Plesio-Filter 1 (60 kV)	iso	1	552.3	500.0	10.5
	Mean of the absolute values of EBT3-Prescribed (%)						4.6

(a)
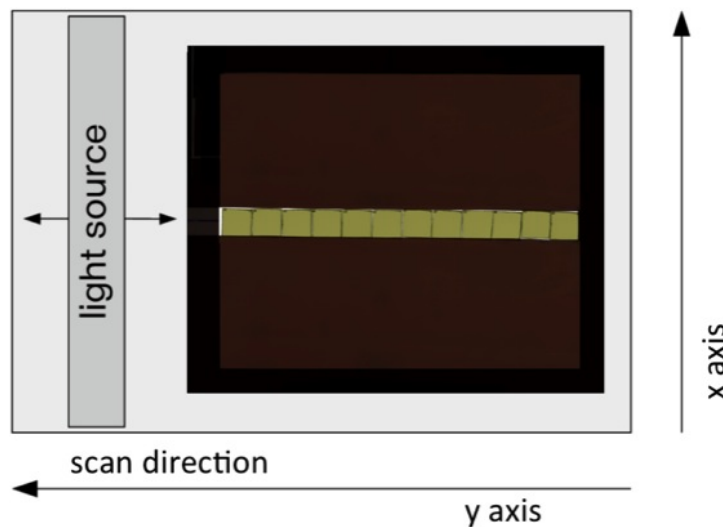
(b)

Figure 5.2: EBT3 film pieces of 2x2 cm² cut and prepared with a plastic film envelop to perform in vivo measurements (5.2a). Reading position of the film pieces along the central axis of the scanner (5.2b).

Table 5.5: Comparison of some EBT3 in vivo measurements performed during Plesio-Röntgen treatments read with different calibrations in the red channel. The readings after 3h and 22h from the irradiation, with and without the use of the black, are compared with the prescribed doses.

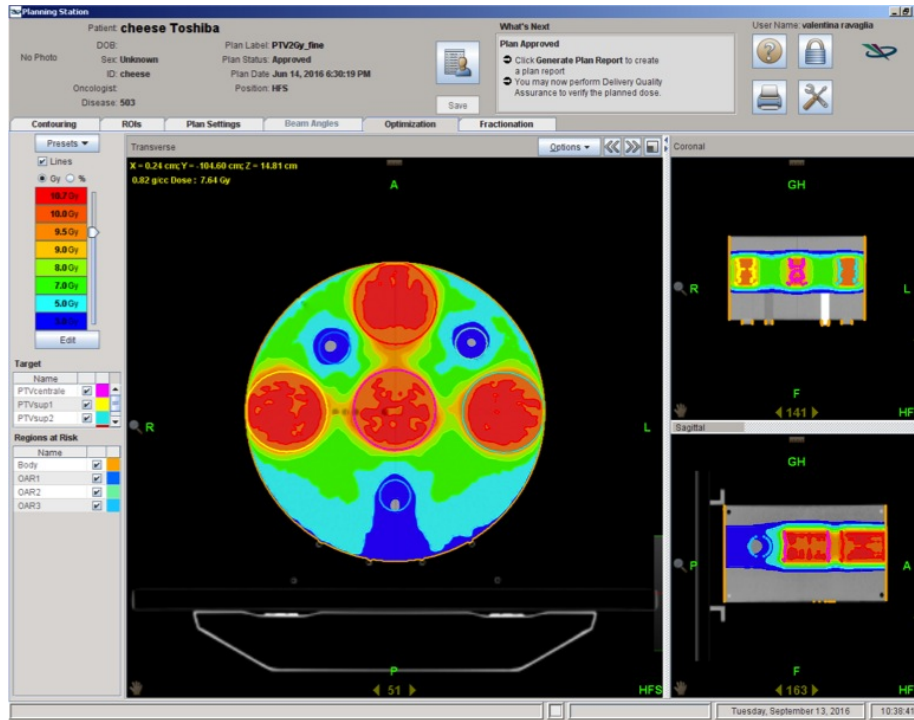| Pat.	Site	Plan	N	EBT3 dose (cGy)				Prescribed	EBT3-Prescribed (%)			
				3h	3h-black	22h	22h-black	dose/fx (cGy)	3h	3h-black	22h	22h-black
16	head	Filter 1	2	277.2 ± 4.5	277.5 ± 4.8	280.3 ± 1.7	280.6 ± 1.3	300.0	-7.6	-7.5	-6.6	-6.5
17	eye sx	Filter 3	2	294.4 ± 6.6	294.5 ± 6.6	298.6 ± 0.0	298.6 ± 0.5	300.0	-1.9	-1.8	-0.5	-0.5
Mean of EBT3-Prescribed (%)									-4.8	-4.7	-3.6	-3.5

Figure 5.3: Tomotherapy plan used for the preliminary measurements performed with the Cheese Phantom.

In tomotherapy the experimental conditions occurring during in vivo measurements in H&N and brain treatments were reproduced. In order to avoid any source of errors due to phantom re-positioning, these measurements were performed in a unique irradiation, being the Cheese covered by the mask only for a part. Then, a film was placed on the part of surface not covered by the mask, and another was fixed below it. The plan was created ad hoc with some superficial PTV having a prescribed dose of 2 Gy per fraction, reproducing the same conditions of in vivo measurements (see Fig. 5.10).

Furthermore, a similar measurement was set up at Linac, with two fields, one impacting perpendicularly to the film placed on the surface of the cheese and covered by the mask, and then another hitting on a part free by the mask. The number of MU of each beam was chosen such that the expected skin dose was similar to the values that on average occur in vivo. The resolutions of dose grids were chose equal to those occurring in vivo, so fine in tomotherapy, and $0.3x0.3x0.3$ mm^2 in Pinnacle.

The results of these measurements are reported in Table 5.6, where they are compared with TPS expected doses. As can be appreciated, the accordances between EBT3 and measurements improve when the thermoplastic mask is used. This is motivated by the fact that the EBT3 measure in a point that is more in depth, hence there is a better accordance with the TPS, that fails on the surface, as reported in literature. These experimental assessments on phantom provide a further explanation of the worse results obtained at Linac without masks. Moreover, in tomotherapy measurements, where the accordance with the TPS in presence of mask is excellent, it seems to be reproduced the trend reported in table 5.3, where the TPS on average overestimates the measurements performed without mask in Pat. 15 and underestimate the others with mask, but having a better agreement with the TPS. Nevertheless, the number of cases taken into account in vivo, especially without mask, and the final measurements performed on phantom should be repeated to obtain a better statistic to confirm a trend. As a consequence, further studies and measurements seem to be necessary to investigate on the behaviour of in vivo skin dose under different
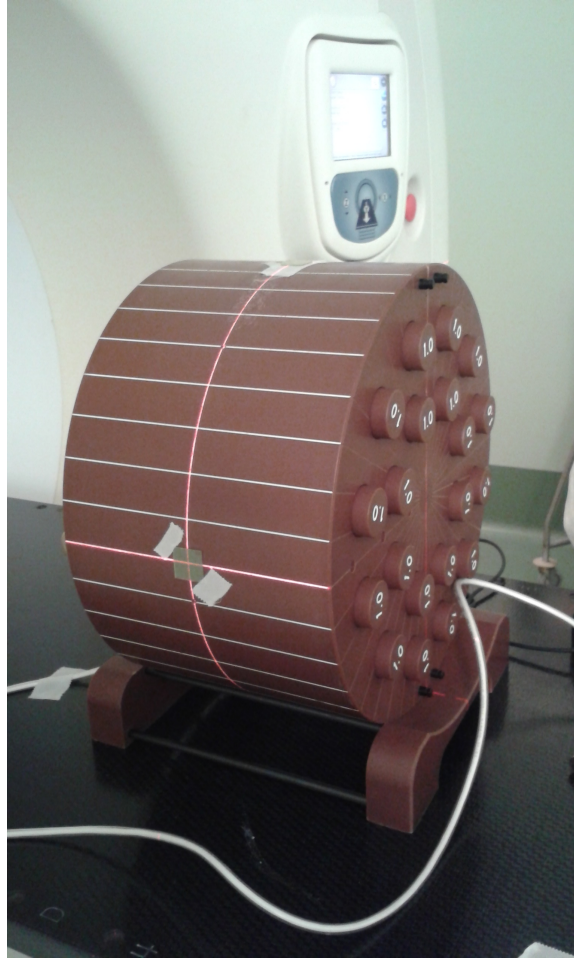
74

Figure 5.4: Experimental setup employed during preliminary measurements on the surface of Cheese Phantom. Three films are located in right, anterior and left positions and two ionizing chambers were used to control the dose. In the figure are visible only the right and the anterior films.

Figure 5.5: An example of in vivo measurement setup with EBT3 in tomotherapy using a thermoplastic mask.

(a)
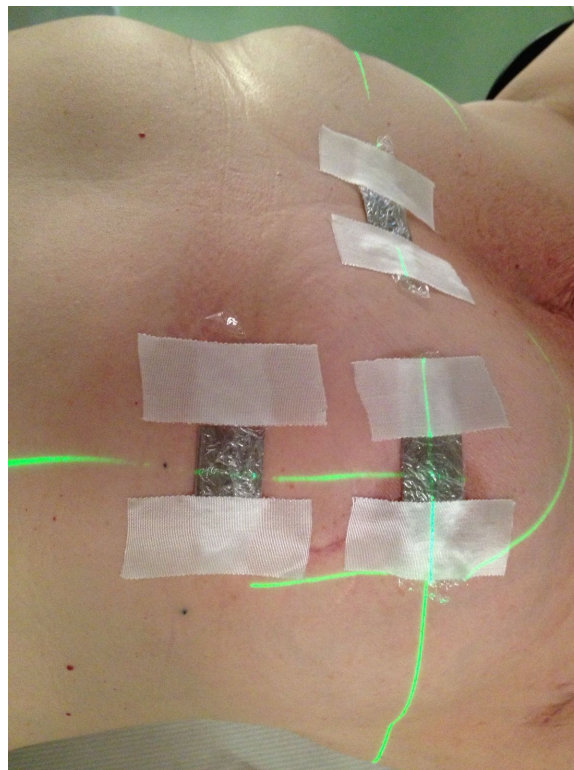
(b)

Figure 5.6: Film pieces positioned on patient skin in Plesio therapy (5.6a) and for breast treated with 3D-CRT at Linac (5.6b). In the latter case, films are placed at the isocenter, at the edge of the light field and in correspondence of the medial tatoo.

Table 5.6: Summary of the results for final tests on Cheese Phantom with EBT3 samples located its surface both in presence and in absence of thermoplastic mask, in Tomotherapy and at Linac.

Machine (TPS)	Experimental condition	EBT3 dose (cGy)	TPS dose (cGy)	EBT3-TPS (%)
Tomotherapy	without mask	124.7	174.6	-28.6
	with mask	137.0	136.1	0.7
Linac (Pinnacle)	without mask	126.1	159.0	-20.7
	with mask	122.5	146.3	-16.3

experimental conditions.
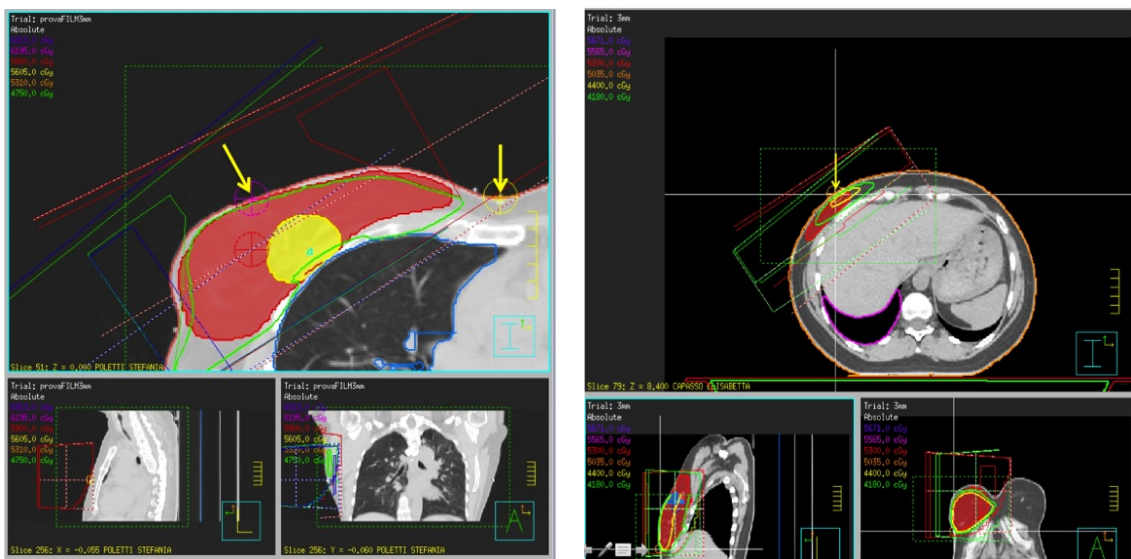
Figure 5.7: Film positioning in breasts treated with 3D-CRT displayed with TPS Pinnacle. Yellow arrows point to chosen measurements positions of isocenter (iso) and medial tatoo (med, 5.7a) and the edge of the field (5.7b).
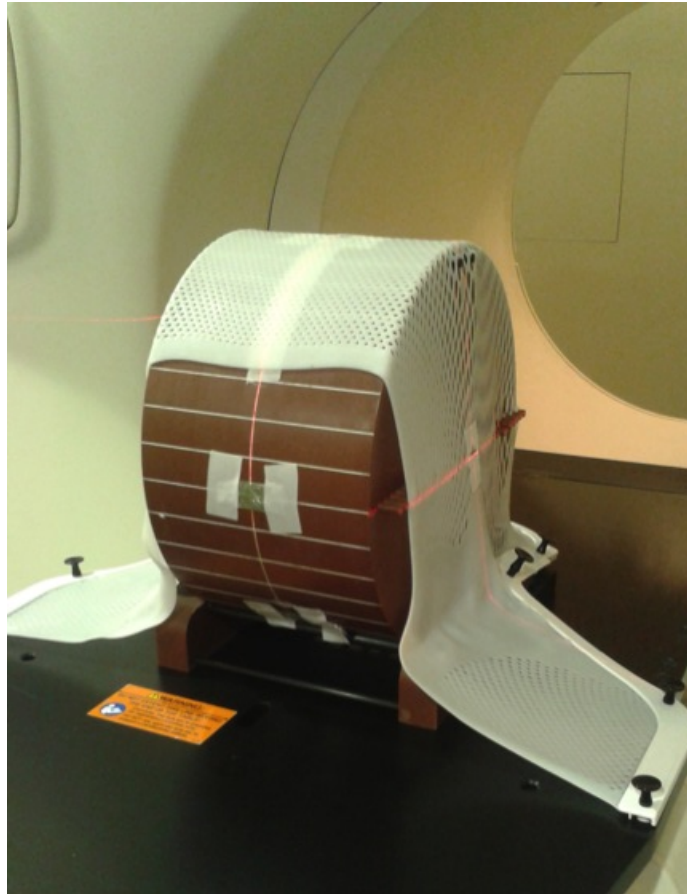
(a) H&N plan in tomotherapy.

(b) Brain plan in tomotherapy

(c) Sarcoma plan in tomotherapy.

Figure 5.8: Film positioning in tomotherapy plans displayed with TPS Tomotherapy. Yellow arrows point to chosen points of measurement: the center of the larinx in a H&N (5.8a), a point in the right and one in the center for a brain plan (5.8b) and two points on the skin of a patient treated without the use of the thermoplastic mask having a sarcoma (5.8c).

Figure 5.9: Final EBT3 measurements performed on Cheese Phantom using a thermoplastic mask built ad hoc for it.
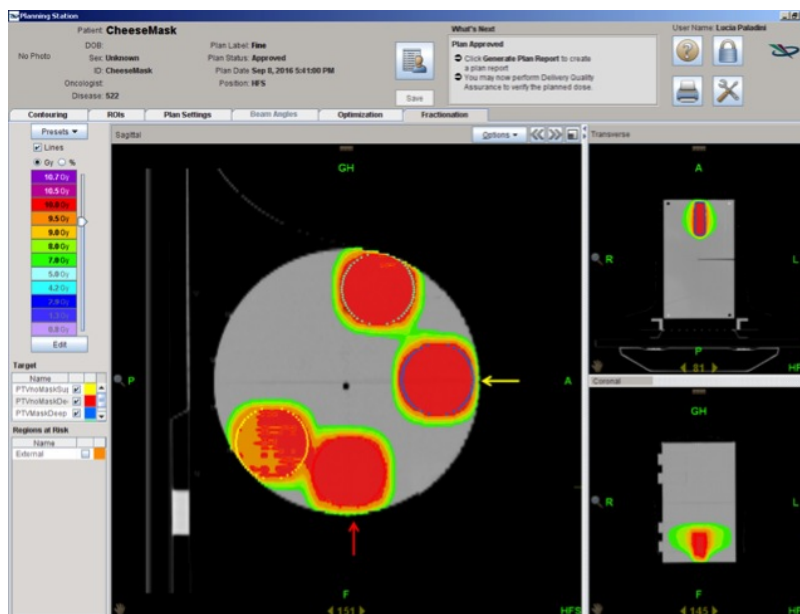

Figure 5.10: Tomotherapy plan used for EBT3 measurements performed on Cheese Phantom simultaneously with and without mask. The yellow arrow points to the surface position covered by the mask, instead the red one is referred to a point not covered from the immobilization device.

Chapter 6

Discussion of the results and concluding remarks

The aim of this thesis was to describe the use of GafChromic EBT3 films for pre-treatment QA applying both single channel and multiple channel methods, and to present the analysis of skin dose measurements using radiochromic film as in vivo dosimeter. EBT3 represent one of the most powerful tools to perform pre-treatment QA verifications and in vivo measurements, due to their high spatial resolution, energy independence in the MV range in radiotherapy, angular independence, easy handling and self-developing.

In first place a characterization of the scanner response at different optical densities and in correspondence of various positions of the scanbed was made. All the channels responses showed a weak and negligible variation along the scan direction, instead, perpendicularly to the scan direction there were higher PV deviations. For the red channel it was measured and fitted a parabolic trend in the mean pixel value reading, with a maximum in correspondence of the central axis of the scanner. When the same film piece was read at the border of the scanner instead that on the central axis, the mean pixel value reached even the 20% less than the central value, when an high OD film was considered. Even if this effect was attenuated for lower ODs, and it became negligible when an unexposed film was read, a correction for this parabolic effect seemed to be necessary. For this reason, a practical method, based on parabolic fits performed at various OD levels, was developed and implemented in a Matlab code. Instead, the green and blue channels showed lower deviations from the readings on the central axis, that were estimated to be about 1-3%, hence no correction methods were implemented for these channels.

Secondly, GafChromic EBT3 films were calibrated in the three channels and various dosimetric methods were developed to obtain an absolute dose measurement from the OD map read with the CCD scanner. All the approaches utilized both the scans of the unexposed and exposed images, in order to take into account film inhomogeneities. The red channel calibration, a method combining both the green and the blue channels [3, 4], the mean of these two methods and a multichannel iterative algorithm [5], were implemented through homemade codes in Matlab. The performances of all the dosimetric approaches were assessed analysing a number of films irradiated using test fields and then they were applied on thirteen pre-treatment clinical QA. The single red channel and the double channel techniques showed moderate performances in terms of $\gamma_{2D}(3\%,3\text{mm})$ pass rates, leading on average to 82% and 83% respectively on the group of QA taken into account. Instead the mean of these two methods led to an average result of 90%, showing a more stable response in the range of doses considered, and the multichannel method achieved the best average performance of 95%. Moreover, the parabolic correction did not improve the mean results for the red, the mean R-GB and the multichannel approaches, probably because in pre-treatment QA the dose maps analysed contain higher dose levels only in the central part

of the film, that is read in the central part of the scanner, where no correction is needed.

Then, the applicability of EBT3 to monitor in vivo skin dose has been assessed. In vivo measurements were performed during radiotherapy treatments in tomotherapy, at Linac both with 3D-CRT and VMAT and in Plesio-Röntgen therapy. Then, skin dose measurements, analysed through single red channel dosimetry, have been compared with TPS planned doses. Overall EBT3 measurements showed a good reproducibility, even if the measurements made without thermoplastic masks had more re-positioning problems. Nevertheless, the comparison between measurements and TPS estimated dose values was more delicate. The average deviations of EBT3 measurements from expected TPS values ranged from 17.7% for Linac treatments to 4.6% for Plesio-Röntgen therapy. Instead Tomotherapy was located at an intermediate position, reaching a mean of 11.6%. In the measurements performed at Linac, the TPS sometimes overestimated and other times underestimated the measurements, instead in tomotherapy a more delineated trend was observed, showing an underestimation of the TPS skin dose, contrary to results reported in literature. Since it was revealed when thermoplastic masks had been used, but not for in vivo measurements made directly on skin in tomotherapy, a set of final measurements on the Cheese Phantom were set up with a mask built ad hoc for it. Here, EBT3 readings showed a similar trend: a worse accordance with the TPS for measurements without the mask, and a better agreement in presence of the mask leading to a soft underestimation by the TPS.

In conclusion, this study has confirmed the importance of GafChromic EBT3 films in pre-treatment QA in radiotherapy and it has provided new in vivo data, showing that they are suitable detectors for surface dose in vivo monitoring. In vivo skin measurements with EBT3 films are a useful tool for QA in radiotherapy treatments, as they lead to a quantification of dose in areas where the TPS may not be accurate.

Bibliography

[1] International Commission on Radiological protection. 1990 reccomendations of the International Commission in Radiological Protection. Pergamon for the Commission, 1991.

[2] International Commission on Radiation Units and Measurements. (1985). Determination of dose equivalents resulting from external radiation sources, 43(2).

[3] Fiandra, C., Fusella, M., Giglioli, F.R., Filippi, A.R., Mantovani, C., Ricardi, U. and Ragona, R. (2013). Comparison of Gafchromic EBT2 and EBT3 for patient-specific quality assurance: Cranial stereotactic radiosurgery using volumetric modulated arc therapy with multiple noncoplanar arcs. *Med. Phys.* 40, 082105.

[4] McCaw, T.J., Micka, J.A. and Dewerd, L.A. (2011). Characterizing the marker-dye correction for Gafchromic EBT2 film: A comparison of three analysis methods. *Med. Phys.* 38, 5771-5777.

[5] Pérez Azorín, J.F., Garcia, L.I.R. and Martí-Climent, J.M.. (2014). A method for multichannel dosimetry with EBT3 radiochromic films. *Med. Phys.* 41(6), 062101.

[6] Low, D.A., Harms, W.B., Mutic, A. and Purdy, J.A. (1998). A technique for the quantitative evaluation of dose distributions. *Med. Phys.*, 25(5), 656-61.

[7] Marrazzo, L., Zani, M., Pallotta, S., Arilli, C., Casati, M., Compagnucci, A., Talamonti, C., and Bucciolini, M. (2015). GafChromic EBT3 films for patient specific IMRT QA using a multichannel approach. *Physica Medica*, 31(8), 1035-42. doi:10.1016/j.ejmp.2015.08.010

[8] Williams, M., and Metcalfe, P. (2011). Radiochromic Film Dosimetry and its Applications in Radiotherapy. *Concepts and Trends in Medical Radiation Dosimetry AIP Conf. Proc.*, 1345, 75-99. doi:10.1063/1.3576160

[9] Rink, A., Lewis, D.F., Varma, S., Vitkin, A. and Jaffray, D.A. (2008). Temperature and hydration effects on absorbance spectra and radiation sensitivity of a radiochromic medium. *Med. Phys.* 35(10), 4545-4555.

[10] McLaughlin, W.L., Puhl, J.M., Al-Sheikhly, Christou, C.A., Miller, A., Kovács, A., Wojnarovits, L. and Lewis, D.F. (1996). Novel Radiochromic Films for Clinical Dosimetry. *Radiat. Prot. Dosimetry* 66(1-4), 263-268.

[11] Hartmann, B., Martisikova, M. and Jakel, O. (2010). Homogeneity of Gafchromic EBT2 film. *Med. Phys.* 37(4), 1753-56.

[12] Zeidan, O.A., Stephenson, S.A., Meeks, S.L. et al. (2006). Characterization and use of EBT radiochromic film for IMRT dose verification. *Med. Phys.* 33(11), 4064-72.

[13] Saur, S. and Frengen J. (2008). GafChromic EBT film dosimetry with flatbed scanner: a novel background correction method and full dose uncertainty analysis. *Med. Phys.* 35(7), 3094-101.

[14] Fuss, M., Sturtewagen, E., De Wagter, C. and Georg, D. (2007). Dosimetric characterization of GafChromic EBT film and its implication on film dosimetry quality assurance. *Phys. Med. Biol.* 52(14), 4211-25.

[15] Matisikova, M., Ackermann, B. and Jakel, O. Analysis of uncertainties in Gafchromic EBT film dosimetry of photon beams. *Phys. Med. Biol.* 53(24), 7013-27.

[16] Desroches, J., Bouchard, H. and Lacroix, F. (2010). Potential errors in optical density measurements due to scanning side in EBT and EBT2 Gafchromic film dosimetry. *Med. Phys.* 37(4), 1565-70.

[17] Andres, C., Del Castillo, A., Tortosa, R., Alonso, D. and Barquero, R. (2010). A comprehensive study of the Gafchromic EBT2 radiochromic film. A comparison with EBT. *Med. Phys.* 37(12), 6271-78.

[18] Meigooni, A. S., Sanders, M.F., Ibbott, G.S. and Szeglin, S.R. (1996). Dosimetric characteristics of an improved radiochromic film. *Med. Phys.* 23(11), 1883-88.

[19] Chiu-Tsao, S.C., Ho, Y., Shankar, R., Wang, L. and Harrison, L.B. (2005). Energy dependence of response of new high sensitivity radiochromic films for megavoltage and kilovoltage radiation energies. *Med. Phys.* 32(11), 3350-54.

[20] Arjomandy, B., Tailor, R., Anand, A. et al. (2010). Energy dependence and dose response of Gafchromic EBT2 film over a wide range of photon, electron and proton beam energies. *Med. Phys.* 37(5), 1942-47.

[21] Butson, M.J., Cheung, T., Yu, P.K.N. and Alnawaf, H. (2009). Dose and absorption spectra response of EBT2. Gafchromic film to high energy x-rays. *Australas Phys. Eng. Sci. Med.* 32(4), 196-202.

[22] Cheung, T., Butson, M.J. and Yu, P.K.N. (2005). Post-irradiation colouration of Gafchromic EBT radiochromic film. *Phys. Med. Biol.* 50(20), N281-N285.

[23] Devic, S., Aldelaijan, S., Mohammed, H. et al. (2010). Absorption spectra time evolution of EBT-2 model GAFCHROMIC film. *Med. Phys.* 37(5), 2207-14.

[24] Lynch, B.D., Kozelka, J., Ranade, M.K., Li, J.G., Simon, W.E. and Dempsey, J.F. (2006). Important considerations for radiochromic film dosimetry with flatbed CCD scanners and EBT Gafchromic film. *Med. Phys.* 33(12), 4551-56.

[25] Casanova Borca, V., Pasquino, M., Russo, G., Grosso, P., Cante, D. (2013) Dosimetric characterization and use of GAFCHROMIC EBT3 film for IMRT dose verification. *Journal of Applied Clinical Medical Physics* 14(2), 158-171. doi:10.1120/jacmp.v14i2.4111.

[26] Rubinstein, A., Tailor, R. and Zhao, Z. (2013). Is EBT3 Energy Independent For Radiation-Therapy Photon & Electron Beams? *Med. Phys.* 40, 226.

[27] Villarreal-Barajas, J.E. and Khan, R.F.H. (2014). Energy response of EBT3 radiochromic films: implications for dosimetry in kilovoltage range. *Journal of Applied Clinical Medical Physics* 15(1).

[28] GAFChromic^{TM} EBT3 film specifications. www.gafchromic.com.

[29] Devic, S. (2011). Radiochromic film dosimetry: Past, present, and future. *Physica Medica* 27, 122-134.

[30] Devic, S., Seuntjens, J., Hegyi, G., Podgorsak, E.B., Soares, C.G., Kirov, A.S. et al. (2004). Dosimetric properties of improved GafChromic films for seven different digitizers. *Med. Phys.* 37, 2207-14.

[31] Technical Report Series Absorbed dose determination in external beam radiotherapy: an International Code of practice for dosimetry based on standards of absorbed dose to water, vol. 398. Vienna: IAEA; 2000.

[32] Almond, P.R., Biggs, P.J., Coursey, B.M., Hanson, W.H., Huq, M.S., Nath, R. et al. (1999). AAPM's TG-51 protocol for clinical reference dosimetry of high-energy photon and electron beams. *Med. Phys.* 26, 1847-70.

[33] Andrés, C., del Castillo, A., Tortosa, R., Alonso, D., and Barquero, R. (2010). A comprehensive study of the Gafchromic EBT2 radiochromic film. A comparison with EBT. *Med. Phys.* 37, 6271-6278. doi:10.1118/1.3512792

[34] Devic, S., Wang, Y., Tomic, N. and Podgorsak, E.B. (2006). Sensitivity of linear CCD array based film scanners used for film dosimetry. *Med. Phys.* 33(11), 3993-6.

[35] Schoenfeld, A.A., Poppinga, D., Harder, D., Doerner, K. and Poppe, B. (2014). The artefacts of radiochromic film dosimetry with flatbed scanners and their causation by light scattering from radiation-induced polymers. *Phys. Med. Biol.* 59(13), 3575.

[36] Gonzalez-Lopez, A. (2007). Useful optical density range in film dosimetry: limitations due to noise and saturation. *Phys. Med. Biol.* 52(15), N321-327.

[37] Devic, S., Seuntjens, J., Sham, E., Podgorsak, E.B., Schmidtlein, C.R., Kirov, A.S. and Soares, C.G. (2005). Precise radiochromic film dosimetry using a flat-bed document scanner. *Med. Phys.* 32(7), 2245-2253.

[38] Ferreira, B.C., Lopes, M.C. and Capela, M. (2009). Evaluation of an Epson flatbed scanner to read Gafchromic EBT films for radiation dosimetry. *Phys. Med. Biol.* 54(4), 1073-1085.

[39] van Battum, L.J., Hoffmans, D., Piersma, H. and Heukelom, S. (2008). Accurate dosimetry with GafChromic EBT film of a 6 MV photon beam in water: what level is achievable? *Med. Phys.* 35(2), 704-716.

[40] Martisíková, M., Ackermann, B., Klemm S. and Jäkel, O. (2008). Nuclear Instruments and Methods in Physics Research Section A: Accelerators, Spectrometers, Detectors and Associated Equipment. 591(1), 171-173.

[41] Fiandra, C., Ricardi, U., Ragona, R., Anglesio, S., Giglioli, F.R., Calamia, E. and Lucio, F. (2006). Clinical use of EBT model Gafchromic (tm) film in radiotherapy. *Med. Phys.* 33, 4314-4319.

[42] Garcia-Garduno, O.A., Celis, M.A., Larraga-Gutierrez, J.M., Moreno-Jimenez, S., Martinez-Davalos, A. and Rodriguez-Villafuerte, M. (2008). Radiation transmission, leakage and beam penumbra measurements of a micro-multileaf collimator using GafChromic EBT film. *J. Appl. Med. Phys.* 9(3), 2802.

[43] Su, F.C., Liu, Y., Stathakis, S., Shi, C., Esquivel, C. and Papanikolaou, N. (2007). Dosimetry characteristics of GAFCHROMIC (R) EBTfilm responding to therapeutic electron beams. *Appl. Rad. Isotop.* 65, 1187-92.

[44] Gerbi, B.J. and Han, E.Y. (2006). The response of radiochromic EBT film in high-energy electron beams. *Med. Phys.* 33, 2144.

[45] Bufacchi, A., Carosi, A., Adorante, N., Delle Canne, S., Malatesta, T., Capparella, R. et al. (2007). In vivo EBT radiochromic film dosimetry of electron beam for Total Skin Electron Theraphy (TSET). *Phys. Med.* 23, 67-72.

[46] Avanzo, M., Drigo, A., Ren Kaiser, S., Roggio, A., Sartor, G. et al. (2013). Dose to the skin in helical tomotherapy: Results of in vivo measurements with radiochromic films. *Physica Medica* 29, 304-311.

[47] Devic, S., Seuntjens, J., Abdel-Rahaman, W., Evans, M., Olivares, M., Podgorsak, E.B. et al. (2006). Accurate skin dose measurements using radiochromic film in clinical applications. *Med. Phys.* 33, 1116-24.

[48] Roland, T.F., Stathakis, S., Ramer, R. and Papanikolaou, N. (2008). Measurement and comparison of skin dose for prostate and head-and-neck patients treated on various IMRT delivery systems. *Appl. Rad. and Isot.* 66, 1844-1849.

[49] Tamponi, M., Bona, R., Poggiu, A. and Marini, P. (2015). A practical tool to evaluate dose distributions using radiochromic film in radiation oncology. *Med. Phys.* 31, 31-6. doi:10.1016/j.ejmp.2014.07.009.

[50] Miras, H. and Arrans, R. (2009). An easy method to account for light scattering dose dependence in radiochromic films. *Med. Phys.* 36(9), 3866-9.

[51] Poppinga, D., Schoenfeld, A., Doerner, K., Blanck, O., Harder, D. and Poppe, B. (2014). A new correction method serving to eliminate the parabola effect of flatbed scanners used in radiochromic film dosimetry. *Med. Phys.* 41(2), 021707. doi:10.1118/1.4861098.

[52] Crijns, W., Maes, F., van der Heide, U. and Van den Heuvel, F. (2013). Calibrating page sized Gafchromic EBT3 films. *Med. Phys.* 40(1),012102.

[53] Lewis, D. and Chan, M. F. (2015). Correcting lateral response artifacts from flatbed scanners for radiochromic film dosimetry. *Med. Phys.* 42(1), 416-29.

[54] Pérez Azorín, J.F., Garcia, L.I.R., Ozcoidi and Almansa J.F. (2016). Polarized dosimetry method for Gafchromic EBT3. *Physica Medica* 32(8), 972-980.

[55] Almond, P.R., Biggs, P.J., Coursey, B. M., Hanson, W.F., Huq, M.S., Nath, R. and Rogers, D.W.O. (1999). AAPM's TG-51 protocol for clinical reference dosimetry of high-energy photon and electron beams. *Med. Phys.* 26, 1847-1870.

[56] Devic, S., Tomic, N., Soares, C. and Podgorsak, E. (2009). Optimizing the dynamic range extension of a radiochromic film dosimetry system. *Med. Phys.* 36, 429-437.

[57] Hupe, O. and Brunzendorf, J. (2006). A novel method of radiochromic film dosimetry using a color scanner.*Med. Phys.* 33, 4085-4094.

[58] Méndez, I., Peterlin, P., Hudej, R., Strojnik, A. and Casar, B. (2014) On multichannel film dosimetry with channel-independent perturbations. *Med. Phys.* 30, 871-7.

[59] Micke, A., Lewis, D.F and Yu, X. (2011). Multichannel film dosimetry with nonuniformity correction. *Med. Phys.* 38, 2523-34.

[60] Lewis, D.F., Micke, A. and Yu, X. (2012). An efficient protocol for radiochromic film dosimetry combining calibration and measurement in a single scan. *Med. Phys.* 39, 6339-50.

[61] Mayer, R.R., Ma, F., Chen, Y., Miller, R.I., Belard, A., McDonough and O'Connell, J.J. (2012). Enhanced dosimetry procedures and assessment for ENT2 radiochromic film. *Med. Phys.* 39, 2147.

[62] Mathot, M., Bobczak, S. and Hoornaert, T. (2014). Gafchromic film dosimetry: Four years experience using FilmQA Pro software and Epson flatbed scanners. *Physica Medica* 30, 871- 877.

[63] Almond, P.R., Biggs, P.J., Coursey, B. M., Hanson, W.F., Huq, M.S., Nath, R. and Rogers, D.W.O. (1999). AAPM's TG-51 protocol for clinical reference dosimetry of high-energy photon and electron beams. *Med. Phys.* 26, 1847-1870.

[64] Press, W.H., Teukolsky, S.A., Vetterling, A. and Flannery B.P. (1999). *Numerical Recipes in FORTRAN 77: The Art of Scientific Computing.* Cambridge University Press, New York, Vol. 2.

[65] Pérez Azorín, J.F., Garcia, L.I.R., Ozcoidi, D.M. and Almansa, J.F. (2016). Polarized dosimetry method for Gafchromic EBT3. *Physica Medica* 32(8), 972-80. doi: 10.1016/j.ejmp.2016.06.013.

[66] Laskar, S., Bahl, G., Muckaden, M., Pai, S.K., Gupta, T., Banavali, S. et al. (2008). Nasopharyngeal carcinoma in children: comparison of conventional and intensity-modulated radiotherapy. *Int. J. Radiat. Oncol. Biol. Phys.* 72,728-36.

[67] Rosenthal, D.I, Chambers, M.S., Fuller, C.D., Rubueno, N.C., Garcia, J., Kies, M.S., et al. (2008). Beam path toxicities to non-target structures during intensity-modulated radiation therapy for head and neck cancer. *Int. J. Radiat. Oncol. Biol. Phys.* 72, 747-55.

[68] Lee, N., Chuang, C., Quivey, J.M., hilips, T.L., Akazawa, P., Verhey, L.J., et al. (2002). Skin toxicity due to intensity-modulated radiotherapy for head-and-neck carcinoma. *Int. J. Radiat. Oncol. Biol. Phys.* 53, 630-7.

[69] Daly, M.E., Le, Q.T., Maxim, P.G., Loo, Jr. B.W., Kaplan, M.J., Fischbein, N.J., et al. Intensity-modulated radiotherapy in the treatment of oropharyngeal cancer: clinical outcomes and patterns of failure. *Int. J. Radiat. Oncol. Biol. Phys.*

[70] Thomas, S.J. and Hoole, A.C. (2004). The effect of optimization on surface dose in intensity modulated radiotherapy (IMRT). *Phys. Med. Biol.* 49, 4919-28.

[71] Sibold, F., Sterzing, F., Sroka-Perez, G., Schubert, K., Wagenknecht, K., Major, G., et al. (2009). Surface dose in the treatment of breast cancer with helical tomotherapy. *Strahlenther Onkol* 185, 574-81.

[72] Tournel, K., Verellen, D., Duchateau, M., Fierens, Y., Linthout, N., Reynders, T. et al. (2007). An assessment of the use of skin flashes in helical tomotherapy using phantom and in-vivo dosimetry. *Radioter. Oncol.* 84, 34-9.

[73] Kinhikar, R.A., Murthy, V., Goel, V., Tambe, C.M., Dhote, D.S., Deshpande, D.D. Skin dose measurements using MOSFET and TLD for head and neck patients treated with tomotherapy. *Appl. Radiat. Isot.* 67, 1683-5.

[74] Higgins, P.D., Alaei, P., Gerbi, B.J., Dusenbery, K.E. (2003). In vivo diode dosimetry for routine quality assurance in IMRT. *Med. Phys.* 30, 3118-23.

[75] Ramsey, C.R., Seibert, R.M., Robison, B. and Mitchell, M. (2007). Helical tomotherapy superficial dose measurements. *Med. Phys.* 34, 3286-93.

[76] Qi, Z.Y., Deng, X.W., Huang, S.M., Zhang, L., He, Z.C., Li, X.A. et al. (2009). In vivo verification of superficial dose for head and neck treatments using intensity-modulated techniques. *Med. Phys.* 36, 59-70.

[77] Cherpak, A., Studinski, R.C. and Cygler, J.E. (2008). MOSFET detectors in quality assurance of tomotherapy treatments. *Radiother. Oncol.* 86, 242-50.

[78] Kinhikar, R.A. (2008). Surface dose for five telecobalt machines, 6 MV photon beam from four linear accelerators and a Hi-Art Tomotherapy. *Technol. Cancer. Res. Treat.* 7,381-4.

[79] Niroomand-Rad, A., Blackwell, C.R., Coursey, B.M., Gall, K.P., Galvin, J.M., McLaughlin, W.L., et al. (1998). Radiochromic film dosimetry: reccomendations of AAPM radiation therapy Committee Task Group 55. *Med. Phys.* 15, 2093-115.

[80] Liu, H.W., Gräfe, J., Khan, R., Olivotto, I. and Villarreal-Barajas, J.E. (2015). Role of in vivo dosimetry with radiochromic films for dose verification during cutaneous radiation therapy. *Radiation Oncology* 10,12.

Ringraziamenti

Domenico, Gaetano, Massimo e Davide.

Ringrazio Cinzia e Chiara per la vostra amicizia, sono contenta di aver affrontato gli anni della specializzazione con due persone che stimo tanto e da cui ho molto da imparare. Un grazie caloroso va a tutti i miei amici conosciuti a Pisa e adesso lontani: Anto e Manu, Gabriele, Claudia, Giusi, Giorgio e Riccardo. Ringrazio le mie amiche speciali ed ex coinquiline Rosalba, Livia, Angela, Lisa, Neda e Martina, siete state una seconda famiglia per me in questi anni a Pisa e per questo vi porterò sempre nel cuore. Ringrazio tutti gli amici di Pisa per il sostegno e per le serate spensierate che continuate a regalarmi e che hanno reso più leggeri gli ultimi mesi di lavoro sulla tesi, grazie per avermi sempre permesso di essere me stessa: Laura, Sara, Giulia, Fede, Antonio e Marta.

Ringrazio di cuore tutta la mia famiglia. Il mio pensiero più grande va a mia zia Carmela, il regalo più bello che avrei desiderato oggi sarebbe stato averti qui e vedere la felicità, l'affetto e l'orgoglio nei tuoi occhi il giorno della mia discussione. Se sono arrivata fin qui lo devo in gran parte alla fiducia che hai sempre riposto in me. Un abbraccio fortissimo va alla mia nonna e a mio fratello Antonio, a zia Rita, zio Toti, e alle mie dolci cuginette, Federica, Lorena e Monica. Grazie per aver sempre creduto in me.

Infine ringrazio enormemente mamma e papà per avermi permesso di raggiungere questo traguardo, sostenendomi in ogni giorno del mio percorso con amore, forza e passione. Vi sono riconoscente per tutti i sacrifici che avete fatto per me e per avermi sempre incoraggiato nel perseguire i miei sogni e le mie passioni.